University of Liège

Faculty of Sciences

Interactions Fondamentales en Physique et en Astrophysique

Primordial abundances of subdominant dark matter

Master Thesis in Space Sciences

Research Focus

Author:
Nico Benincasa

Supervisor:
Prof. Jean-René Cudell

Academic year 2016-2017

Acknowledgements

Pour ce mémoire, je remercie avant tout Jean-René Cudell pour sa grande disponibilité tout au long de cette année ainsi que pour ses conseils lors de nos discussions et ses nombreuses relectures qui améliorèrent grandement la qualité de ce mémoire, tant sur le fond que sur la forme.

Mes sincères remerciements vont également à Martin et Laura dont la contribution, certes modeste, fut néanmoins d'une aide cruciale pour le bon déroulement de ce mémoire.

Plus généralement, concernant mes études, je tiens à remercier chaleureusement Martin, Laura, Manu et Sophie.

Je tiens en outre à exprimer ma profonde gratitude envers mon frère qui m'accorda un peu de son temps chaque fois que cela fut nécessaire et ce, tout au long de ces cinq années d'études.

Enfin, un grand merci à ma famille et mes amis dont la présence, durant toute mes études, permis de ne pas lâcher prise lors des moments difficiles.

Contents

Introduction

> *The universe around us is not what it appears to be. The stars make up less than one percent of its mass; all the loose gas and other forms of ordinary matter, less than five percent. The motions of this visible material reveal that it is mere flotsam on an unseen sea of unknown material. We know little about that sea. The terms we use to describe its components, "dark matter" and "dark energy", serve mainly as expressions of our ignorance.*
>
> – David B. Cline [1]

Dark matter is a hypothetical matter that can account for several problems encountered in astrophysics (see Chapters 1 and 2). Throughout this thesis, dark matter will be investigated by only focusing on its particle-physics aspects. In particular, we will consider exotic dark-matter particles. The purpose of this work is to determine the characteristics of self-interacting dark matter, where this self-interacting part accounts for a few percentage of the total amount of dark matter.

The outline of this thesis is as follows. In the first chapter we introduce dark matter by talking about its historical presumed discovery and then we describe the different types of dark matter. In the second chapter, we briefly introduce the cosmological model currently in use, namely the ΛCDM model. Next, we mention its successes as well as its defects (especially its small-scales problems). In doing so, we then introduce the dark-matter model called PIDM model that we will consider in the fourth chapter and which can solve these small-scales problems that the popular too basic WIMP model, while being appreciated for its famous WIMP miracle, cannot resolve. In the third chapter, we develop the formalism to compute the relic density of dark-matter particles and apply it to the WIMP model in a first phase. Then we develop in detail a precise analytical formula to compute the thermally averaged annihilation cross section for our processes implying dark-matter particles. In the fourth chapter, we determine the value of the different parameters associated with the subdominant part of our two-type dark-matter model so that we obtain the right abundance established in the second chapter. The determination of the characteristics of these subdominant dark-matter particles will be performed in a case where we consider a kinetic mixing between the traditional photon of the visible sector and a photon belonging to the dark sector.

For information, for some equations in Chapter 3 and 4, in order not to slow down the reading of the thesis by their cumbersome developments, the latter were done in the Appendix A. Actually, whenever we will encounter the concerned equations, it will be indicated that the excessively detailed calculations are available in Appendix A.

As a final note, we would like to mention that all the Feynman diagrams realized by ourselves were drawn with the aid of Joshua Ellis' article [2].

Conventions

Natural units

As in customary in particle physics we will work in natural units throughout this thesis.

This consists in expressing all physical quantities with the energy, traditionally in GeV, and two fundamental constants: one from the relativistic world, namely the speed of light c and the other one from the quantum world, namely the reduced Planck constant $\hbar$.

Practically, it consists in working with

$$c = \hbar = k_B = 1 \tag{1}$$

where $c = 2.99792458 \cdot 10^8$ m/s, $\hbar = 1.0545718 \cdot 10^{-34}$ J·s and $k_B = 1.38064852 \cdot 10^{-23}$ J/K is the Boltzmann constant, which links the energy to the temperature [3].

Some useful relations between natural and SI units are given in the following table [4]:

Variable	Natural unit $\rightarrow$ SI unit
mass	1 GeV $\rightarrow 1.7824 \cdot 10^{-27}$ kg
length	1 GeV^{-1} $\rightarrow 1.9733 \cdot 10^{-16}$ m
time	1 GeV^{-1} $\rightarrow 6.5823 \cdot 10^{-25}$ s
energy	1 GeV $\rightarrow 0.6022 \cdot 10^{-10}$ J
momentum	1 GeV $\rightarrow 5.3444 \cdot 10^{-19}$ kg m s^{-1}
temperature	1 GeV $\rightarrow 1.1605 \cdot 10^{13}$ K
velocity	1 $\rightarrow 2.9979 \cdot 10^8$ m s^{-1}
energy density	1 GeV^4 $\rightarrow 2.0852 \cdot 10^{37}$ J m^{-3}
number density	1 GeV^{-3} $\rightarrow 7.6836 \cdot 10^{-42}$ m^{-3}

Table 1 – Conversion from natural units (expressed in GeV) to SI units.

This conversion table leads to

- parsec: 1 pc $= 3.0857 \cdot 10^{16}$ m $= 1.5637 \cdot 10^{32}$ GeV$^{-1} = 3.2616$ lyr
- Planck mass: $m_{\text{pl}} = 2.1764 \cdot 10^{-8}$ kg $= 1.2209 \cdot 10^{19}$ GeV
- present photon temperature: $T_0 = 2.7255$ K $= 2.3524 \cdot 10^{-13}$ GeV

- Hubble constant: $H_0 = 100h$ km s^{-1} Mpc^{-1} $= 2.1331h \cdot 10^{-42}$ GeV
- critical density: $\rho_c = \frac{3H_0}{8\pi} m_{\rm pl}^2 = 8.0843 \cdot 10^{-47}$ GeV^{-4} $= 1.0521 \cdot 10^{-5}$ GeV cm^{-3}
- picobarn: 1 pb $= 10^{-36}$ cm^2 $= 2.9979 \cdot 10^{-26}$ cm^3 s^{-1} $= 2.5682 \cdot 10^{-9}$ GeV^{-2}

Tensorial notations

In special relativity one utilizes 4-vectors. The first component refers to time whereas the three others components refer to space. The contravariant and covariant position vectors are respectively expressed as

$$x^\mu = (x^0, x^i) = (t, \vec{x}) \tag{2}$$

and

$$x_\mu = (x_0, x_i) = (t, -\vec{x}) \tag{3}$$

where Greek indices denote space-time components ($\mu = 0, 1, 2, 3$) whereas Latin indices only refer to space components ($i = 1, 2, 3$) by convention.

Along the same lines, for the 4-momentum, one has

$$p^\mu = (p^0, p^i) = (E, \vec{p}) \tag{4}$$

and

$$p_\mu = (p_0, p_i) = (E, -\vec{p}) \tag{5}$$

The same treatment holds for the derivatives:

$$\frac{\partial}{\partial x^\mu} = \partial_\mu = (\partial_0, \partial_i) = (\partial_t, \nabla_x) \tag{6}$$

and

$$\frac{\partial}{\partial x_\mu} = \partial^\mu = (\partial^0, -\partial^i) = (\partial_t, -\nabla_x) \tag{7}$$

The generalization in four dimensions of the metric of Euclidian space is the metric of Minkowski space (flat spacetime) represented by the metric tensor $g_{\mu\nu}$:

$$g_{\mu\nu} = \begin{pmatrix} 1 & 0 & 0 & 0 \\ 0 & -1 & 0 & 0 \\ 0 & 0 & -1 & 0 \\ 0 & 0 & 0 & -1 \end{pmatrix} = g^{\mu\nu} \tag{8}$$

where $g^{\mu\nu}$ is the inverse matrix of $g_{\mu\nu}$. One chose the $(+---)$ metric signature as it is conventionally the case in quantum field theory. Note that in general relativity the $(-+++)$ metric is employed instead.

The metric tensor acts as an index lift. Indeed, using the Einstein summation convention, one has

$$x^\mu = x_\nu g^{\nu\mu} \quad \text{and} \quad x_\mu = x^\nu g_{\nu\mu} \tag{9}$$

where, in the first case, the metric tensor $g^{\mu\nu}$ raises the ν and transforms it into the μ index and where, in the second case, the metric tensor $g_{\mu\nu}$ lowers the ν and transforms it into the μ index.

Thus the scalar product between the 4-momenta is

$$p^2 = p^\mu p^\nu g_{\mu\nu} = p^\mu p_\mu = p^0 p_0 + p^i p_i = E^2 - |\vec{p}|^2 = m^2 \tag{10}$$

where the last equality originates from the energy-momentum relation.

Chapter 1

The necessity for dark matter

1.1 Evidence for dark matter

Several astronomical observations made during the 20^{th} century led to the conclusion that there is some non-luminous matter that plays a considerable gravitational role in our Universe. A few historical indications of the existence of this aptly named dark matter will be briefly discussed in the following subsections.

1.1.1 Galaxy rotation curves

In 1978, Rubin, Ford and Thonnard demonstrated that in several spiral galaxies, contrarily to what one would have expected from Keplerian dynamics, the rotation curves [1] were rather flat at large distances (up to a radius of 50 kpc) [5]. For a star of mass m orbiting circularly in a galaxy of mass M, the gravitational force exerted by the galaxy on the star is counterbalanced by the centrifugal force. One therefore has, for a spherical distribution of matter, the following equality at a radial distance r to the center of this galaxy [6]:

$$G\frac{mM_r}{r^2} = \frac{mv(r)^2}{r} \tag{1.1}$$

where M_r refers to the mass of the galaxy up to r and v is the rotational velocity.

The central galactic area can be considered as a spherical region where the mean density can be expressed as $\rho = \frac{M_r}{\frac{4}{3}\pi r^3}$. As a result, for a star at radius r, (1.1) yields the following dependency for $v(r)$:

$$v(r) \sim r \tag{1.2}$$

On the other hand, outside the central region, the mass of the galaxy is rather constant and (1.1) thus implies

$$v(r) \sim \frac{1}{\sqrt{r}} \tag{1.3}$$

1. A galaxy rotation curve is obtained by plotting the star and gas orbital speed around the galactic center as a function of the distance to this center.

Thereby, the expected evolution of $v(r)$ is clear: in the beginning, it increases linearly with r and then it slowly falls as $r^{-1/2}$. Nevertheless, the observations do not lead to the same conclusion. Indeed, despite the fact that the linear dependence on r for the orbital speed is effectively observed, the curve, when it reaches its maximum value, then remains approximately constant (see Fig. 1.1).

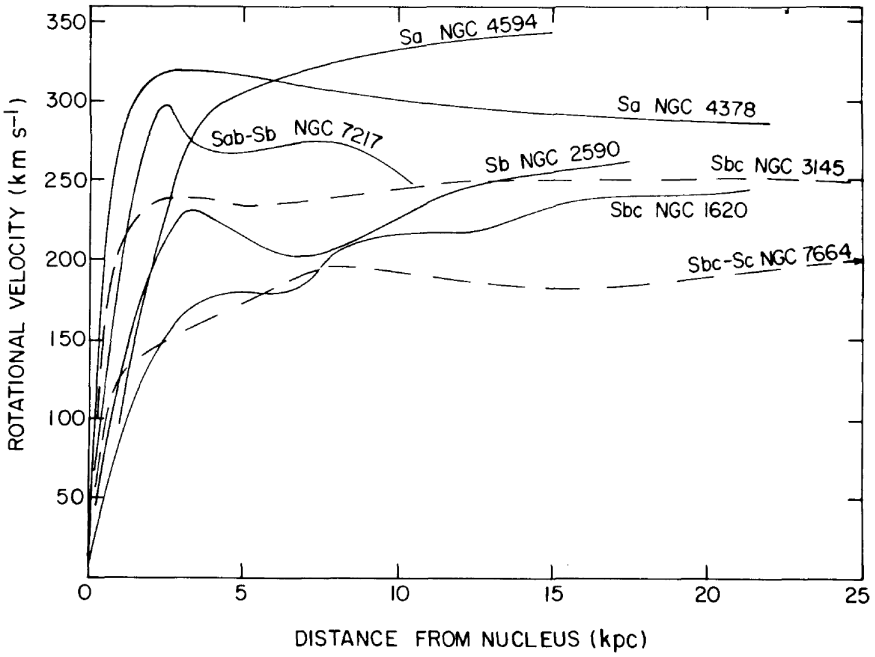

Figure 1.1 – Rotation curves for several spiral galaxies from [5]. After the maximum, one can observe a rather flat trend instead of a decrease with r.

The fact that the orbital speed does not decrease as one moves away from the dense areas of the galaxy is symptomatic of the presence of an amount of matter which, given its gravitational influence, prevents the stars from slowing down as the distance to the galactic center grows. Moreover, it should be noted that a more recent study [7] yields the rotation curves of a much larger set of spiral galaxies (see Fig. 1.2). Nowadays, it is commonly accepted that the distribution of this unobservable matter forms a halo containing the galaxy: the dark matter halo.

Finally, a study [9], published very recently, showed that, at the time of formation of the galaxies (about 10^{10} years ago), one observes that their dark-matter content was by far dominated by stars and gas. The authors of this article studied six massive star-forming galaxies and obtained rotation curves (see Fig. 1.3) that show a decrease where a rather flat trend is observed in Fig. 1.1.

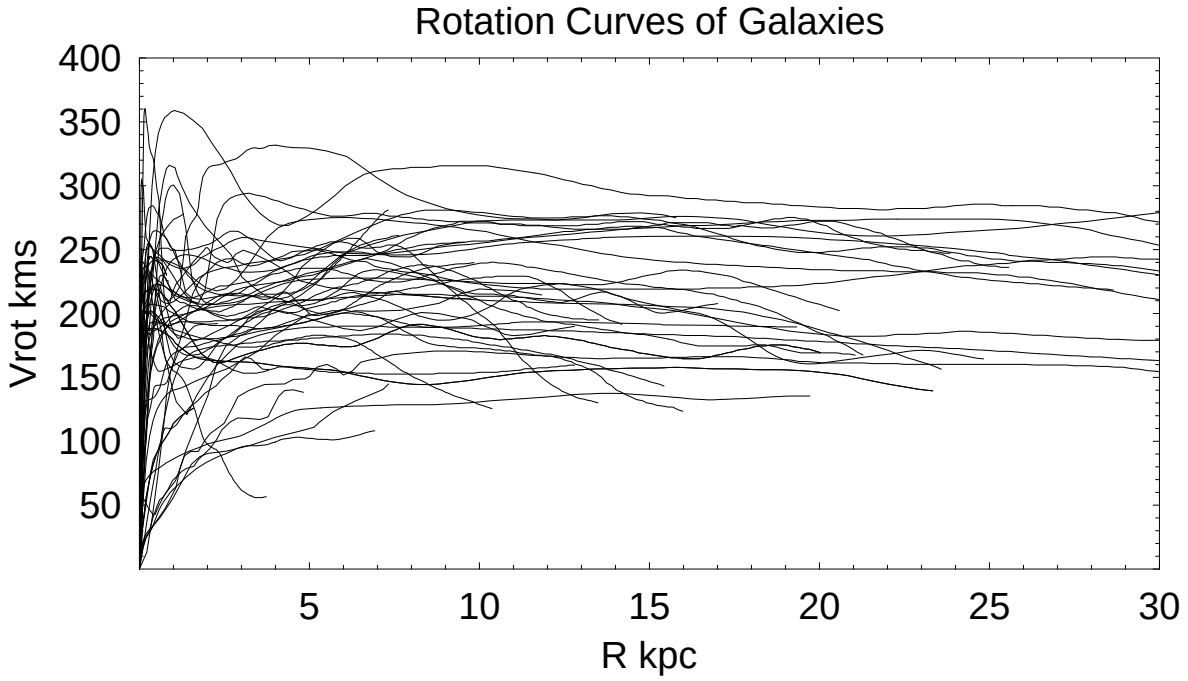

Figure 1.2 – Rotation curves from [8]. They all show a steep increase in the beginning which reaches a maximum value, then followed by an approximately constant rotational velocity with growing radius. These results reinforce those originally shown in Fig. 1.1.

1.1.2 The virial theorem in galaxy clusters

Regarding galaxy clusters, one famous example concerns the Coma Cluster, studied by Zwicky in 1933, where the velocity of the galaxies seemed to be too high to be kept inside the cluster when considering only the visible mass of the cluster [11]. By measuring the redshift of eight galaxies, he calculated their radial velocity and then computed the velocity dispersion [2] σ of this cluster by comparing these eight velocities to the mean velocity of the cluster [12, 13]. Next Zwicky used the virial theorem in order to obtain the mass of the Coma Cluster. The virial theorem links the kinetic energy T with the potential energy V of a system in equilibrium. More precisely it states that $T = -\frac{1}{2}V$ [6]. For a galaxy cluster, V corresponds to the total gravitational potential energy of the system and since the latter is quite spherical and assumed to be in equilibrium, an expression for V can easily be obtained [6]:

$$V = -\frac{3}{5}\frac{GM^2}{R} \tag{1.4}$$

with M and R respectively the mass and the radius of the cluster. As for the kinetic energy of this system, it can be expressed as [6]

$$T = \frac{1}{2}M\sigma^2 \tag{1.5}$$

2. The velocity dispersion corresponds here to the statistical dispersion of the velocities of the different galaxies around the mean velocity of the galaxy cluster.

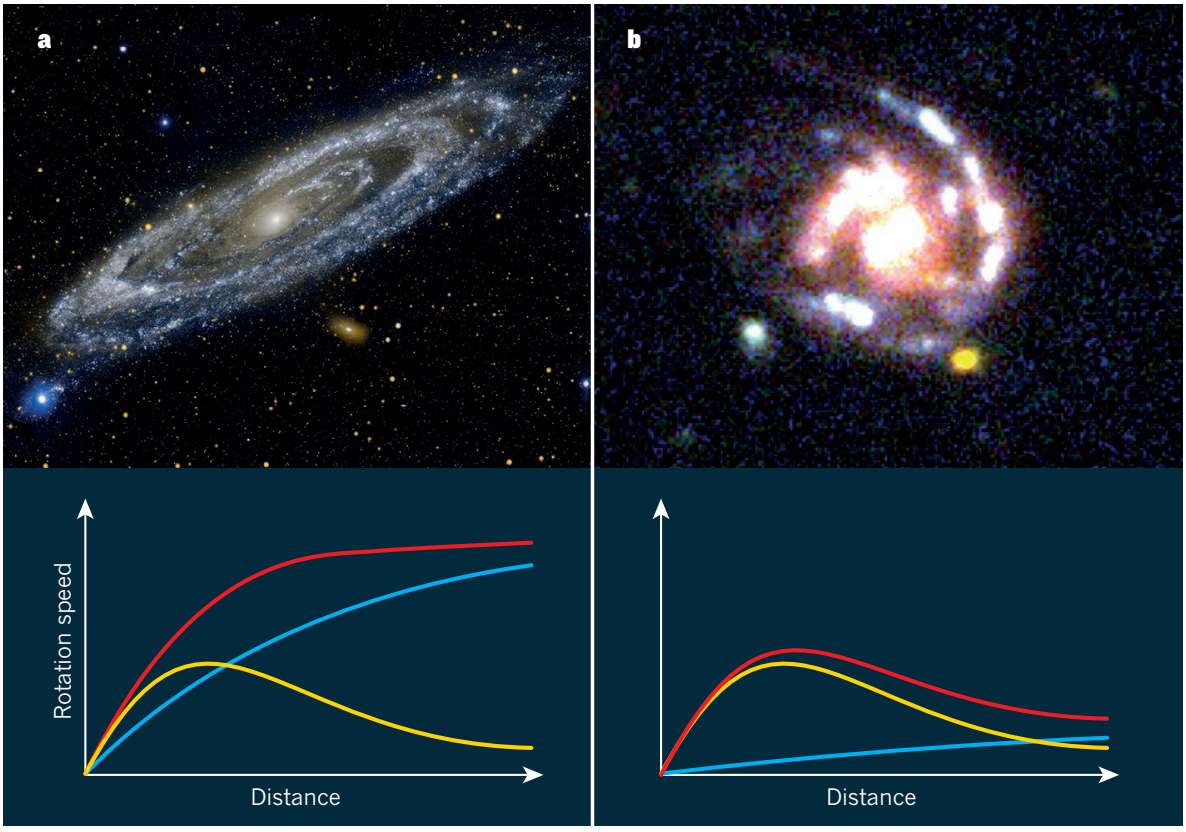

Figure 1.3 – Galaxy rotation curves from [10]. The left image shows the Andromeda galaxy. As discovered nearly 40 years ago, the rotational velocity of the visible matter (red curve) does not follow the originally expected Keplerian law (yellow curve) at large radii. This is due to the fact that the mass of dark matter (blue curve) increases with increasing radius. As for the right picture, it displays the rotation curve of a massive star-forming galaxy studied in [9]. It demonstrates that the red curve fits closely the yellow one since such galaxies contained little dark matter 10^{10} years ago.

By measuring R and σ, Zwicky could therefore estimate the mass needed for such a high velocity for the galaxies. The resulting mass was by far greater than the mass obtained via visible observations (about 400 times larger) [13]. It should be noted at that time, Zwicky was not aware of the presence of a hot ionized gas emitting in X-ray inside the galaxy cluster. However this intra-cluster medium, when taken into consideration, is still not sufficient to explain the discrepancies between the visible mass and the one computed with the virial theorem. It thus implied that there is some dark matter that fills the regions between the galaxies constituting the galaxy cluster.

1.1.3 Galaxy-cluster collision

The well-known example of dark matter evidence in a galaxy-cluster collision was reported in the Bullet cluster in 2006 by Clowe et al. [14]. It arises from the collision of two galaxy clusters which happened 100 million years ago [14]. One analysed the resulting merging in X-rays, for the hot ionized intra-cluster gas of both clusters, in the range of visible light for

the stars that the galaxies contain and one revealed the dark-matter distribution through gravitational lensing (see Fig. 1.4). Since the size of stars is negligible compared to the mean distance between two closer stars in a galaxy-cluster-collision process, the visible material remains intact. In this figure, one can clearly note that dark matter is at the same place as the galaxy distribution whereas the intra-cluster gas clouds of both clusters collided with each other. The latter result implies that dark matter is collisionless.

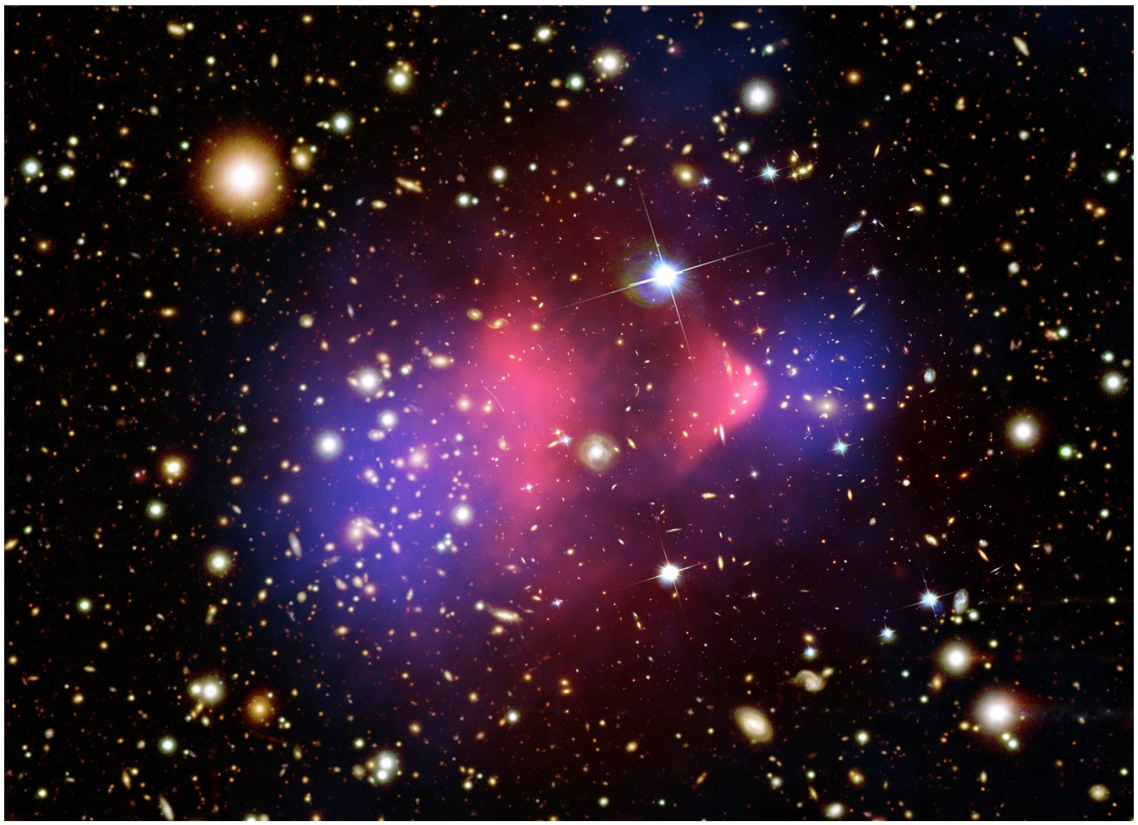

Figure 1.4 – This composite picture of the Bullet cluster results from the association of hot intra-cluster gas (in red) analysis via X-rays (NASA/CXC/CfA/M.Markevitch et al.), galaxies observation in the visible range of the electromagnetic spectrum (NASA/STScI; Magellan/U.Arizona/D.Clowe et al.) and dark matter (in blue) mapping by means of gravitational lensing (NASA/STScI; ESO WFI; Magellan/U.Arizona/D.Clowe et al.). This image can be found at `https://apod.nasa.gov/apod/ap060824.html`.

Another interesting instance of galaxy clusters collision is the Abell 520 galaxy cluster. In Fig. 1.5, similarly to the Bullet cluster, one can observe a separation between the hot intra-cluster gas and the galaxies [15]. Nevertheless, the presence of dark matter and intra-cluster gas as well as a deficiency of luminous galaxies in the core, drastically contrast with what is encountered in the Bullet cluster [16]. Moreover, in the area encircled in green for example, Fig. 1.5 presents some galaxies with intra-cluster gaz but devoid of dark matter.

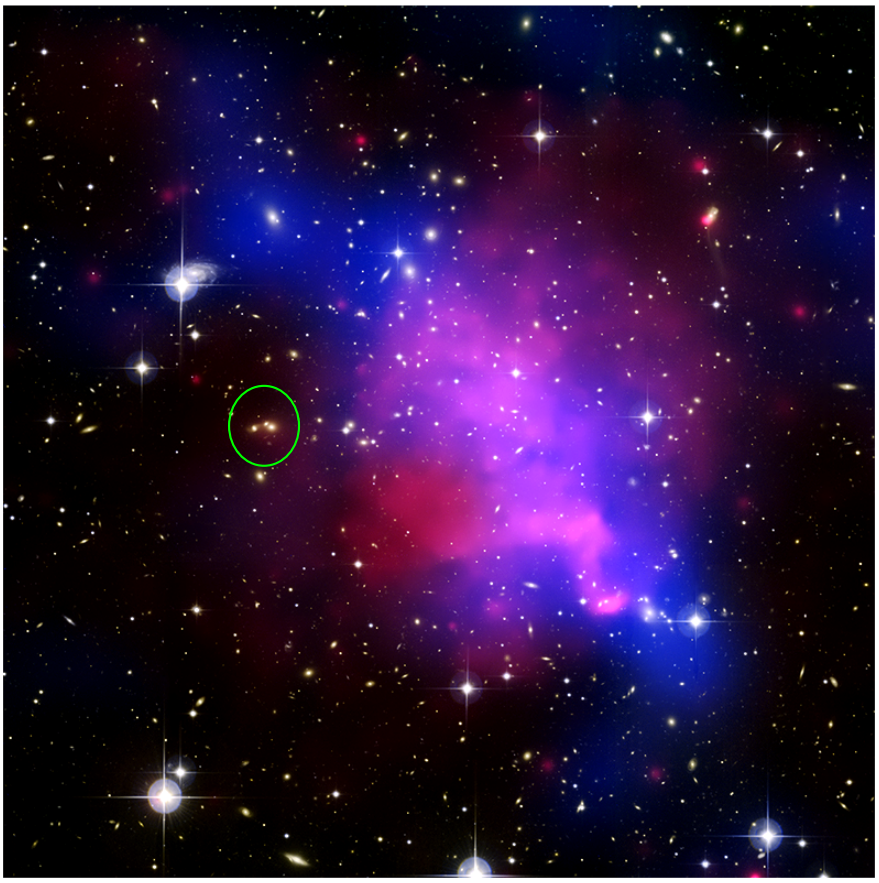

Figure 1.5 – This composite picture of Abell 520 results from the association of hot intra-cluster gas (in red) analysis via X-rays (NASA/CXC/UVic./A.Mahdavi et al.). The optical and the lensing (dark matter is displayed in blue) part is obtained thanks to CFHT/UVic./A.Mahdavi et al. This image can be found at `https://www.nasa.gov/mission_pages/chandra/multimedia/photos07-090.html`.

Thereby, originally considered as collisionless, dark matter seems to behave in a more complex manner. The fact that, in Abell 520, dark matter coincides with intra-cluster gas, which underwent a violent collision, might suggest that a non-negligible dark matter self-interaction should be taken into account.

The self-interactions that are responsible for a drag force that separates dark matter from stars, often occur and with little momentum transferred during each interaction [17]. This small momentum transfer can be due to a light mediator (particle which mediates the interaction) for instance. In this case, the resulting range of the mediated force will be long and the scattering will be anisotropic [17]. The self-interaction cross section of dark matter per unit mass σ/m in the Bullet cluster was actually calculated by S. W. Randall et al. in 2007 and they found [18]

$$\sigma/m < 2.23 \text{ barn/GeV} = 5.72 \cdot 10^3 \text{ GeV}^{-3} \tag{1.6}$$

with a 1σ error [3].

In a more recent paper, 72 cluster collisions were studied which allowed to constrain σ/m better. The obtained result was [17]

$$\sigma/m < 0.84 \text{ barn/GeV} = 2.15 \cdot 10^3 \text{ GeV}^{-3} \tag{1.7}$$

with a 2σ error.

To conclude, one can also mention a recently lower bound found in [19], namely

$$\sigma/m > (3.03 \pm 1.25) \cdot 10^{-4} \text{ barn/GeV} = (0.78 \pm 0.32) \text{ GeV}^{-3} \tag{1.8}$$

1.2 Types of dark matter

The dark matter that fills our Universe can be of two types. The first one is called baryonic dark matter. A baryon is made of three quarks which are elementary particles of the standard model. Two well-known examples are the proton (uud) and the neutron (udd), where u and d denote the up-quark and the down-quark respectively. Actually, when one mentions baryonic dark matter, it can also refers to electrons when they form bound states with protons and neutrons like atoms for instance. By contrast, non-baryonic dark matter is made of non-baryonic standard-model particles such as neutrinos or of exotic particles that are different from standard-model particles.

1.2.1 Baryonic dark matter

Baryonic dark matter is made of *our* particles, thereby the only possibility not to detect them is that this massive amount of matter is non-luminous or too faint. These typical bodies are called Massive Compact Halo Objects (MACHOs). One can cite the brown dwarfs that are stars the mass of which is lower than $0.08M_\odot$ and which thus cannot start the first thermonuclear reactions. Another instance concerns the white dwarfs. These faint objects are what remains after the life on the main sequence for stars of mass between $0.08M_\odot$ and $9M_\odot$. A white dwarf sees its luminosity decrease with time. As a last example, one can also mention the neutron stars. These very dense objects arise from massive stars ($>9M_\odot$) which ended their life through a type II supernova.

By virtue of their large mass, general relativity states that MACHOs locally distort space-time in the vicinity so that if a MACHO is between a bright source and the observer, the photons from the emitting source will be deflected when they pass near the MACHO (the geodesics that the photons follow become curved in the area around the MACHO). This results in a lens effect (the MACHO acts as a gravitational lens) except that contrary to a traditional lens, the light beams converge not by passing through the lens but via its exterior.

3. One can note that this cross section is typical of what one encounters in collisions between two nuclei, the cross section of this process being in the order of 1 barn.

1.2.2 Non-baryonic dark matter

As already stated above, non-baryonic dark matter corresponds to exotic particles. This dark matter cannot be charged (if one is in the presence of a single type of particle dark matter) since charged particles interact with the gauge boson of the electromagnetic interaction, namely the photon. Moreover, non-baryonic dark-matter interactions with the standard-model particles (constituents of the ordinary matter) are extremely weak or could even be null which explains the difficulty to detect these exotic particles [6]. Finally, the non-baryonic dark matter can be classified into two categories: the hot or the cold dark matter (see Section 1.2.4).

1.2.3 Immaterial dark matter

Black holes, which are defined as spacetime singularities, can also account for dark matter. Although classical physics states that they are non-luminous given that they prevent the light from escaping once it enters their horizon, they are actually not completely dark. Indeed, within the framework of quantum physics, Stephen Hawking predicted that black holes can emit some radiation, the Hawking radiation. This radiation leads to what is called the black hole evaporation since, by emitting particles, black holes lose their energy and thus their mass. As for the Hawking temperature, it refers to the temperature of the Hawking radiation and is expressed as [20]

$$T_H = \frac{1}{8\pi MG} \tag{1.9}$$

with M, the black-hole mass and G the gravitational constant.

Black holes that result from the evolution of a massive star have a terribly low Hawking temperature. For instance, the Hawking temperature of a solar-mass black hole is $T_H \simeq 5.29 \cdot 10^{-21}$ GeV $\simeq 6.16 \cdot 10^{-8}$ K. Since the mass M of a black hole decreases at a rate given by [21]

$$\frac{dM}{dt} = -L \sim -\frac{1}{M^2G^2} \tag{1.10}$$

with L the black-hole luminosity, then, by integrating, it implies that the lifetime of a black hole is

$$t_L \sim \frac{M_0^3G^2}{3} \tag{1.11}$$

where M_0 is the initial mass of the black hole.

One therefore concludes that one can detect Hawking radiation only near the end of the black-hole life since at this time, the luminosity in (1.10) becomes significant. However, the age of the Universe is about 10^{10} yr or equivalently $3 \cdot 10^{17}$ s and the lifetime for a solar-mass black hole is $t_L \sim 10^{74}$s [20] so one is not likely to observe it.

In fact, only black holes of mass $\sim 10^{12}$ kg or lower [20] can completely evaporate in a time interval inferior to the age of the Universe. These hypothetical black holes cannot be the fruit of a star but could have been present before the Big Bang nucleosynthesis. To be present today, these *primordial* black holes need a mass higher than 10^{12} kg and in doing so, they would contribute to the dark-matter amount in a non-negligible way.

1.2.4 Decoupling and freeze-out

When the rate of interaction Γ and the expansion rate H are such that $\Gamma \gg H$, the expansion of the Universe does not affect the interactions between particles. Indeed, if one defines [22] $t_{int} \equiv \frac{1}{\Gamma}$ and $\tau_H \equiv \frac{1}{H}$ one obtains $t_{int} \ll \tau_H$. The time scale for the interaction is thus much shorter than that for the expansion which means a local thermal equilibrium can take place [22]. Starting from the moment where $\Gamma = H$, the reactions do not occur sufficiently rapidly, which implies that the dark-matter particles and those from the thermal bath progressively stop seeing each other and become decoupled. This decoupling arises from the fact that the temperature of the Universe (this corresponds to the temperature of the photons that are embedded in it and to that of the particles which are in thermal equilibrium with photons) decreases with time and so does the interaction rate [22]. Given the decoupling, the number of particles per comoving volume will no longer change, this is also known as *freeze-out*. According to the value of the mass of the particles and the temperature of the Universe at the time of decoupling, the dark matter is either relativistic or non-relativistic at freeze-out [6].

If the mass M of the dark-matter particles and the freeze-out temperature T_f are such that $\frac{M}{T_f} \ll 1$, then these particles are relativistic (since their mass is negligible compared to their kinetic energy) at the freeze-out and the dark matter is said to be *hot* [6]. If however one has $\frac{M}{T_f} \gg 1$ at the decoupling, then the dark matter is non-relativistic and is called *cold* dark matter. Is should be noted that a case of dark matter, between the two previous ones, could exist and is referred to as *warm* dark matter [6].

1.2.5 Complex dark matter

One usually argues that non-baryonic dark matter must be made of one specific particle like the WIMP (see Section 2.3) but one could imagine a Universe consisting of dark matter as complex as ordinary matter [23]. In this case, one is not constrained by single-type dark matter: it can be composed of two, three or even many more different particles. Actually, there exists a theory which claims the existence of dark matter that is a reflection of *our* matter. It is naturally called *mirror* dark matter.

It was initially suggested by Yang and Lee in 1956 in order to reconcile the principle of relativity with the parity violation of weak interactions [24]. Indeed an important characteristic of this mirror dark matter is that only right-handed [4] particles can interact through the weak interaction whereas it only concerns left-handed particles for ordinary matter [25]. This property aim to restore the parity symmetry in physical laws. This model thus requires that our Universe is separated into two sectors: the visible one consisting of the ordinary particles and the *hidden* one consisting of mirror dark matter [25]. The sole link between these two sectors is of gravitational nature [25]. Thereby, if for instance a quark interacts with a photon, this gauge boson cannot interacts with a mirror quark and vice versa. The interactions between mirror dark matter and mirror gauge bosons unfold exactly in the same way as those between the gauge bosons and ordinary matter. It follows

4. The helicity of a particle is defined as the projection of the angular momentum $\vec{J}$ onto the momentum $\vec{p}$ but since $\vec{J} = \vec{L} + \vec{S}$ with $\vec{L}$ and $\vec{S}$ respectively the orbital momentum and the spin, it amounts to considering the projection of $\vec{S}$ onto $\vec{p}$ for the helicity. Then a particle is said to be right-handed if its helicity is positive and left-handed in the opposite case.

that in the manner of the processes which lead to the formation of complex structures such as atoms or molecules or even planets and stars, the mirror world contains mirror atoms or mirror molecules or mirror planets and mirror stars [25].

Chapter 2

The ΛCDM model

The ΛCDM model is the current cosmological model. CDM stands for cold dark matter whereas Λ denotes the cosmological constant or the dark energy, a mysterious repulsive force responsible for the acceleration of the expansion of the Universe.

Why was cold dark matter introduced? In the beginning of the 1980s, one had already become aware of the existence of anistropies in the Cosmic Microwave Background (CMB) [1] since they were supposed to be the manifestation of seeds that develop to yield the structures one currently observes [27]. At the same time, hot [2] dark matter was thought to be the right model of dark matter [27]. However, with this type of dark matter one should have expected to measure relatively high temperature fluctuations in the CMB. Indeed in a hot dark matter model, structures would form through a *top-down* approach [29], that is superclusters would form first and then, by a fragmentation process, all smaller structures would be obtained. Small-scale fluctuations are smoothed out by the free streaming relativistic particles (hot dark matter), thus there only remains large-scale fluctuations which are responsible for the formation of superclusters. Since these large fluctuations were not detected, one switched from the hot to the cold dark matter scenario. With cold dark matter, the predicted fluctuations from the CMB were observed by several space missions such as COBE, WMAP or more recently, by the Planck satellite.

As for the cosmological constant Λ, it was introduced in the CDM model (and thus reintroduced in the Einstein equations) since one has discovered the acceleration of the Universe expansion. Indeed, in 1998, Riess et al. observed, by analysing ten type-Ia supernovae at a given redshift, that the luminosity distance [3] of the latter was larger than expected [30]. These results could not be explained in a matter-dominated Universe but were consistent with a cosmological model where Λ was higher than zero [30].

Various predictions of the ΛCDM model were observed on large scales, demonstrating the success of this theory. One can cite a few of them [31]: polarization and anisotropies of the CMB (in agreement with the Planck data), baryon acoustic oscillations (BAO), gravitational lensing and large-scale galaxy distribution. The phenomenon of BAO [27] results from the fact that, at some point (before the matter-radiation decoupling), a

1. The CMB anisotropies were actually predicted in 1967 by Silk [26].
2. The *hot* and *cold* terms were introduced by Joel Primack and Dick Bond in 1983 [28].
3. The luminosity distance d_L, the apparent magnitude m and the absolute magnitude M are connected through $m - M = -5 + 5\log_{10}(d_{L,pc})$, where the subscript pc indicates that the luminosity distance is expressed in parsecs.

primordial density fluctuation starts to collapse but not completely since by reducing its volume, it increases its density and its temperature. The radiation pressure is therefore large enough to counterbalance the collapse by repelling the matter. As a consequence the density and the temperature drop, the collapse can thus start again, etc. This oscillatory motion is defined as the baryon acoustic oscillation. The BAO stops as soon as the matter-radiation decoupling occurs since, starting from this moment, the photons do not interact with the matter anymore and thereby cannot push the matter outward. Consequently, the matter can eventually collapse to form structures.

2.1 The FLRW metric

In general relativity, it is known that a body, through its energy, locally distorts spacetime. The way it modifies the geometry of spacetime is given by the key equation of the general relativity, namely, the Einstein equation [32]:

$$R_{\mu\nu} - \frac{1}{2} g_{\mu\nu} R - g_{\mu\nu}\Lambda = 8\pi G T_{\mu\nu} \tag{2.1}$$

where $R_{\mu\nu}$ is the Ricci tensor, $g_{\mu\nu}$ the metric tensor, R the scalar curvature, Λ the cosmological constant, G the gravitational constant and $T_{\mu\nu}$ the energy-momentum tensor.

The Einstein tensor $G_{\mu\nu} \equiv R_{\mu\nu} - \frac{1}{2} g_{\mu\nu} R$ describes how spacetime is curved whereas the right-hand side of (2.1) represents the energy-momentum content responsible for this curvature.

In cosmology, there is an important assumption one makes, namely, the cosmological principle. It assumes that the observable Universe is homogeneous (the Universe is the same at any place) and isotropic [4] (the Universe is the same, whatever the direction in which one observes) on large scales. Actually, this principle is based on the Copernican principle, stating there is no privileged position in the Universe (it arises from Copernicus's heliocentrism) [27]. Thereby, by extrapolating this principle, one can conclude that, from our position or from another one in the Universe, one is supposed to observe the same phenomena [27]. Nowadays, this principle seems to be verified.

The Einstein equations correspond to a set of non-linear differential equations in which the unknown is the metric tensor $g_{\mu\nu}$. For an homogeneous and isotropic spacetime, the metric is given by the Friedmann-Lemaître-Robertson-Walker (FLRW) equation [33]:

$$ds^2 = dt^2 - a^2(t) \left[\frac{dr^2}{1 - kr^2} + r^2 d\theta^2 + r^2 \sin^2\theta d\phi^2 \right] \tag{2.2}$$

where (t, r, θ, ϕ) are the comoving coordinates, $a(t)$ is the scale factor and k is a parameter that characterizes the curvature of the Universe ($k = -1, 0, 1$ denotes an hyperbolic, a flat and a spherical space respectively (see Fig. 2.1).

The metric tensor therefore takes the following form:

$$g_{\mu\nu} = \begin{pmatrix} 1 & 0 & 0 & 0 \\ 0 & \frac{-a^2}{1-kr^2} & 0 & 0 \\ 0 & 0 & -a^2 r^2 & 0 \\ 0 & 0 & 0 & -a^2 r^2 \sin^2\theta \end{pmatrix} \tag{2.3}$$

4. The isotropy of the Universe at every point implies its homogeneity.

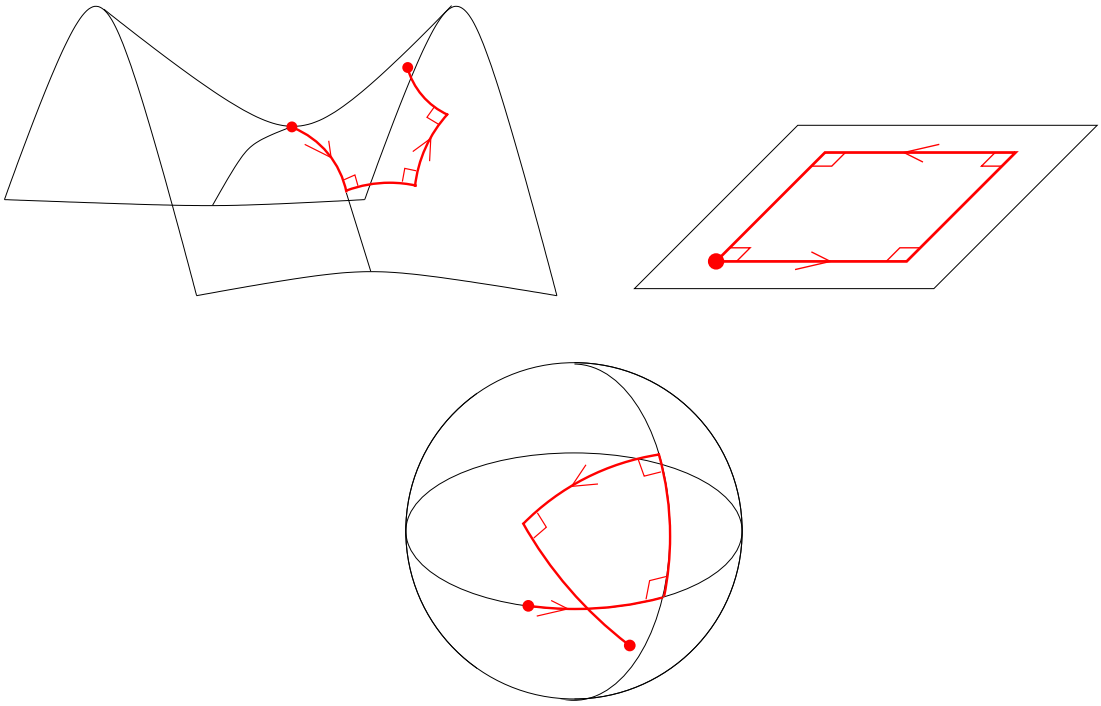

Figure 2.1 – Two-dimension spatial surfaces from [34]. The red lines correspond to a trajectory where each change of direction is made at a right angle. In the top-left, image the red line does not cross itself: this corresponds to a hyperbolic geometry. In the top-right image, the starting point coincide with the point of arrival: this is an Euclidean (or flat) geometry. In the bottom image, the trajectory is closed but not a the origin point: this corresponds to a spherical geometry.

It is important to note that the ΛCDM model is based on the assumption that general relativity is applicable on cosmological scales [27]. One only tested general relativity on galactic scales, thereby it is possible that this theory suffers from some shortcoming at larger distances. In this case one should appeal to an alternative theory such as MOND (Modified Newtonian Dynamics) for instance. Invented in 1983, one owes this conceptually simple theory to Milgrom [35]. Indeed it consists in modifying Newton's second law ($\vec{F} = m\vec{a}$) by introducing a new function $f(\frac{|\vec{a}|}{a_0})$ in it such that

$$\begin{cases} F = mf\left(\frac{a}{a_0}\right)a = ma & \text{with } f\left(\frac{a}{a_0}\right) = 1 \text{ if } a \gg a_0, \\ F = mf\left(\frac{a}{a_0}\right)a = m\frac{a^2}{a_0} & \text{with } f\left(\frac{a}{a_0}\right) = \frac{a}{a_0} \text{ if } a \ll a_0, \end{cases}$$

where $a_0 \sim 1.2 \cdot 10^{-10}$ m/s^2 [28]. One therefore notes that for high accelerations, one recovers Newton's law but for lower acceleration the latter formula is slightly modified.

This alternative theory is supposed to explain what one observes without bringing dark matter into play. Indeed, MOND naturally explains the flat trend in galaxy rotation curves as well as the Baryonic Tully-Fisher Relation [5] for instance [27]. Nevertheless,

5. The Tully-Fisher relation is an empirical correlation between the luminosity (or stellar mass) and

although this model is successful at small scales, it remains incapable of explaining what one observes at larger scales such as in galaxy clusters (Bullet cluster for example) unless one invokes a significant additional neutrino content which is equivalent to involving some dark matter in this dark-matterless theory [27]. Since the ΛCDM model is effective at large scales but encounters some problems at small scales (see Section 2.4), a certain complementarity can be emphasized between this model and MOND. Thereby, one could combine both these theories as in [38] into a new one in which each of both theories is utilized on scales where it is the most appropriate.

Furthermore, it should be noted that, in its original form, MOND had two main defects: it did not satisfy the energy, momentum and angular-momentum conservation and was not consistent with general relativity [28]. Thanks to Milgrom and Bekenstein [39], the first problem was resolved in 1984, with AQUAL (Aquadratic Lagrangian), a theory based upon a Lagrangian [40]. Moreover, contrary to MOND, it respects the weak equivalence principle[28], that is the inertial mass is proportional to the gravitational mass and thus all objects identically fall when they are subject to the same gravitational field. Then, an attempt to correct the second default was RAQUAL (Relativistic AQUAL) but could not, among others, explain gravitational lensing as one observes it. This is not before 2004, that a relativistic extension of MOND theory, coherent with general relativity, was developed by Bekenstein [40]. In addition, this Tensor-Vector-Scalar (TeVeS) modified gravity yields MOND theory in the weak-gravitational-field approximation.

2.2 Density parameters

If one considers the Universe as an ideal fluid in a homogeneous and isotropic spacetime one obtains [32] $T^{\mu}_{\ \nu}$ =diag$(\rho(t), -p(t), -p(t), -p(t))$ with ρ and p, the density and the pressure respectively. Then considering the fact that $g_{\mu\nu}$ is given by (2.3), one can derive, via (2.1), two equations for the scale factor $a(t)$ [33, 32]:

$$\left(\frac{\dot{a}}{a}\right)^2 + \frac{k}{a^2} = \frac{8\pi G}{3}\rho + \frac{\Lambda}{3} \tag{2.4}$$

from the temporal part ($\mu = \nu = 0$) of (2.1) and

$$2\frac{\ddot{a}}{a} + \left(\frac{\dot{a}}{a}\right)^2 + \frac{k}{a^2} = -8\pi G p + \Lambda \tag{2.5}$$

from the spatial part ($\mu = \nu = i$) of (2.1).

By subtracting (2.4) from (2.5) one obtains

$$\frac{\ddot{a}}{a} = -\frac{4\pi G}{3}(\rho + 3p) + \frac{\Lambda}{3} \tag{2.6}$$

the rotation velocity of spiral galaxies. This relationship is well-fitted with a power law but does not behave as a single power law at low luminosities and velocities since the influence of cold gas becomes important [36]. Therefore, in order to take this contribution into account, one can use the Baryonic Tully-Fiher Relation which, as indicated, considers the mass of baryons and not just the mass of stars [36]. This new relationship yields, for the baryonic mass, a dependence in the fourth power of the rotation velocity [37].

Equations (2.4) and (2.6) are known as the Friedmann equations.

One defines the critical density ρ_c as the density for a flat model without cosmological constant and with the same expansion rate $H \equiv \frac{\dot{a}}{a}$ as currently. Therefore, from the Friedmann equation (2.4), with k and Λ vanishing, one finds $\rho_c = \frac{3H_0^2}{8\pi G}$ where the subscript 0 denotes the present time. Then one defines the current density parameters for the matter, the radiation and the vacuum as

$$\Omega_{m,0} \equiv \frac{\rho_{m,0}}{\rho_c}, \quad \Omega_{r,0} \equiv \frac{\rho_{r,0}}{\rho_c}, \quad \Omega_\Lambda \equiv \frac{\rho_\Lambda}{\rho_c} \tag{2.7}$$

One can show [22] that the Friedmann equation (2.4) can be rewritten as

$$H^2(a) = H_0^2 \left[\Omega_{r,0} \left(\frac{a_0}{a} \right)^4 + \Omega_{m,0} \left(\frac{a_0}{a} \right)^3 + \Omega_{k,0} \left(\frac{a_0}{a} \right)^2 + \Omega_\Lambda \right] \tag{2.8}$$

where one defined $\Omega_{k,0} \equiv -\frac{k}{a_0 H_0^2}$.

As a consequence, if one looks at (2.8) today, one obtains

$$\Omega_{r,0} + \Omega_{m,0} + \Omega_{k,0} + \Omega_\Lambda = 1 \tag{2.9}$$

Instead of Ω, one usually utilizes Ωh^2 with h defined such that the Hubble constant H_0 is expressed as [33] $H_0 \equiv 100h$ km s^{-1} Mpc^{-1} $= 2.1332h \cdot 10^{-42}$ GeV. The most recent values provided by the Planck satellite data (1σ error) for the density parameters are [41]:

$$\begin{aligned} &\Omega_{m,0} = 0.3089 \pm 0.0062, \quad \Omega_b h^2 = 0.02230 \pm 0.00014, \\ &\Omega_{\text{CDM}} h^2 = 0.1188 \pm 0.0010, \quad \Omega_\Lambda = 0.6911 \pm 0.0062 \end{aligned} \tag{2.10}$$

with Ω_b and Ω_{CDM} respectively the baryon and the dark matter density parameter.

From the black body spectrum and the temperature of the CMB, the radiation density is estimated as [32]

$$\Omega_{r,0} h^2 \sim 10^{-5} \tag{2.11}$$

The data from the Planck mission [6] yield [41] $H_0 = 67.74 \pm 0.46$km s^{-1} Mpc^{-1}. One thus obtains the following values for the baryon and the dark matter density parameters:

$$\Omega_b = 0.0485976 \pm 0.0004494, \quad \Omega_{\text{CDM}} = 0.258896 \pm 0.002800 \tag{2.12}$$

One can therefore observe that to reach such a value for $\Omega_{m,0}$, the baryon density, which contains the visible and the dark matter (MACHOs), is lower than that required. A non-baryonic dark matter is thus necessary to explain this value. Thereby, by analysing

6. Actually, a more recent value was obtained by the Hubble Space Telescope, namely $H_0 = 71.9^{+2.4}_{-3.0}$ km s^{-1} Mpc^{-1} [42]. Nevertheless, we still use the Hubble constant calculated by the Planck satellite in order to remain coherent since we utilize parameter densities from Planck data.

the CMB, one proved in a cosmological way that dark matter must essentially be non-baryonic and constitute about 85% of the total matter density of the Universe. The value of Ω_k found by Planck is [41]

$$\Omega_k = 0.0008^{+0.0040}_{-0.0039} \tag{2.13}$$

One therefore cannot establish the sign of the curvature of the Universe but given the value of Ω_k, one can consider that one lives in a nearly flat Universe. Starting from now, for the rest of this thesis, when we will mention dark matter, it will implicitly refer to non-baryonic dark matter.

2.3 WIMPs

At present the most accepted representative of cold dark matter is the Weakly Interacting Massive Particle (WIMP). This exotic stable (or long-lived) neutral massive particle obviously interacts gravitationally with ordinary matter but also through the weak interaction. Moreover, since this particle is not confined in atoms or nuclei, it cannot be implied in a process ruled by strong interaction [11].

It can be demonstrated (see Section 3.2) that the WIMP freeze-out or relic density Ω_{WIMP} can be expressed as follows [43]:

$$\Omega_{\text{WIMP}} \sim \frac{10^{-10}\ \text{GeV}^{-2}}{<\sigma v_{\text{rel}}>} \tag{2.14}$$

and that the thermally averaged annihilation cross section $<\sigma v_{\text{rel}}>$ can be written as [43]

$$<\sigma v_{\text{rel}}> \sim \frac{\alpha^2}{M^2_{\text{weak}}} \tag{2.15}$$

with σ the annihilation cross section, v_{rel} the relative velocity between the interacting particles, α the weak coupling constant and M_{weak} the weak scale mass. A typical value for electroweak cross section is $<\sigma v_{\text{rel}}> \sim 10^{-9}$ GeV^{-2} [43] which yields $\Omega_{\text{WIMP}} \sim 0.1$. The relic density is therefore of the same order as the dark matter abundance given by the Planck data (2.12). Thus one notes that this astonishing coincidence naturally arises from the weak nature of the WIMPs [44]. The latter result, known as the *WIMP miracle*, is the major reason for which the WIMP model is so seductive.

2.4 Small-scale problems

Despite the aforementioned successes of the ΛCDM model, some of its predictions are problematic at small scales. Indeed, the ΛCDM model is efficient at large scales but encounters some issues at galactic or lower scales. These main problems are

- the *cusp-core* problem [45]: dissipationless (without collisions between dark matter particles) N-body simulations indicate that the CDM halo density in the inner part

of dwarf or low-surface-brightness [7] galaxies behaves as $\rho^{-\alpha}$ with $\alpha \simeq 1$ and that the resulting inner profile is rather cuspy (see Fig. 2.2). However, this trend is in contradiction with the inner-core observed profile (see Fig. 2.3).

- the *missing satellite* problem [45]: if, with each dark matter subhalo, one (maybe mistakenly) associates a satellite galaxy [46], then one concludes that N-body simulations predict a larger (by at least one order of magnitude) amount of dwarf galaxies with respect to what is observed in the Milky Way or in the Andromeda galaxy for instance.

- the *too big to fail* problem [45]: From simulations, one obtains that the halo of the Milky Way contains about ten subhalos that are more massive and denser than the observed satellite galaxies. They would thus seem to be too big to fail to form a large amount of stars (thereby, they would be too bright to miss them). The observational issue manifests itself through the fact that one does not detect fast-moving stars in these subhalos contrarily to what is expected.

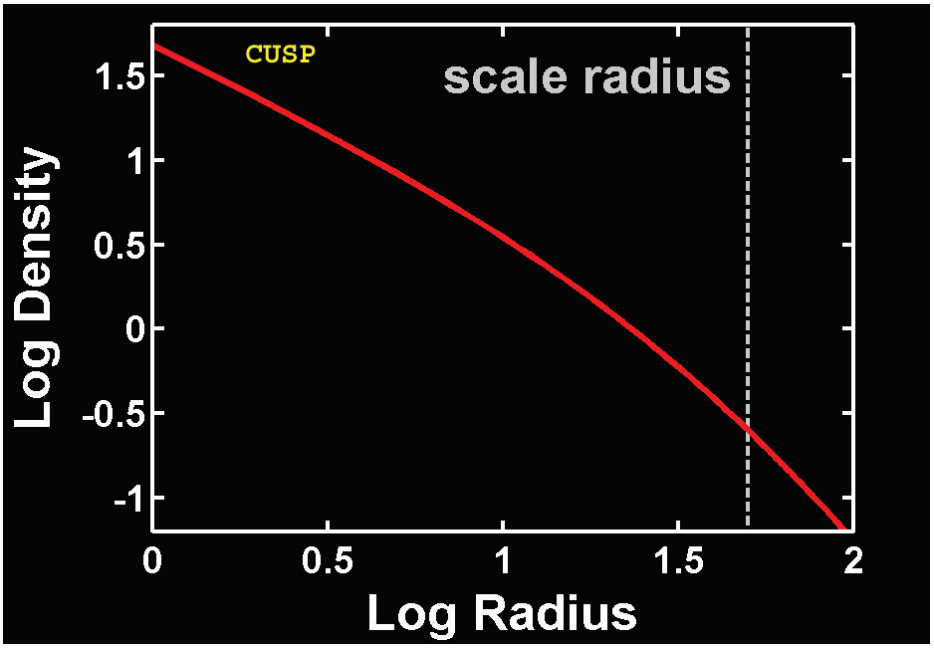

Figure 2.2 – Cuspy profile from [45].

7. Low-surface-brightness galaxies are interesting for testing dark matter models since the main contribution to their mass is due to dark matter (the mass contribution of the visible content is rather anecdotal) [46].

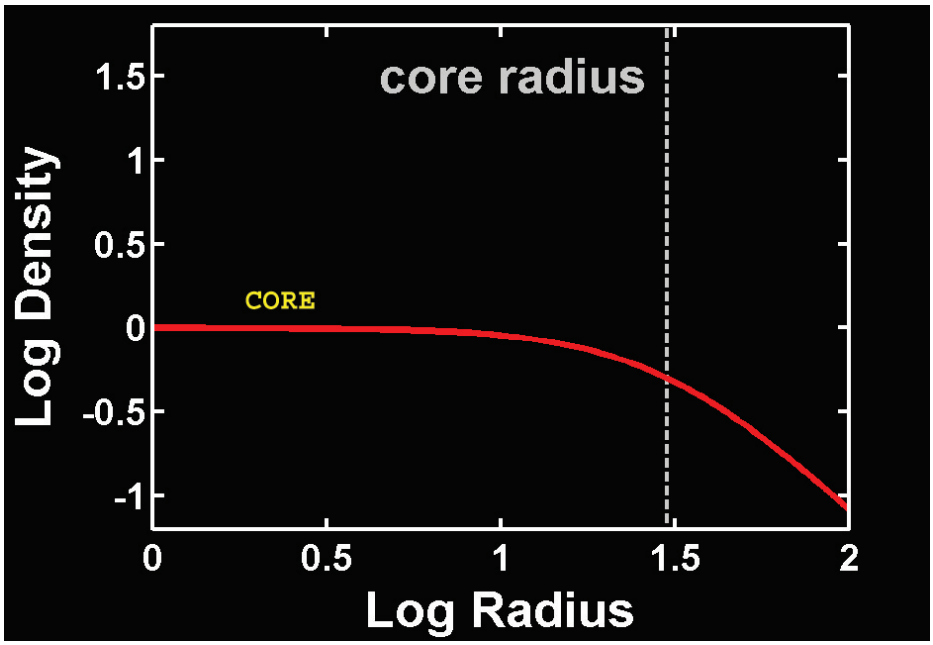

Figure 2.3 – Cored profile from [45].

2.5 A remedy: subdominant dark matter

The small-scale problems evoked in Section 2.4 cannot be explained by the ΛCDM model with a dark matter model like WIMPs, namely a single-type collisionless dark matter interacting *weakly*. For the purpose of eluding this difficulty, one can appeal to a self-interacting dark matter (SIDM) model, that is, dark matter which has a large scattering cross section with itself [47]. In this model, the density profile of the central region of the dark matter halo tends to be flattened because of the collisions between dark matter particles which transport heat from the hotter outer to the cooler inner parts of the halo [48]. Moreover, scattering is responsible for the randomization of the particle velocities. It should therefore make the inner part of the halo more homogeneous since, in this region, the scattering rate becomes high [49]. SIDM can have a velocity-dependent self-interacting cross section and in doing so, lead to the resolution of some small-scale problems while slightly modifying the results at large scales [50]. In order to obtain such modifications of the dark matter halo, the self-interaction cross section per unit mass σ/m_X must be [48]

$$\sigma/m_X \sim 1 \text{ barn/GeV} = 2.57 \cdot 10^3 \text{ GeV}^{-3} \tag{2.16}$$

Therefore one cannot model self-interacting dark matter with a WIMP since its weak scale mass and cross section are of order 100 GeV-1 TeV and 1 picobarn respectively. Thus

$$\sigma/m_X \sim 10^{-14}\text{-}10^{-15} \text{ barn/GeV} \tag{2.17}$$

which is much too small.

One simple extension of the SIDM which allows to obtain sufficiently large cross section considers that SIDM can interacts through a new force non-necessarily limited to the

dark sector (it could couple to the photon for instance). This force is mediated by a light (m_ϕ = 1-100 MeV) vector (or spin-1) gauge boson ϕ_μ [48]. This is a sort of electromagnetic interaction (the gauge group of which is $U(1)_{\text{elm}}$), thereby implying that dark matter is charged under the gauge group of this *dark* interaction (one considers fermionic dark matter). One is thus in the presence of composite dark matter (made of X, $\bar{X}$ and ϕ_μ). The corresponding interaction term that intervenes in the Lagrangian density [8] $\mathcal{L}$ is [48]

$$\mathcal{L}_{\text{int}} = g_X \bar{X} \gamma^\mu X \phi_\mu \tag{2.18}$$

where g_X is defined as $\alpha_X \equiv \frac{g_X^2}{4\pi}$ with α_χ the coupling constant of the new dark interaction. In general, with such a light particle, self-interactions depend on the velocity and thus, in the manner of Rutherford scattering ($\propto v^{-4}$), one can neglect self-interactions for high velocity but they are dominant for small ones [50]. An expression for the cross section can be found in the approximation of small velocities [48]:

$$\sigma \approx 50 \text{ barn} \left(\frac{\alpha_\chi}{0.01}\right)^2 \left(\frac{m_X}{10 \text{ GeV}}\right)^2 \left(\frac{10 \text{ MeV}}{m_\phi}\right)^4 \tag{2.19}$$

In the case of asymmetric SIDM, only the dark matter particle X is present nowadays. The scattering is therefore repulsive since self-interactions are only between two X particles. However, in the symmetric case, since both the X particle and the $\bar{X}$ antiparticle are present, one can have repulsive and attractive scattering.

Besides scattering, annihilation into ϕ_μ particles can also occur (leading to relic density). Moreover, direct and indirect detection can be possible if ϕ_μ also interacts with charged baryonic particles [50]. All these situations are depicted in Fig. 2.4.

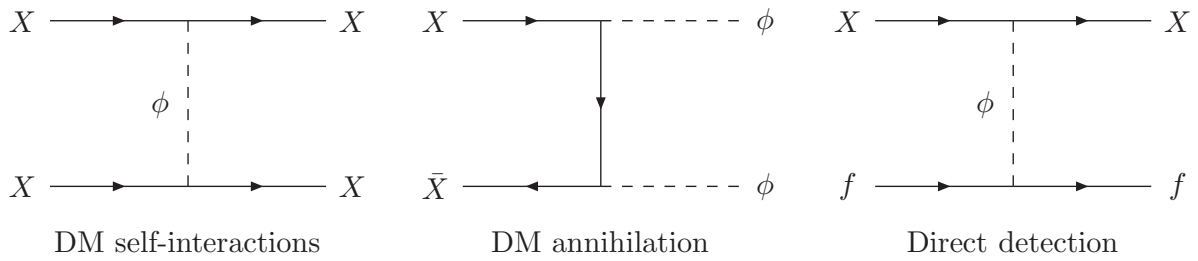

Figure 2.4 – Feynman diagrams (from [50]) for the self-interaction (which is mediated by ϕ_μ) between X particles, for the annihilation (by exchanging a X particle) of X with its antiparticle $\bar{X}$ and for the interaction between a fermionic dark matter particle X and an ordinary fermion f via ϕ_μ.

Another example of a composite SIDM model is considered in [51]. In this article, Cline et al. worked on the basis that nuclei and atoms (from the visible world) have a large cross section. Indeed, for the nuclei, it is explained by the fact that nuclei interact through the

8. The Lagrangian density $\mathcal{L}$ is defined as $\mathcal{S} = \int d^4x \; \mathcal{L} \equiv \int dt \; L$ where $\mathcal{S}$ and L are respectively the action and the Lagrangian.

nuclear force [9] [51]. As for the atoms, it results from their large area. Thus, in the manner of mirror dark matter (not exactly since, for instance, the mass of the dark electron will be higher than that of the visible one [51]), one can postulate the existence of dark nuclei and atoms in order to reach sufficiently large self-interacting cross section.

Finally, as a last model, which will be of interest for the rest of this manuscript, one can mention the Partially Interacting Dark Matter (PIDM) model [52]. It consists in self-interacting dark matter but not for the whole dark matter content: it only concerns a small fraction of the total amount of dark matter while the rest remains the traditional cold collisionless dark matter. In fact, since it has cross section similar to that of baryon-baryon interactions, one considers that this *subdominant* component (which is referred to as PIDM) can amount up to the proportion of baryonic matter compared to dark matter, that is it constitutes about 5% to 15% [52].

The specific case dealt in [52] is Double-Disk Dark Matter (DDDM). It corresponds to a portion of PIDM which is energy dissipative. Dissipation of energy is possible by postulating an interaction with a massless (or nearly so) dark $U(1)$ gauge boson analogous to the photon [52]. According to the DDDM model the energy dissipation sufficiently cools dark matter so that it eventually ends into a dark rotating disk.

Previous bounds on self-interacting dark-matter cross sections do not directly concern PIDM since these bounds were for a model in which the whole dark matter was self-interacting but in a PIDM model, the small amount of self-interacting dark matter can have a large interaction without actually altering what one observes [23]. The bound computed for DDDM is [52]

$$\epsilon \equiv \frac{M_{\rm DDDM}^{\rm disk}}{M_{\rm DM}^{\rm gal}} \lesssim 0.05 \tag{2.20}$$

with $M_{\rm DDDM}^{\rm disk}$ and $M_{\rm DM}^{\rm gal}$, the mass of DDDM in the Milky Way disk and the mass of all dark matter in the Milky Way respectively.

One can also define the portion of self-interacting dark matter as [52]

$$\epsilon_\Omega \equiv \frac{\Omega_{\rm PIDM}}{\Omega_{\rm DM}} \tag{2.21}$$

where $\Omega_{\rm PIDM}$ and $\Omega_{\rm DM}$ are respectively the PIDM and the total dark-matter energy density.

Moreover, since one considers that the proportion of different type of matter in our galaxy is similar to those in the Universe [52], then one can approximate ϵ_Ω by

$$\epsilon_\Omega \approx \frac{M_{\rm PIDM}^{\rm gal}}{M_{\rm DM}^{\rm gal}} \tag{2.22}$$

with $M_{\rm PIDM}^{\rm gal}$, the PIDM mass in the Milky Way.

9. Nuclear force or strong residual force is, by analogy with the residual electromagnetic force which allows atoms to bind into molecules, a force that allows the nucleons to be bound with each other to form a nucleus by exchange of mesons such as pions.

Since about one-third of baryonic matter is located in the galactic disk [23], if DDDM concentrates in the same way as baryonic matter (that is DDDM constitutes one-third of PIDM), then one has $M_{\rm PIDM}^{\rm gal} \approx 3M_{\rm DDDM}^{\rm disk}$ which is equivalent to

$$\epsilon_\Omega \approx 3\epsilon \tag{2.23}$$

which means that about one-third of PIDM is in the disk.

On the other hand, if, as evoked above, PIDM constitutes about 5% of dark matter, one thus obtains that

$$\epsilon_\Omega \approx \epsilon \tag{2.24}$$

that is, almost all of PIDM is in the disk.

In Chapter 4 we drew our inspiration from the PIDM model and thereby want to determine the characteristics of subdominant dark matter so that it accounts for 5% to 15% of the total dark-matter abundance.

Chapter 3

Relic Density

We want to compute the abundance of dark matter that currently fills our Universe. As stated in Section 1.2.4, the relic abundance arises from the fact that at a given moment, the interaction rate Γ is of the same order as the expansion rate H which implies that there is no interactions between the particles in question anymore. The abundance of these particles literally freezes out. However the transition between the equilibrium situation and the moment when $\Gamma = H$ is not abrupt. Actually, when $\Gamma > H$, the particles are in equilibrium with the thermal plasma so that one has as much annihilation as creation of these particles which means that there is no net production or destruction of particles. Nevertheless, as the Universe expands the temperature and thus the energy of the photons and the particles that are in equilibrium with them diminishes. As a consequence, at some point, the energy of X particles will be inferior to the rest mass energy of the dark-matter particles they used to produce. Starting from this moment the reaction only occurs in one direction: the equilibrium is shifted towards the X particle production. Thereby, the particle number density starts to decrease (so it becomes more and more difficult for a particle to find a partner with which it can interact) until $\Gamma \leq H$ when it remains constant. Thus, in order to describe the evolution of the particle number density in a out-of-equilibrium situation, one has to resort to the Boltzmann equation.

3.1 The Boltzmann equation

In this section we will derive the usual expression for the Boltzmann equation.

The evolution of the phase space distribution function $f(p^\mu, x^\mu)$ is given by the Boltzmann equation [33]:

$$\hat{\mathbf{L}}[f] = \mathbf{C}[f] \tag{3.1}$$

with $\hat{\mathbf{L}}$ the Liouville operator, which describes the variation of f, and $\mathbf{C}$ the collision operator.

In its traditional non-relativistic form the Liouville operator is expressed as [33]

$$\hat{\mathbf{L}}_{\mathrm{NR}} = \frac{d}{dt} = \frac{\partial}{\partial t} + \frac{d\vec{x}}{dt} \cdot \vec{\nabla}_x + \frac{d\vec{v}}{dt} \cdot \vec{\nabla}_v = \frac{\partial}{\partial t} + \frac{\vec{p}}{m} \cdot \vec{\nabla}_x + \vec{F} \cdot \vec{\nabla}_p \tag{3.2}$$

with the rest mass m and the force $\vec{F}$ such that $\vec{F} = \frac{d\vec{p}}{dt} = \frac{d(m\vec{v})}{dt}$.

In general relativity, the extension of the Liouville operator $\hat{\mathbf{L}}_{\rm NR}$ takes the form (see Appendix A)

$$\hat{\mathbf{L}} = p^\alpha \frac{\partial}{\partial x^\alpha} - \Gamma^\alpha_{\beta\gamma} p^\beta p^\gamma \frac{\partial}{\partial p^\alpha} \tag{3.3}$$

In the FLRW metric (2.2), f does not depend on x^i (homogeneity). Therefore, $f(p^\mu, x^\mu) = f(p^\mu, t)$. Moreover it does not depend on the direction of observation (isotropy): there is no vectorial dependence. Thus $f(p^\mu, t) = f(E, t)$ (or $f(|\vec{p}|, t)$), which means that it is enough to consider only $\alpha = 0$ in the Eq. (3.3). Therefore, the formulation of $\hat{\mathbf{L}}$ in this metric is (see Appendix A)

$$\hat{\mathbf{L}}[f(E,t)] = E\frac{\partial f}{\partial t} - \frac{\dot{a}}{a}|\vec{p}|^2 \frac{\partial f}{\partial E}. \tag{3.4}$$

By definition

$$dn(t) = f(E,t) g \frac{d^3x d^3p}{(2\pi)^3} \tag{3.5}$$

where n is the proper number density of particles and g represents the number of internal degrees of freedom (or equivalently, the number of spin states of the particle).

Thus, knowing that the number of particles is $N = \int dn$, the proper volume is $V = \int d^3x$ and that the proper number density can be expressed as $n = \frac{N}{V}$, we have

$$\begin{aligned} n(t) &= \frac{1}{V} \int f(E,t) g \frac{d^3x d^3p}{(2\pi)^3} \\ &= \frac{g}{(2\pi)^3} \int d^3p \; f(E,t) \end{aligned} \tag{3.6}$$

We can therefore express the Boltzmann equation in the following way (see Appendix A) for the species of interest χ:

$$\frac{dn_\chi}{dt} + 3\frac{\dot{a}}{a} n_\chi = \frac{g_\chi}{(2\pi)^3} \int \frac{d^3p_\chi}{E_\chi} \mathbf{C}[f] \tag{3.7}$$

Defining $d\Pi \equiv g \frac{1}{(2\pi)^3} \frac{d^3p}{2E}$, the right-hand side of (3.7) for the reaction $\chi + a + b + ... \longleftrightarrow i + j + ...$, can be written as [33]

$$\begin{aligned} \frac{g_\chi}{(2\pi)^3} \int \frac{d^3p_\chi}{E_\chi} \mathbf{C}[f] = -\int d\Pi_\chi d\Pi_a d\Pi_b ... d\Pi_i d\Pi_j ... (2\pi)^4 \delta^{(4)}(p_\chi + p_a + p_b + ... - p_i - p_j - ...) \\ \times \Big[|\overline{\mathcal{M}}|^2_{\chi+a+b+...\to i+j...} f_a f_b ... f_\chi (1 \pm f_i)(1 \pm f_j) ... \\ - |\overline{\mathcal{M}}|^2_{i+j+...\to\chi+a+b+...} f_i f_j ... (1 \pm f_a)(1 \pm f_b) ... (1 \pm f_\chi) \Big] \end{aligned} \tag{3.8}$$

where the Dirac delta function translates the 4-momentum conservation. The "+" sign is for bosons (Bose enhancement) and the "−" sign is for fermions (Pauli exclusion principle).

However these two phenomena can be neglected as explained hereafter, thereby it follows that $1 \pm f \simeq 1$.

Then, both invariant amplitudes [1] in (3.8) can be replaced with $|\overline{\mathcal{M}}|^2$ by time-reversal invariance. Furthermore, fermions and bosons distributions are supposed to obey Fermi-Dirac and Bose-Einstein statistics respectively but here one will use the Maxwell-Boltzmann distribution to describe the phase space density of both types of particles (thus $f_i(E_i) = e^{-(E_i-\mu_i)/T}$, with μ the chemical potential). This assumption is justified by the fact that one focuses only on the study of non-relativistic particles at the decoupling time ($\frac{m}{T} \gg 1$).

These hypothesis lead to a new expression for the Boltzmann equation:

$$\dot{n}_\chi + 3Hn_\chi = -\int d\Pi_\chi d\Pi_a d\Pi_b ... d\Pi_i d\Pi_j ... (2\pi)^4 \delta^{(4)}(p_i + p_j ... - p_\chi - p_a - p_b ...) \times |\overline{\mathcal{M}}|^2 [f_a f_b ... f_\chi - f_i f_j ...] \quad (3.9)$$

where n_χ represents the number density of species χ, the dot denotes the derivative with respect to time and H, the expansion rate, is defined as $H \equiv \frac{\dot{a}}{a}$.

The second term of the left-hand side of (3.9) has thus a dilution impact which tends to decrease n_χ because of the expansion of the Universe whereas the right-hand side represents all the collisions between particles (these collisions can lead to an increase or decrease of n_χ).

Next, in order to counter the dilatation [2] of the proper volume in which n_χ is measured, one defines the number density of particles χ per comoving volume: [53]

$$Y \equiv \frac{n_\chi}{s} \quad (3.10)$$

with $s \equiv \frac{S}{V}$ the entropy density and S the entropy.

Since the entropy per comoving volume is constant ($sa^3 =$ constant) [33], one can show that $\dot{n}_\chi + 3Hn_\chi = s\dot{Y}$. Indeed

$$s\dot{Y} = \dot{n}_\chi - n_\chi \frac{\dot{s}}{s} = \dot{n}_\chi - n_\chi \frac{(\dot{a^{-3}})}{a^{-3}} = \dot{n}_\chi + 3n_\chi a^3 a^{-4} \dot{a} = \dot{n}_\chi + 3Hn_\chi \quad (3.11)$$

Therefore, using the latter relation, the Boltzmann equation (3.9) becomes

$$s\dot{Y} = -\int d\Pi_\chi d\Pi_a d\Pi_b ... d\Pi_i d\Pi_j ... (2\pi)^4 \delta^{(4)}(p_i + p_j ... - p_\chi - p_a - p_b ...) |\overline{\mathcal{M}}|^2 [f_a f_b ... f_\chi - f_i f_j ...] \quad (3.12)$$

1. The squared complex modulus of the matrix element (or invariant amplitude) $i\mathcal{M}$ for the initial-final state transition is averaged in the following way: one sums over the spins of the particles in the final state and one averages over the spins of the particles in the initial state.

2. The increase in size of the proper volume is due to the expansion of the Universe which increases the scale factor. The proper volume V increases as the scale factor does, thereby, it is more convenient to utilize the comoving volume, which is proportionnal to $\frac{V}{a^3}$ and thus remains constant as the Universe expands.

Then one wants to find a relation between the time t and the temperature T in a radiation-dominated Universe. For that, one has to start with the energy density ϵ. In the same way as one obtained (3.6), one has

$$\epsilon_i = \frac{g_i}{(2\pi)^3} \int d^3p_i \; E_i f_i \tag{3.13}$$

the energy density of species i.

It can be shown that [33]

$$\epsilon_i = \begin{cases} \frac{\pi^2}{30} g_i T^4 & \text{for bosons} \\ \frac{7}{8}\frac{\pi^2}{30} g_i T^4 & \text{for fermions,} \end{cases}$$

$$n_i = \begin{cases} \frac{\zeta(3)}{\pi^2} g_i T^3 & \text{for bosons} \\ \frac{3}{4}\frac{\zeta(3)}{\pi^2} g_i T^3 & \text{for fermions} \end{cases}$$

and

$$p = \rho/3$$

in the relativistic limit where T is the photon temperature and where $\zeta(3) = 1.20206...$ is the Riemann zeta function [54]

$$\zeta(s) = \sum_{n=1}^{\infty} \frac{1}{n^s} \tag{3.14}$$

Thus, for a system of relativistic particles in equilibrium, if one distinguishes bosons from fermions, the energy density of the system is

$$\begin{aligned} \epsilon &= \sum_i \epsilon_i \\ &= \sum_{i=\text{bosons}} \frac{\pi^2}{30} g_i T^4 + \sum_{i=\text{fermions}} \frac{7}{8}\frac{\pi^2}{30} g_i T^4 \\ &= \frac{\pi^2}{30} g_* T^4 \end{aligned} \tag{3.15}$$

with

$$g_* \equiv \sum_{i=\text{bosons}} g_i \left(\frac{T_i}{T}\right)^4 + \frac{7}{8} \sum_{i=\text{fermions}} g_i \left(\frac{T_i}{T}\right)^4 = \sum_{i=\text{bosons}} g_i + \frac{7}{8} \sum_{i=\text{fermions}} g_i \tag{3.16}$$

the effective number of relativistic degrees of freedom [22] and where the last equality is only valid at the equilibrium.

Then one can utilize the Friedmann equation (2.4) (with $\epsilon = \rho \simeq \rho_r$ given the relativistic-particle domination) in order to compute H:

$$\left(\frac{\dot{a}}{a}\right)^2 = H^2 = \frac{8\pi G}{3}\rho = \frac{8\pi G}{3}\frac{\pi^2}{30} g_* T^4 \tag{3.17}$$

$$\Rightarrow H(T) = \left(\frac{4\pi^3}{45}\right)^{1/2} \frac{g_*^{1/2}}{m_{\rm Pl}} T^2 \simeq 1.66 \frac{g_*^{1/2}}{m_{\rm Pl}} T^2 \tag{3.18}$$

with $m_{\rm Pl} \equiv G^{-1/2}$ the Planck mass.

However during the radiation-dominated epoch, it can be shown that the energy-momentum conservation and the use of Friedmann equations yields that the time t is related to H by $t = \frac{1}{2H}$ [33]. Thus the relation connecting t and T is

$$t = \frac{1}{2}\left(\frac{45}{4\pi^3}\right)^{1/2} \frac{m_{\rm Pl}}{g_*^{1/2}} \frac{1}{T^2} \simeq 0.301 g_*^{-1/2} \frac{m_{Pl}}{T^2} = 0.301 g_*^{-1/2} \frac{m_{Pl}}{m^2} \xi^2 \tag{3.19}$$

where one introduced the dimensionless variable $\xi \equiv m/T$.

Using (3.19) one finds

$$dt = 0.602 g_*^{-1/2} \frac{m_{\rm Pl}}{m^2} \xi d\xi \tag{3.20}$$

and thus

$$\dot{Y} = \frac{dY}{dt} = \frac{1}{\xi}\frac{dY}{d\xi}\frac{1}{0.602} g_*^{1/2} \frac{m^2}{m_{\rm Pl}} \equiv \frac{1}{\xi}\frac{dY}{d\xi} H(m) \tag{3.21}$$

where

$$H(m) \equiv 1.66 g_*^{1/2} \frac{m^2}{m_{\rm Pl}} = H(T)\xi^2 \tag{3.22}$$

The latter result, combined with (3.12) yields

$$\frac{dY}{d\xi} = -\frac{\xi}{H(m)s} \int d\Pi_\chi d\Pi_a d\Pi_b ... d\Pi_i d\Pi_j ... (2\pi)^4 \delta^{(4)}(p_i + p_j ... - p_\chi - p_a - p_b ...) \times |\overline{\mathcal{M}}|^2 [f_a f_b ... f_\chi - f_i f_j ...] \tag{3.23}$$

Now one considers the annihilation process of a stable species χ into any possible species X and the reverse one, so $\chi\bar{\chi} \longleftrightarrow X\bar{X}$. Moreover, one considers that there is a symmetry between χ and $\bar{\chi}$, namely one has as many χ particles as $\bar{\chi}$ particles [33], thereby $\mu_\chi = \mu_{\bar{\chi}} = 0$ [55]. Thus the phase space density of χ and $\bar{\chi}$ at equilibrium is $f_\chi^{\rm eq} = e^{-E_\chi/T}$ and $f_{\bar{\chi}}^{\rm eq} = e^{-E_{\bar{\chi}}/T}$. The collision term in (3.9) then reduces to

$$-\int d\Pi_\chi d\Pi_{\bar{\chi}} d\Pi_X d\Pi_{\bar{X}} (2\pi)^4 \delta^{(4)}(p_\chi + p_{\bar{\chi}} - p_X - p_{\bar{X}}) |\overline{\mathcal{M}}|^2 [f_\chi f_{\bar{\chi}} - f_X f_{\bar{X}}] \tag{3.24}$$

where $f_X = e^{-(E_X - \mu_X)/T}$ and $f_{\bar{X}} = e^{-(E_{\bar{X}} - \mu_{\bar{X}})/T}$ because one assumed that X and $\bar{X}$ are in thermal equilibrium since they can have stronger interaction with other particles than χ and $\bar{\chi}$ [33].

Next, due to the delta function, one has the energy conservation $E_\chi + E_{\bar{\chi}} = E_X + E_{\bar{X}}$ and thus, if one considers $\mu \ll T$, then $\mu_X \simeq \mu_{\bar{X}} \simeq 0$. Thus one obtains

$$f_X f_{\bar{X}} = e^{-(E_X + E_{\bar{X}})/T} = e^{-(E_\chi + E_{\bar{\chi}})/T} = f_\chi^{\rm eq} f_{\bar{\chi}}^{\rm eq} \tag{3.25}$$

which implies that in (3.24), $[f_\chi f_{\bar{\chi}} - f_X f_{\bar{X}}] = [f_\chi f_{\bar{\chi}} - f_\chi^{\rm eq} f_{\bar{\chi}}^{\rm eq}]$.

In addition one has

$$\left.\begin{array}{l} \frac{n_\chi}{n_\chi^{\rm eq}} = \frac{f_\chi}{f_\chi^{\rm eq}} \\ \frac{n_{\bar\chi}}{n_{\bar\chi}^{\rm eq}} = \frac{f_{\bar\chi}}{f_{\bar\chi}^{\rm eq}} \end{array}\right\} \Rightarrow f_\chi f_{\bar\chi} = \frac{n_\chi}{n_\chi^{\rm eq}}\frac{n_{\bar\chi}}{n_{\bar\chi}^{\rm eq}} f_\chi^{\rm eq} f_{\bar\chi}^{\rm eq}$$

Therefore Eq. (3.9) and (3.23) respectively take the following form

$$\frac{dn_\chi}{dt} + 3Hn_\chi = -\langle\sigma_{\chi\bar\chi\to X\bar X} v_{\rm rel}\rangle[n_\chi^2 - (n_\chi^{\rm eq})^2] \tag{3.26}$$

$$\frac{dY}{d\xi} = \frac{-\xi\langle\sigma_{\chi\bar\chi\to X\bar X} v_{\rm rel}\rangle s}{H(m)}(Y^2 - Y_{\rm eq}^2) \tag{3.27}$$

with n_χ the present number density of χ's, $n_\chi^{\rm eq}$ the number density of χ's when they are in equilibrium, $Y \equiv n_\chi/s = n_{\bar\chi}/s$, $Y_{\rm eq} \equiv n_\chi^{\rm eq}/s = n_{\bar\chi}^{\rm eq}/s$ and where the thermally averaged annihilation cross section is defined as [33]

$$\langle\sigma_{\chi\bar\chi\to X\bar X} v_{\rm rel}\rangle \equiv (n_\chi^{\rm eq})^{-2}\int d\Pi_\chi d\Pi_{\bar\chi} d\Pi_X d\Pi_{\bar X}(2\pi)^4\delta^{(4)}(p_\chi + p_{\bar\chi} - p_X - p_{\bar X})|\overline{\mathcal{M}}|^2 e^{-E_\chi/T}e^{-E_{\bar\chi}/T} \tag{3.28}$$

with $v_{\rm rel}$ the relative velocity between the interacting particles and $\langle\ \rangle$ the thermal average.

Finally, one can note that the final state F is not automatically composed of only two particles. Therefore one can generalize by replacing the previous thermally averaged cross section in (3.26) and (3.27) with $\langle\sigma_{\chi\bar\chi\to F} v_{\rm rel}\rangle$. Then one can sum over all annihilation channels what results in $\langle\sigma_A v_{\rm rel}\rangle$ [33], the total annihilation cross section. Inserting the latter in (3.26) and (3.27), one obtains

$$\frac{dn_\chi}{dt} + 3Hn_\chi = -\langle\sigma_A v_{\rm rel}\rangle[n_\chi^2 - (n_\chi^{\rm eq})^2] \tag{3.29}$$

$$\frac{dY}{d\xi} = \frac{-\xi\langle\sigma_A v_{\rm rel}\rangle s}{H(m)}(Y^2 - Y_{\rm eq}^2) \tag{3.30}$$

which are the well-known forms of the Boltzmann equation.

3.2 Approximate abundance calculation

Let us consider cold relics which are species that decouple when they are non-relativistic. One has [33]

$$n_{\rm eq} = g\left(\frac{mT}{2\pi}\right)^{3/2} e^{-m/T} = g\left(\frac{\xi T^2}{2\pi}\right)^{3/2} e^{-\xi} \tag{3.31}$$

and since the entropy density s is dominated by that of relativistic particles, one finds [22]

$$s = \frac{2\pi^2}{45} g_{*s} T^3 \tag{3.32}$$

where

$$g_{*s} \equiv \sum_{i={\rm bosons}} g_i\left(\frac{T_i}{T}\right)^3 + \frac{7}{8}\sum_{i={\rm fermions}} g_i\left(\frac{T_i}{T}\right)^3 \tag{3.33}$$

is the effective number of degrees of freedom in the entropy [22].

Thus the value of ξ at the decoupling epoch is $\xi_f \gg 1$ and $Y_{\rm eq}$ is given by

$$Y_{\rm eq}(\xi) = \frac{n_\chi^{\rm eq}}{s} = \frac{45}{(2\pi)^{5/2}} \frac{1}{\pi} \frac{g}{g_{*s}} \xi^{3/2} e^{-\xi} \simeq 0.145 \frac{g}{g_{*s}} \xi^{3/2} e^{-\xi} \tag{3.34}$$

If one uses (3.22), knowing that $\Gamma_A \equiv n_{\rm eq} \langle \sigma_A v_{\rm rel} \rangle$, one can reformulate (3.30) in a interesting way:

$$\frac{dY}{d\xi} = -\xi \frac{\Gamma_A}{n_{\rm eq}} \frac{s}{H(T)\xi^2} Y_{\rm eq}^2 \left[\left(\frac{Y}{Y_{\rm eq}} \right)^2 - 1 \right] = -\Gamma_A \frac{1}{H(T)\xi} \frac{n_{\rm eq}}{s} \left[\left(\frac{Y}{Y_{\rm eq}} \right)^2 - 1 \right] \tag{3.35}$$

$$\Rightarrow \frac{\xi}{Y_{\rm eq}} \frac{dY}{d\xi} = -\frac{\Gamma_A}{H} \left[\left(\frac{Y}{Y_{\rm eq}} \right)^2 - 1 \right] \tag{3.36}$$

With this formulation one clearly sees that the variation of species χ depends on the previously mentioned $\frac{\Gamma}{H}$. Moreover the terms within brackets represent the deviation of Y with respect to its equilibrium value.

In the case of cold dark matter, (3.31) states that $n_{\rm eq} \sim (mT)^{3/2} e^{-m/T}$, thereby Γ diminishes because of the exponential in the Maxwell-Boltzmann distribution: $n_{\rm eq}$ is said to be Boltzmann suppressed. However a quick dimensional analysis of (3.36) yields

$$-\frac{\Delta Y}{Y} \sim \frac{\Gamma}{H} \tag{3.37}$$

As a consequence when $\Gamma \lesssim H$, one concludes that the relative variation of Y has to slow down (since $\Delta Y < 0$) until it becomes negligible when $\Gamma \ll H$.

In an non-relativistic regime, $\langle \sigma_A v_{\rm rel} \rangle$ can be approximated by an expansion in powers of v^2 [56]:

$$\begin{aligned} \langle \sigma_A v_{\rm rel} \rangle &= \langle a + b v^2 + c v^4 + \ldots \rangle \\ &= a + b \langle v^2 \rangle + c \langle v^4 \rangle + \ldots \\ &= a + 3b \frac{T}{m} + 15c \left(\frac{T}{m} \right)^2 + \ldots \\ &= a + 3b\xi^{-1} + 15c\xi^{-2} + \ldots \end{aligned} \tag{3.38}$$

where the calculation of $\langle v^2 \rangle$ and $\langle v^4 \rangle$ is given in Appendix B.

One thus has that each term of $\langle \sigma_A v_{\rm rel} \rangle$ is proportional to T^n where $n = 0$ denotes a s-wave annihilation, $n = 1$ denotes a p-wave annihilation and so on [57].

After a few steps given in [33] one finds the expression of ξ_f and Y_∞ (defined as $Y(\xi \to \infty)$, the asymptotic value of Y):

$$\xi_f = \ln \left[0.038(n+1) \frac{g}{g_*^{1/2}} m_{\rm Pl}\ m\ \sigma_0 \right] - \left(n + \frac{1}{2} \right) \ln \left\{ \ln \left[0.038(n+1) \frac{g}{g_*^{1/2}} m_{\rm Pl}\ m\ \sigma_0 \right] \right\} \tag{3.39}$$

$$Y_\infty = \frac{3.79(n+1)\xi_f^{n+1}}{(g_{*s}/g_*^{1/2})m_{\rm Pl}\ m\ \sigma_0} \tag{3.40}$$

where σ_0 is defined as $\langle\sigma_A v_{\rm rel}\rangle \equiv \sigma_0 \left(\frac{T}{m}\right)^n = \sigma_0\xi^{-n}$ (σ_0 therefore corresponds to the first term in the expansion given in (3.38) which is constant).

The numerical resolution of the Boltzmann equation yields the evolution of the abundance as a function of ξ. This result is depicted in Fig. 3.1.

Using (3.39) and (3.40), one can compute Y_∞ in the expression of the present number density $n_{\chi 0} = s_0 Y_\infty$, where the subscript 0 denotes the current epoch. Therefore it remains to compute s_0 which will be done in the following paragraphs.

Because of (3.33) and (3.32), one can compute $g_{*s,0}$ and s_0 (with the present photon temperature $T = 2.73$ K $\simeq 1694.25$ cm^{-3}):

$$\begin{aligned} g_{*s,0} &= g_\gamma + \frac{7}{8}\sum_{i=e,\mu,\tau} g_{\nu_i}\left(\frac{T_\nu}{T}\right)^3 \\ &= 2 + \frac{7}{8}\times 2\times 3\times\frac{4}{11} \\ &\simeq 3.91 \end{aligned} \tag{3.41}$$

where the subscrpit γ denotes the photon whereas that of neutrinos [3] is indicated by ν_i (with $i = e$ is for electron neutrinos, $i = \mu$ is for muon neutrinos and $i = \tau$ is for tau neutrinos). A photon has two polarization modes, thereby $g_\gamma = 2$. As for the factor 2 and 3 in the fermion part, they respectively arise from the fact that $g_{\nu_i} = 2$, since neutrinos are spin-$\frac{1}{2}$ particles, and that one has 3 flavours for the neutrinos [4]. The factor $\frac{4}{11}$, the origin of which will be explained just below, results from the conservation of sa^3, the entropy in a comoving volume in thermal equilibrium, which can be demonstrated via the two first laws of thermodynamics [33]. Thus, (3.32) implies

$$g_{*s}a^3T^3 \sim \text{ constant.} \tag{3.42}$$

while the expansion of the Universe continues.

Around $T \sim$ MeV, the neutrinos decouple from the thermal bath [22]. A short time after that, when $T \sim m_e$ (m_e is the electron mass), the photon energy is no longer sufficient to create electron-positron pairs and the equilibrium is then shifted towards photon production. Thus the annihilation process that ensues heats the photons but not the decoupled neutrinos.

3. We consider Majorana neutrinos, that is neutrinos which are their own antiparticles.

4. Actually the fermion part of (3.41) should contain $N_{\rm eff}$, which is the effective number of neutrinos, instead of the factor 3. Indeed, while the neutrinos decouple, the electrons and positrons start to annihilate despite the fact that the neutrino decoupling is still in process. Therefore a little energy and entropy due to the electron-positron annihilation are provided to the neutrinoss. Thereby one obtains $N_{\rm eff} = 3.046$ which implies $g_{*s,0} = 3.94$ [22].

Indeed one has

$$\begin{aligned} \text{for } T \gtrsim m_e: \ g_{*s} &= g_\gamma + \frac{7}{8}(g_{e^-} + g_{e^+}) \\ &= 2 + \frac{7}{8}(2+2) \\ &= \frac{11}{2} \end{aligned} \tag{3.43}$$

whereas

$$\begin{aligned} \text{for } T \ll m_e: \ g_{*s} &= g_\gamma \\ &= 2 \end{aligned} \tag{3.44}$$

Therefore, using (3.42), one obtains

$$(aT)^3_{ad} = \frac{11}{4}(aT)^3_{bd} \tag{3.45}$$

where the subscripts ad and bd respectively refer to after and before the electron annihilation.

In conclusion, at the present time one has

$$\left(\frac{T}{T_\nu}\right)^3 = \frac{11}{4} \tag{3.46}$$

since the temperature of the neutrinos has continued to decrease in the same way as the photon temperature would have if the photons were not heated because of the electron annihilation, put another way $T_\nu \simeq T_{bd}$. Therefore

$$\begin{aligned} s_0 &= \frac{2\pi^2}{45} g_{*s,0} T^3 \\ &\simeq \frac{2\pi^2}{45} 3.91 \times 1694.25 \text{ cm}^{-3} \\ &= 2905.83 \text{ cm}^{-3} \end{aligned} \tag{3.47}$$

and then

$$n_{\chi 0} = s_0 Y_\infty = 2905.83 \ Y_\infty \text{ cm}^{-3} = 1.1013 \cdot 10^4 \frac{(n+1)\xi_f^{n+1}}{(g_{*s}/g_*^{1/2}) m_{\rm Pl} m \langle \sigma_A v_{\rm rel} \rangle \xi^n} \text{ cm}^{-3} \tag{3.48}$$

The relic abundance of χ, Ω_χ ($\rho = mn$ in the non-relativistic limit) can thus be expressed as

$$\Omega_\chi h^2 = \frac{\rho_{\chi 0}}{\rho_c} h^2 = \frac{m n_{\chi 0}}{\rho_c} h^2 = 1.0467 \cdot 10^9 \frac{(n+1)\xi_f^{n+1}}{(g_{*s}/g_*^{1/2}) m_{Pl} \langle \sigma_A v_{\rm rel} \rangle \xi^n} \text{ GeV}^{-1} \tag{3.49}$$

It is interesting to note that the relic abundance is proportional to the inverse of the thermally averaged annihilation cross section, which means that the higher the interaction rate, the lower the relic abundance.

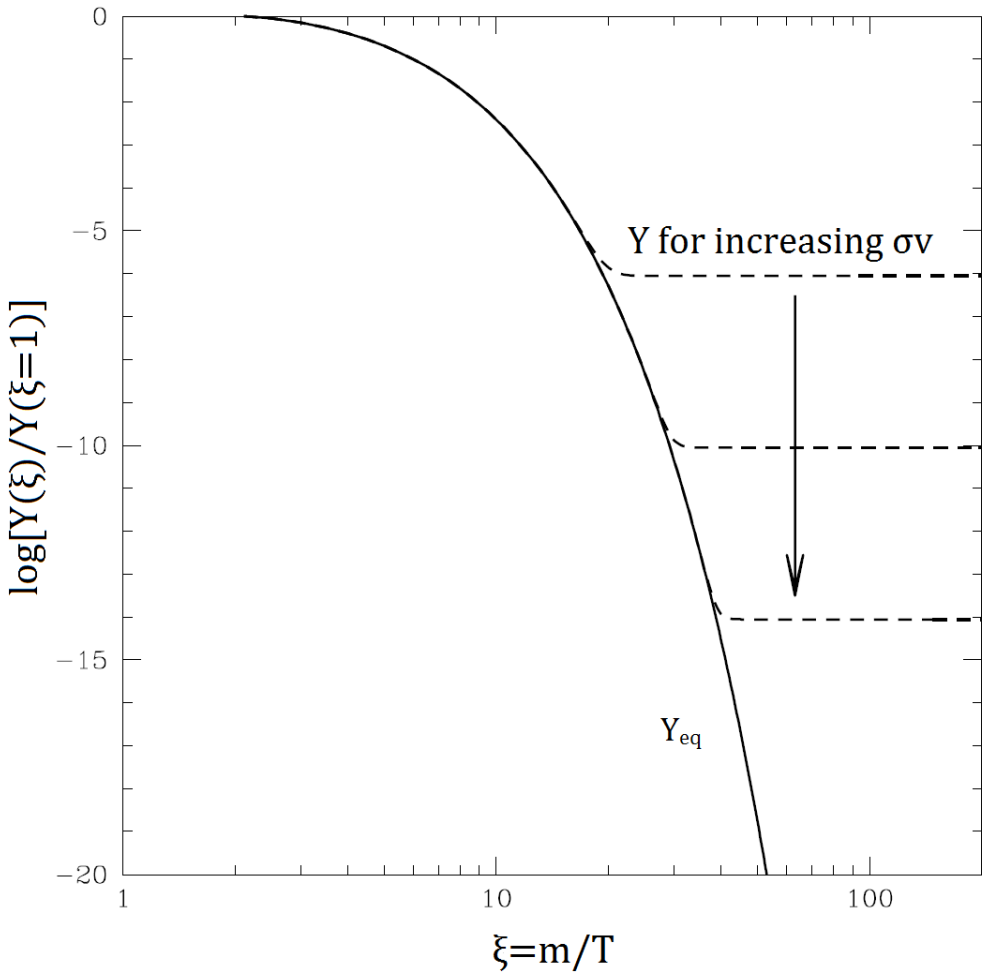

Figure 3.1 – This representation from [58] gives the evolution of Y in terms of ξ. When $\xi < 1$ (outside of the graph), the particles are relativistic and thus $n \sim T^3$ which implies $Y \sim$ constant. When $\xi > 1$, one notes that if the particles were still in equilibrium with the thermal bath (solid line) , then, as stated before, the abundance would be Boltzmann suppressed (see (3.31)) and thus the current relic abundance would be insignificant. However, in reality, Y deviates (dashed line) from Y_{eq} when $\Gamma \sim H$ (at the inflection point). Before and after this inflection point one respectively has $\Gamma \gtrsim H$ and $\Gamma \lesssim H$. Furthermore, as one can observe, the relic abundance is lower for increasing $\langle \sigma v_{\text{rel}} \rangle$. Indeed the higher $\langle \sigma v_{\text{rel}} \rangle$, the higher Γ thereby, the inflection point is shifted towards the right of the graph. Physically speaking, if the interaction rate is large, then although the Universe expands, the particles can still interact (therefore the annihilation makes the abundance decrease) until the expansion is sufficiently important.

3.2.1 Results

We tested the formula (3.49) to compute the relic abundance of WIMPs, which has to be approximately equal to $\Omega_{\rm CDM} \simeq 25.89\%$ ($\Omega_{\rm CDM}h^2 \simeq 11.88\%$). Using $n = 0$ (thus $\langle\sigma_A v_{\rm rel}\rangle$ is independent of T and then it is also the case for $\Omega_\chi h^2$), $g = 2$ (if WIMPs are fermions for instance) and

$$\langle\sigma_A v_{\rm rel}\rangle \sim 3 \cdot 10^{26}{\rm cm}^3/s \simeq 1 \text{ picobarn} = 2.5682 \cdot 10^{-9}{\rm GeV}^{-2}. \tag{3.50}$$

We obtained the following results for different values of m (see Tab. 3.1 and Tab. 3.2), with g_* and g_{*s} equal at the epoch when the dark-matter particles freeze out (see Fig. 3.2).

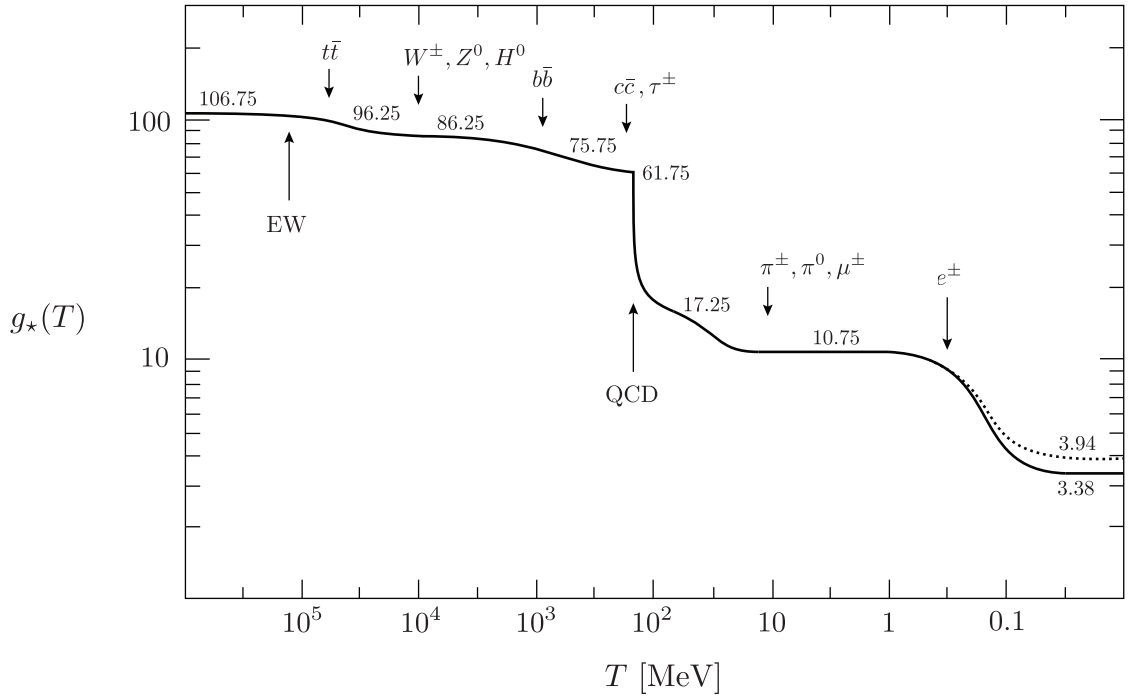

Figure 3.2 – Graph from [22] displaying the evolution of g_* et g_{*s} as a function of the temperature of the Universe. One notes that g_* and g_{*s} remain equal until the neutrino decoupling occurs.

m	ξ_f	T_f	g_*	$\Omega_\chi h^2$
100 GeV	22.38	4.47 GeV	86.25	8.05%
1 TeV	24.64	40.59 GeV	86.25	8.86%
10 TeV	26.79	373.25 GeV	106.75	8.66%
100 TeV	29.06	3441.71 GeV	106.75	9.39%

Table 3.1 – Computation of relic abundances in the case of an s-wave annihilation.

We notice that the relic abundance remains under the upper limit $\Omega_{\rm CDM}h^2$ even for the most massive particles. However, in a recent article [59], it is stated that ξ_f is comprised

m	ξ_f	T_f	g_*	$\Omega_\chi h^2$
100 GeV	52.31	1.91 GeV	75.75	$4.94{\cdot}10^{-12}\%$
1 TeV	56.74	17.63 GeV	86.25	$5.45{\cdot}10^{-13}\%$
10 TeV	67.50	163.45 GeV	96.25	$6.00{\cdot}10^{-14}\%$
100 TeV	65.64	1523.54 GeV	106.75	$6.55{\cdot}10^{-15}\%$

Table 3.2 – Computation of relic abundances in the case of a p-wave annihilation.

between 30 and 40 which suggests that the expression of ξ_f in (3.39) is not adequate in the sense that it may be too approximative. Following these considerations, we obtained the right abundance for the following values of the parameters in a s-wave annihilation case (see Tab. 3.3). As for the p-wave annihilation case, the values of $\Omega_\chi h^2$ remains still negligible with the new range of ξ_f (see Tab. 3.4).

m	ξ_f	T_f	g_*	$\Omega_\chi h^2$
100 GeV	30.95	3.23 GeV	75.75	11.88%
1 TeV	33.03	30.28 GeV	86.25	11.88%
10 TeV	36.74	272.17 GeV	106.75	11.88%
100 TeV	36.74	2721.65 GeV	106.75	11.88%

Table 3.3 – Values of the different parameters in the case of an s-wave annihilation.

m	ξ_f	T_f	g_*	$\Omega_\chi h^2$
100 GeV	40	2.5 GeV	75.75	$2.89{\cdot}10^{-12}\%$
1 TeV	40	25 GeV	86.25	$2.71{\cdot}10^{-13}\%$
10 TeV	40	250 GeV	106.75	$2.43{\cdot}10^{-14}\%$
100 TeV	40	2500 GeV	106.75	$2.43{\cdot}10^{-15}\%$

Table 3.4 – Values of the different parameters yielding the abundance that is the closest to 11.88% in the case of an p-wave annihilation.

We can remark in Tab. 3.3 that we obtained the same ξ_f for both $m = 10$ TeV and $m = 100$ TeV. This is because these two cases display the same value for g_* thus since it is the only parameter which can induce a change in the value of $\Omega\chi h^2$ at fixed $\langle\sigma_A v_{\rm rel}\rangle$, thereby, starting from the moment when g_* does not vary anymore, this also holds true for ξ_f. Therefore, even a mass such that $m > 100$ TeV yields the right relic abundance.

In conclusion the WIMP miracle already introduced in Section 2.3, is not so miraculous since although we find the right abundance for a typical weak scale mass (100 GeV - 1000 GeV), we obtain the same result for particle even heavier.

3.3 Beyond leading order

In the previous section one established the formula for the relic abundance of particles. However the formalism one developed does not allow to compute the thermally averaged annihilation cross section. Thus Eq. (3.49) can be used only for processes the thermally averaged annihilation cross section of which is already known. Therefore, it would be interesting to derive an exact expression for $\langle \sigma v_{\rm rel} \rangle$, which is the purpose of this section.

One starts with the following well-known result of the quantum field theory [60]:

$$\sigma v_{\rm rel} = \frac{1}{4E_1E_2} \int \left(\prod_f \frac{d^3p_f}{(2\pi)^3 2E_f} \right) |\overline{\mathcal{M}}(k_1k_2 \to \{p_f\})|^2 (2\pi)^4 \delta^{(4)}(k_1 + k_2 - \sum_f p_f) \quad (3.51)$$

where 1, 2 and f respectively denote the first incident particle, the second incident particle and the final particles. Moreover, for the average of the matrix element $\mathcal{M}$, one averages $|\mathcal{M}|^2$ over the initial spins and sums over the final spins.

One can also write (3.51) as

$$\sigma v_{\rm rel} = \frac{1}{4E_1E_2} \int dLIPS \ |\overline{\mathcal{M}}|^2 \quad (3.52)$$

where $dLIPS$ (for Lorentz Invariant Phase Space) is written as

$$dLIPS = (2\pi)^4 \delta^{(4)}(k_1 + k_2 - \sum_f p_f) \prod_f \frac{d^3p_f}{(2\pi)^3 2E_f} \quad (3.53)$$

Since $\int dLIPS \ |\overline{\mathcal{M}}|^2$ is Lorentz-invariant, one can express it by means of Lorentz invariant variables, the Mandelstam variables (see Appendix C). Next, similarly to (3.28), one can define $\langle \sigma v_{\rm rel} \rangle$ as

$$\langle \sigma v_{\rm rel} \rangle \equiv \frac{g^2}{(2\pi)^6 n_0^2} \int d^3k_1 d^3k_2 \ f(E_1) f(E_2) \frac{1}{E_1E_2} w(s) \quad (3.54)$$

with $n_0 = \frac{g}{(2\pi)^3} \int d^3p \ f(E)$ the particle density at the equilibrium and $w(s)$ defined as

$$w(s) \equiv \frac{1}{4} \int dLIPS \ |\overline{\mathcal{M}}|^2 = E_1E_2 \sigma v_{\rm rel} \quad (3.55)$$

where

$$s = (k_1 + k_2)^2 = (k_1^2 + k_2^2 + 2k_1 \cdot k_2) = 2(M^2 + E_1E_2 - |\vec{k_1}||\vec{k_2}| \cos\theta) \quad (3.56)$$

is a Mandelstam variable and M and θ are respectively the mass of the initial particles and the angle between the 3-momenta of the incoming particles in the lab frame.

Contrary to the previous section, one defines $x \equiv \frac{T}{m} \equiv \xi^{-1}$. However one still neglects the Pauli blocking and the Bose enhancement, which means that $f(E) = e^{-E/T}$ comes down to the Maxwell-Boltzmann distribution.

For a $2 \to 2$ process, (3.54) becomes

$$\langle \sigma v_{\rm rel} \rangle = \frac{g^2}{(2\pi)^6 n_0^2} \int d^3k_1 d^3k_2 \; e^{-E_1/T} e^{-E_2/T} \frac{1}{E_1 E_2} w(s) \tag{3.57}$$

Thus in spherical coordinates, one has

$$\begin{aligned}\langle \sigma v_{\rm rel} \rangle &= \frac{g^2}{(2\pi)^6 n_0^2} \int_0^\infty d|\vec{k_1}| d|\vec{k_2}| \frac{|\vec{k_1}|^2 |\vec{k_2}|^2}{E_1 E_2} e^{-E_1/T} e^{-E_2/T} (2\pi)^2 \underbrace{\int_0^\pi d\Theta \; \sin\Theta}_{=2} \int_0^\pi d\theta \; \sin\theta \; w(s) \\ &= \frac{g^2}{8\pi^4 n_0^2} \int_0^\infty d|\vec{k_1}| d|\vec{k_2}| \frac{|\vec{k_1}|^2 |\vec{k_2}|^2}{E_1 E_2} e^{-E_1/T} e^{-E_2/T} \int_{-1}^1 d\cos\theta \; w(s) \end{aligned} \tag{3.58}$$

Then, given $|\vec{k}| = \sqrt{E^2 - k^2} = \sqrt{E^2 - M^2}$, one obtains $|\vec{k}| d|\vec{k}| = E dE$ and thus

$$\langle \sigma v_{\rm rel} \rangle = \frac{g^2}{8\pi^4 n_0^2} \int_M^\infty dE_1 dE_2 |\vec{k_1}| |\vec{k_2}| e^{-E_1/T} e^{-E_2/T} \int_{-1}^1 d\cos\theta \; w(s) \tag{3.59}$$

Next, for E_a and $|\vec{k_a}|$, with $a = 1, 2$, one can make a change of variables of the form [61]

$$E_a = M(1 + x y_a) \Rightarrow dE_a = M x dy_a \tag{3.60}$$

$$|\vec{k_a}| = M(2x)^{1/2}(y_a + \frac{1}{2}x y_a^2)^{1/2} \Rightarrow d|\vec{k_a}| = \frac{1}{2} M (2x)^{1/2} (1 + x y_a)(y_a + \frac{1}{2} x y_a)^{-1/2} \tag{3.61}$$

Finally $\langle \sigma v_{\rm rel} \rangle$ can be written as

$$\langle \sigma v_{\rm rel} \rangle = \frac{g^2 M^4 x^3 e^{-2/x}}{4\pi^4 n_0^2} \int_0^\infty dy_1 dy_2 \; (y_1 + \frac{1}{2} x y_1^2)^{1/2} (y_2 + \frac{1}{2} x y_2^2)^{1/2} e^{-y_1} e^{-y_2} \int_{-1}^1 d\cos\theta \; w(s) \tag{3.62}$$

where

$$\begin{aligned} n_0 &= \frac{g}{(2\pi)^3} \int d^3k \; e^{-E/T} \\ &= \frac{g}{(2\pi)^3} 4\pi \int_0^\infty d|\vec{k}| \; |\vec{k}|^2 \; e^{-E/T} \\ &= g(2\pi)^{-2} M^3 (2x)^{3/2} \int_0^\infty dy \; (1 + xy)(y + \frac{1}{2} x y^2)^{1/2} e^{-\frac{M}{T} - y} \\ &= g(2\pi)^{-2} (2x)^{3/2} x^{-3} T^3 e^{-1/x} \int_0^\infty dy \; (1 + xy)(y + \frac{1}{2} x y^2)^{1/2} e^{-y} \\ &= \left[g(2\pi x)^{-3/2} T^3 e^{-1/x} \right] 2\pi^{-1/2} \int_0^\infty dy \; (1 + xy)(y + \frac{1}{2} x y^2)^{1/2} e^{-y} \end{aligned} \tag{3.63}$$

Thus, injecting the latter result in (3.62), we obtain

$$\langle \sigma v_{\rm rel} \rangle = \frac{1}{2M^2} \frac{\int_0^\infty dy_1 dy_2 \; (y_1 + \frac{1}{2} x y_1^2)^{1/2} (y_2 + \frac{1}{2} x y_2^2)^{1/2} e^{-y_1} e^{-y_2} \int_{-1}^1 d\cos\theta \; w(s)}{\left[\int_0^\infty dy \; (1 + xy)(y + \frac{1}{2} x y^2)^{1/2} e^{-y} \right]^2} \tag{3.64}$$

Starting from now, in compliance with [61], we will make some approximations through a Taylor expansion of the same type as (3.38) in order to calculate $\langle \sigma v_{\text{rel}} \rangle$ analytically. Then, after all these calculations, we will compute $\langle \sigma v_{\text{rel}} \rangle$ numerically in the next chapter and will compare both results with the aim of verifying how precise are the approximations made in this article.

Since x is small ($x \leq \frac{1}{20}$ [61]), the Taylor approximation of n_0 around $x = 0$ yields (see Appendix A)

$$\frac{1}{n_0^2} = \frac{8\pi^3 e^{2/x}}{g^2 x^3 M^6} \left[1 - \frac{15}{4}x + \frac{285}{32}x^2 - \frac{2115}{128}x^3 + \mathcal{O}(x^4)\right] \tag{3.65}$$

We can therefore inject this result in (3.62) and we obtain

$$\begin{aligned}\langle \sigma v_{\text{rel}} \rangle =& \frac{2}{\pi M^2} \left[1 - \frac{15}{4}x + \frac{285}{32}x^2 - \frac{2115}{128}x^3 + \mathcal{O}(x^4)\right] \\ &\times \int_0^\infty dy_1 dy_2 \ (y_1 + \frac{1}{2}xy_1^2)^{1/2}(y_2 + \frac{1}{2}xy_2^2)^{1/2} e^{-y_1} e^{-y_2} \int_{-1}^{1} d\cos\theta \ w(s)\end{aligned} \tag{3.66}$$

The Mandelstam variable s, defined above in (3.56), can be written, using (3.60) and (3.61), as

$$\begin{aligned}s &= 2\left(M^2 + M^2(1 + xy_1)(1 + xy_2) - 2M^2 x(y_1 + \frac{1}{2}xy_1^2)^{1/2}(y_2 + \frac{1}{2}xy_2^2)^{1/2}\cos\theta\right) \\ &= 2\left(2M^2 + M^2 x(y_1 + y_2) + M^2 x^2 y_1 y_2 - 2M^2 x(y_1 + \frac{1}{2}xy_1^2)^{1/2}(y_2 + \frac{1}{2}xy_2^2)^{1/2}\cos\theta\right)\end{aligned} \tag{3.67}$$

$$\Rightarrow \frac{s}{4M^2} = 1 + \frac{1}{2}x(y_1 + y_2) + \frac{1}{2}x^2 y_1 y_2 - x(y_1 + \frac{1}{2}xy_1^2)^{1/2}(y_2 + \frac{1}{2}xy_2^2)^{1/2}\cos\theta \tag{3.68}$$

When $x = 0$, $\frac{s}{4M^2} = 1$. Therefore, we can make a Taylor expansion of $w(s)$ around $\frac{s}{4M^2} = 1$ and we obtain (see Appendix A)

$$\begin{aligned}\langle \sigma v_{\text{rel}} \rangle = \frac{2}{\pi M^2}&\left[1 - \frac{15}{4}x + \frac{285}{32}x^2 - \frac{2115}{128}x^3\right] \int_0^\infty dy_1 dy_2 \ (y_1 + \frac{1}{2}xy_1^2)^{1/2}(y_2 + \frac{1}{2}xy_2^2)^{1/2} \\ &\times e^{-y_1} e^{-y_2} \Bigg[2w(s) + w'(s)\left(x(y_1 + y_2) + x^2 y_1 y_2\right) + \frac{w''(s)}{2}\Bigg(\frac{x^2}{2}(y_1 + y_2)^2 \\ &+ \frac{2}{3}x^2(y_1 + \frac{1}{2}xy_1^2)(y_2 + \frac{1}{2}xy_2^2) + x^3(y_1 + y_2)y_1 y_2\Bigg) + \frac{w'''(s)}{6}\Bigg(\frac{x^3}{4}(y_1 + y_2)^3 \\ &+ x^3(y_1 + y_2)(y_1 + \frac{1}{2}xy_1^2)(y_2 + \frac{1}{2}xy_2^2)\Bigg) + \mathcal{O}(x^4)\Bigg]_{\frac{s}{4M^2}=1}\end{aligned} \tag{3.69}$$

where the prime denotes the derivative with respect to $\frac{s}{4M^2}$.

Then we compute the integrals of the latter equation and after a long computation (see Appendix A), we obtain

$$\langle \sigma v_{\text{rel}} \rangle = \frac{1}{M^2}\Big[w(s) - \frac{3}{2}\left(2w(s) - w'(s)\right)x + \frac{3}{8}\left(16w(s) - 8w'(s) + 5w''(s)\right) - \frac{5}{16}(30w(s) - 15w'(s) + 3w''(s) - 7w'''(s)) + \mathcal{O}(x^4)\Big]_{\frac{s}{4M^2}=1} \tag{3.70}$$

Then one can show that $w(s)$ can be expressed as [61]

$$w(s) = \sum_f \left(1 - \frac{4m_f^2}{s}\right)^{1/2} \left[C_{0f} + C_{1f}\frac{s}{4M^2} + C_{2f}\left(\frac{s}{4M^2}\right)^2\right] \tag{3.71}$$

where m_f denotes the mass of the final particles, the sum over f is a sum over the permitted types of final particle-antiparticle pairs and C_{0f}, C_{1f} and C_{2f} are constants which have to be calculated for each annihilation process. The factor next to the sum of C_f is a threshold factor since it implies that s has to be at least equal to twice the final mass so that the process occurs.

We can then derive the final expression for $\langle \sigma v_{\text{rel}} \rangle$ by injecting (3.71) in (3.70) and we obtain (see Appendix A)

$$\langle \sigma v_{\text{rel}} \rangle = \sum_f \frac{1}{M^2}\left(1 - \frac{m_f^2}{M^2}\right)^{1/2}\left[a_f + b_f x + c_f x^2 + d_f x^3 + \mathcal{O}(x^4)\right] \tag{3.72}$$

where

$$a_f = C_{0f} + C_{1f} + C_{2f} \tag{3.73}$$

$$b_f = -\frac{3}{2}\left(2C_{0f} + C_{1f}\right) + \frac{3}{4}\beta_f\left(C_{0f} + C_{1f} + C_{2f}\right) \tag{3.74}$$

$$c_f = \frac{3}{4}\left(8C_{0f} + 4C_{1f} + 5C_{2f}\right) - \frac{3}{8}\beta_f\left(9C_{0f} + 4C_{1f} - C_{2f}\right) - \frac{15}{32}\beta_f^2\left(C_{0f} + C_{1f} + C_{2f}\right) \tag{3.75}$$

$$d_f = -\frac{15}{16}\left(10C_{0f} + 5C_{1f} + 2C_{2f}\right) + \frac{15}{32}\beta_f\left(21C_{0f} + 5C_{1f} + 3C_{2f}\right) + \frac{15}{64}\beta_f^2\left(15C_{0f} + 8C_{1f} + C_{2f}\right) + \frac{105}{128}\beta_f^3\left(C_{0f} + C_{1f} + C_{2f}\right) \tag{3.76}$$

with $\beta_f \equiv \frac{m_f^2}{M^2 - m_f^2}$.

In the next chapter, we will apply what we have derived in the present chapter, namely the equation allowing to compute the relic abundance for a specific species, the approximate expression of the thermally averaged annihilation cross section (3.72) as well as its exact formulation (see Eq. 3.64). The two latter equations (we will utilize the exact formulation

of the thermally averaged annihilation cross section in numerical treatments) will be used in order to compute the thermally averaged annihilation cross section for one specific process.

Chapter 4

Toy model

In this chapter, we will consider the annihilation process of subdominant dark-matter particles (see PIDM model in the end of Section 2.5) into standard-model particles. The aim will be to determine the different parameters involved in the calculation of the abundance of this subdominant dark matter so that the latter abundance remains comprised between 5% and 15% of Ω_{CDM} as stated in Section 2.5.

If we want to calculate $\langle \sigma v_{\text{rel}} \rangle$ with (3.72), we have to know the coefficients C_{0f}, C_{1f} and C_{2f}. These can be obtained by computing $w(s)$, which is different for each annihilation process, and then by comparing the resulting $w(s)$ with (3.71).

Given (3.55) for a $2 \to 2$ process, we have

$$\begin{aligned} w(s) &= \frac{1}{4} \int \frac{d^3p_1}{(2\pi)^3 2E_1} \int \frac{d^3p_2}{(2\pi)^3 2E_2} (2\pi)^4 \delta^{(4)}(k_1 + k_2 - p_1 - p_2) |\overline{\mathcal{M}}|^2 \\ &= \frac{1}{4} \int \frac{d^3p_1}{(2\pi)^3 2E_1} \int \frac{d^4p_2}{(2\pi)^3} \delta^{(1)}(E_2^2 - |\vec{p_2}|^2 - m_f^2)(2\pi)^4 \delta^{(4)}(k_1 + k_2 - p_1 - p_2) |\overline{\mathcal{M}}|^2 \\ &= \frac{1}{4} \int \frac{d^3p_1}{(2\pi)^3 2E_1} \int d^4p_2 \; \delta^{(1)}(p_2^2 - m_f^2) 2\pi \delta^{(4)}(k_1 + k_2 - p_1 - p_2) |\overline{\mathcal{M}}|^2 \end{aligned} \tag{4.1}$$

with f the same subscript as that in 3.71 and where, in order to obtain the second equality, we used the following property of the Dirac delta function:

$$\int_{-\infty}^{+\infty} dx \; f(x) \delta(g(x)) = \sum_i \frac{f(x_i)}{|\frac{dg}{dx}(x_i)|} \tag{4.2}$$

Then, if we express (4.1) in spherical coordinates, we obtain

$$w(s) = \frac{1}{4} \int_0^\infty \frac{d|\vec{p_1}|}{(2\pi)^2} \frac{|\vec{p_1}|^2}{2E_1} \int d\Omega \; \delta^{(1)} \left((k_1 + k_2 - p_1)^2 - m_f^2 \right) |\overline{\mathcal{M}}|^2 \tag{4.3}$$

Let us compute the expression within the delta function. If we work in the center-of-mass frame we have

$$k_1 = (E_k, 0, 0, |\vec{k}|) \tag{4.4}$$
$$k_2 = (E_k, 0, 0, -|\vec{k}|) \tag{4.5}$$
$$p_1 = (E_p, |\vec{p}| \sin\theta' \sin\phi', |\vec{p}| \sin\theta' \cos\phi', |\vec{p}| \cos\theta') \tag{4.6}$$
$$p_2 = (E_p, -|\vec{p}| \sin\theta' \sin\phi', -|\vec{p}| \sin\theta' \cos\phi', -|\vec{p}| \cos\theta') \tag{4.7}$$

where E_k, E_p, θ' and ϕ' are the rest energy of the initial particles, the rest energy of the final particles ($E_1 = E_2 = E_p$), the angle between the final momenta and the longitude respectively.

Thus the delta function becomes

$$\begin{aligned}
&\delta^{(1)}\left((2E_k - E_p, -|\vec{p}| \sin\theta' \sin\phi', -|\vec{p}| \sin\theta' \cos\phi', -|\vec{p}| \cos\theta')^2 - m_f^2\right) \\
&= \delta^{(1)}\left((2E_k - E_p)^2 - |\vec{p}|^2 - m_f^2\right) \\
&= \delta^{(1)}\left(\left(\sqrt{s} - \sqrt{|\vec{p}|^2 + m_f^2}\right)^2 - |\vec{p}|^2 - m_f^2\right) \\
&= \delta^{(1)}\left(s + |\vec{p}|^2 + m_f^2 - 2\sqrt{s}\sqrt{|\vec{p}|^2 + m_f^2} - |\vec{p}|^2 - m_f^2\right) \\
&= \delta^{(1)}\left(s - 2\sqrt{s}\sqrt{|\vec{p}|^2 + m_f^2}\right) \\
&= \frac{1}{2\sqrt{s}}\delta^{(1)}\left(\frac{\sqrt{s}}{2} - \sqrt{|\vec{p}|^2 + m_f^2}\right)
\end{aligned}$$

with $s = (E_k + E_k)^2$ the Mandelstam variable in the center-of-mass frame.

Therefore, using $|\vec{p}|d|\vec{p}| = E_p dE_p$, we can write (4.3) as

$$\begin{aligned}
w(s) &= \frac{1}{4}\int_0^\infty \frac{dE_p}{2(2\pi)^2}|\vec{p}| \int d\Omega \frac{1}{2\sqrt{s}}\delta^{(1)}\left(\frac{\sqrt{s}}{2} - \sqrt{|\vec{p}|^2 + m_f^2}\right)|\overline{\mathcal{M}}|^2 \\
&= \int \frac{d\Omega}{64\pi^2}\frac{1}{\sqrt{s}}\left(\frac{s}{4} - m_f^2\right)^{1/2}|\overline{\mathcal{M}}|^2 \\
&= \int_0^{2\pi} d\phi' \int_0^\pi d\theta' \ \sin\theta' \frac{1}{128\pi^2}\left(1 - \frac{4m_f^2}{s}\right)^{1/2}|\overline{\mathcal{M}}|^2 \\
&= \int_{-1}^1 d\cos\theta' \frac{1}{64\pi}\left(1 - \frac{4m_f^2}{s}\right)^{1/2}|\overline{\mathcal{M}}|^2
\end{aligned} \tag{4.8}$$

Now, in order to derive the expression of $w(s)$, we need to determine $|\overline{\mathcal{M}}|^2$ which will be computed in the following section.

4.1 Photon kinetic mixing

Let us consider the annihilation of fermionic dark matter, χ_f and $\bar{\chi}_f$ into standard-model fermions f and $\bar{f}$ via a dark photon γ' kinetically mixed with the photon γ. This process is depicted in Fig. 4.1.

The Lagrangian density for this model is [60, 62]

$$\begin{aligned}\mathcal{L} &= \mathcal{L}_{\mathrm{SM}} + \mathcal{L}_{\mathrm{DM}} + \mathcal{L}_{\mathrm{mix}} \\ &= i\bar{\psi}\gamma^{\mu}\partial_{\mu}\psi - m_f\bar{\psi}\psi - \frac{1}{4}F_{\mu\nu}F^{\mu\nu} - e\bar{\psi}\gamma^{\mu}A_{\mu}\psi \\ &\quad + i\bar{\psi}'\gamma^{\mu}\partial_{\mu}\psi' - M\bar{\psi}'\psi' - \frac{1}{4}G_{\mu\nu}G^{\mu\nu} - g_D\bar{\psi}'\gamma^{\mu}B_{\mu}\psi' \\ &\quad + \frac{1}{2}\epsilon F_{\mu\nu}G^{\mu\nu} - \frac{1}{2}\Lambda^2 B^{\mu}B_{\mu} \end{aligned} \tag{4.9}$$

where $\mathcal{L}_{\mathrm{SM}}$, $\mathcal{L}_{\mathrm{DM}}$ and $\mathcal{L}_{\mathrm{mix}}$ are respectively the Lagrangian density of the visible sector, the Lagrangian density of the dark sector and the kinetically mixed term between the massless (or nearly) $U(1)_{\mathrm{D}}$ and the $U(1)_{\mathrm{elm}}$ gauge bosons, the former being a *dark* photon γ' and the latter being the *standard* photon γ. The mass Λ of this dark photon can be introduced in a gauge-invariant way via the Higgs mechanism. The fermionic fields for standard-model and dark-matter particles are respectively described by ψ and $\bar{\psi} = \psi^{\dagger}\gamma^0$ with the gamma matrices γ^{μ} defined in Appendix C and ψ' and $\bar{\psi}'$. The tensor fields $F_{\mu\nu}$ and $G_{\mu\nu}$ are respectively defined as $F_{\mu\nu} = \partial_{\mu}A_{\nu} - \partial_{\nu}A_{\mu}$ and $G_{\mu\nu} = \partial_{\mu}B_{\nu} - \partial_{\nu}B_{\mu}$ with A_{μ} the gauge field of the photon γ and B_{μ} the gauge field of the dark photon γ'. The mass of the standard-model particles is m_f and that of dark-matter particles is M. As for e, g_D and ϵ, they respectively denote the charge of the electromagnetic coupling in the visible sector, the charge of the electromagnetic coupling in the dark sector (that is a *dark* charge) and a dimensionless kinetic mixing parameter. For the calculations, we consider the effective coupling $g' = \epsilon g_D$.

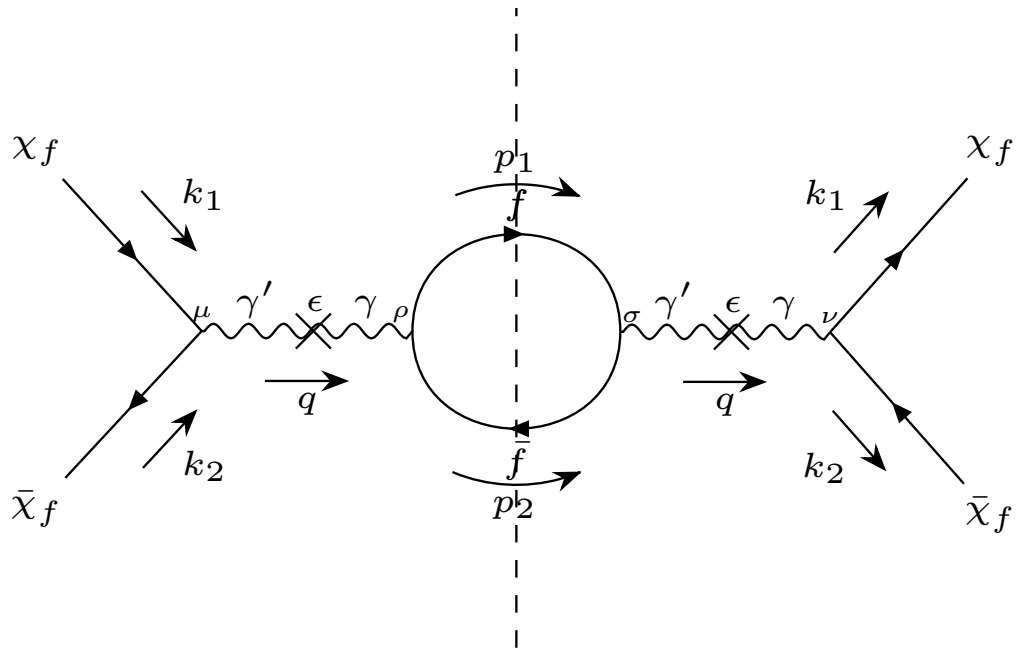

Figure 4.1 – Feynman diagram for $\chi_f\bar{\chi}_f \to \gamma' \to \gamma \to f\bar{f}$.

The $|\overline{\mathcal{M}}|_f^2$ given by the Feynman diagram in Fig. 4.1 is

$$\begin{aligned}
|\overline{\mathcal{M}}|_f^2 &= \left(\frac{1}{2}\right)^2 |-ig'|^2 |-iQ_f e|^2 \frac{-ig_{\mu\rho}}{q^2-\Lambda^2}\frac{-i^* g_{\sigma\nu}}{q^2-\Lambda^2} \times \mathrm{Tr}\left[(k_1\cdot\gamma + M)\cdot\gamma^\nu(-k_2\cdot\gamma+M)\cdot\gamma^\mu\right] \\
&\qquad \times \mathrm{Tr}\left[(p_1\cdot\gamma + m_f)\cdot\gamma^\rho(-p_2\cdot\gamma+m_f)\cdot\gamma^\sigma\right] \\
&= \frac{Q_f^2 e^2 g'^2}{4(q^2-\Lambda^2)^2} \times 4\left(-k_1^\nu k_2^\mu - k_1^\mu k_2^\nu + k_1\cdot k_2\ g^{\mu\nu} + M^2 g^{\mu\nu}\right) \\
&\qquad \times 4\left(-p_{1\mu}p_{2\nu} - p_{1\nu}p_{2\mu} + p_1\cdot p_2\ g_{\mu\nu} + m_f^2 g_{\mu\nu}\right) \\
&= \frac{4Q_f^2 e^2 g'^2}{(q^2-\Lambda^2)^2}\big(k_1\cdot p_2\ k_2\cdot p_1 + k_1\cdot p_1\ k_2\cdot p_2 - k_1\cdot k_2\ p_1\cdot p_2 - k_1\cdot k_2\ m_f^2 \\
&\qquad + k_1\cdot p_1\ k_2\cdot p_2 + k_1\cdot p_2\ k_2\cdot p_1 - k_1\cdot k_2\ p_1\cdot p_2 - k_1\cdot k_2\ m_f^2 \\
&\qquad - k_1\cdot k_2\ p_1\cdot p_2 - k_1\cdot k_2\ p_1\cdot p_2 + 4\ k_1\cdot k_2\ p_1\cdot p_2 + 4\ k_1\cdot k_2\ m_f^2 \\
&\qquad - p_1\cdot p_2\ M^2 - p_1\cdot p_2\ M^2 + 4\ p_1\cdot p_2\ M^2 + 4M^2 m_f^2\big) \\
&= \frac{4Q_f^2 e^2 g'^2}{(q^2-\Lambda^2)^2}\big(2\ k_1\cdot p_2\ k_2\cdot p_1 + 2\ k_1\cdot p_1\ k_2\cdot p_2 + 2\ k_1\cdot k_2\ m_f^2 + 2\ p_1\cdot p_2\ M^2 \\
&\qquad + 4M^2 m_f^2\big) \quad (4.10)
\end{aligned}$$

where q is the propagator momentum and e and g' are respectively defined as $\alpha = \frac{e^2}{4\pi}$ and $\alpha' = \frac{g'^2}{4\pi}$ with α and α' the coupling constants. The charge of a particle is defined as $Q_f e$, thereby $Q_f = -1$ for the electron, $Q_f = \frac{2}{3}$ for the up-quark, $Q_f = -\frac{1}{3}$ for the down-quark, and so on. The charge g' refers to the $\bar{\chi}_f\chi_f\gamma'$-vertex whereas e refers to the $\bar{f}f\gamma$-vertex.

Expressing the latter equation through Mandelstam variables $s = (k_1+k_2)^2$ $= (p_1+p_2)^2$, $t = (k_1-p_1)^2 = (k_2-p_2)^2$ and $u = (k_1-p_2)^2 = (k_2-p_1)^2$, we obtain

$$\begin{aligned}
s &= k_1^2 + k_2^2 + 2\ k_1\cdot k_2 = M^2 + M^2 + 2\ k_1\cdot k_2 && (4.11)\\
&= p_1^2 + p_2^2 + 2\ p_1\cdot p_2 = m_f^2 + m_f^2 + 2\ p_1\cdot p_2 && (4.12)
\end{aligned}$$

$$\begin{aligned}
t &= k_1^2 + p_1^2 - 2\ k_1\cdot p_1 = M^2 + m_f^2 - 2\ k_1\cdot p_1 && (4.13)\\
&= k_2^2 + p_2^2 - 2\ k_2\cdot p_2 = M^2 + m_f^2 - 2\ k_2\cdot p_2 && (4.14)
\end{aligned}$$

$$\begin{aligned}
u &= k_1^2 + p_2^2 - 2\ k_1\cdot p_2 = M^2 + m_f^2 - 2\ k_1\cdot p_2 && (4.15)\\
&= k_2^2 + p_1^2 - 2\ k_2\cdot p_1 = M^2 + m_f^2 - 2\ k_2\cdot p_1 && (4.16)
\end{aligned}$$

and then

$$\begin{aligned}
|\overline{\mathcal{M}}|_f^2 = \frac{4Q_f^2 e^2 g'^2}{(s-\Lambda^2)^2}\Bigg(&2\frac{-1}{2}\Big(u - M^2 - m_f^2\Big)\frac{-1}{2}\Big(u - M^2 - m_f^2\Big) \\
&+ 2\frac{-1}{2}\Big(t - M^2 - m_f^2\Big)\frac{-1}{2}\Big(t - M^2 - m_f^2\Big) \\
&+ 2\frac{1}{2}\Big(s - 2M^2\Big)m_f^2 + 2\frac{1}{2}\Big(s - 2m_f^2\Big)M^2 + 4M^2 m_f^2\Bigg) \qquad (4.17)
\end{aligned}$$

Next, we use $s+t+u = 2m_f^2+2M^2$ (see Appendix C) in order to eliminate s and we find

$$\begin{aligned}|\overline{\mathcal{M}}|_f^2 = \frac{4Q_f^2e^2g'^2}{(s-\Lambda^2)^2}\Bigg[&\frac{1}{2}\Big(u^2+M^4+m_f^4-2uM^2-2um_f^2+2M^2m_f^2\Big)\\ &+\frac{1}{2}\Big(t^2+M^4+m_f^4-2tM^2-2tm_f^2+2M^2m_f^2\Big)\\ &+\Big(-um_f^2-tm_f^2+2m_f^4-uM^2-tM^2+2M^4+4M^2m_f^2\Big)\Bigg]\\ = \frac{4Q_f^2e^2g'^2}{(s-\Lambda^2)^2}&\left(\frac{u^2+t^2}{2}-2(u+t)(M^2+m_f^2)+3(M^4+m_f^4)+6M^2m_f^2\right)\end{aligned} \tag{4.18}$$

Before injecting the latter expression in (4.8), let us calculate $\frac{u^2+t^2}{2}$ and $(u+t)$. Given (4.4)-(4.7) we obtain, in the center-of-mass frame of reference,

$$\begin{aligned}&s=(k_1+k_2)^2=2M^2+2\ k_1\cdot k_2=2M^2+2\Big(E_k^2+|\vec{k}|^2\Big)=2M^2+\frac{s}{2}+2|\vec{k}|^2\\ &\Rightarrow|\vec{k}|=\frac{1}{2}(s-4M^2)^{1/2}\end{aligned} \tag{4.19}$$

and

$$\begin{aligned}&s=(p_1+p_2)^2=2m_f^2+2\ p_1\cdot p_2=2m_f^2+2\Big(E_p^2+|\vec{p}|^2\Big)=2m_f^2+\frac{s}{2}+2|\vec{p}|^2\\ &\Rightarrow|\vec{p}|=\frac{1}{2}(s-4m_f^2)^{1/2}\end{aligned} \tag{4.20}$$

Thus

$$\begin{aligned}t&=(k_1-p_1)^2\\ &=k_1^2+p_1^2-2\ k_1\cdot p_1\\ &=M^2+m_f^2-2(E_kE_p-|\vec{k}||\vec{p}|\cos\theta')\\ &=M^2+m_f^2-\frac{s}{2}+\frac{1}{2}(s-4M^2)^{1/2}(s-4m_f^2)^{1/2}\cos\theta'\end{aligned} \tag{4.21}$$

Then using $s+t+u=2M^2+2m_f^2$ (see Appendix C) we have

$$u=M^2+m_f^2-\frac{s}{2}-\frac{1}{2}(s-4M^2)^{1/2}(s-4m_f^2)^{1/2}\cos\theta' \tag{4.22}$$

Finally, we find

$$\frac{u^2+t^2}{2}=(M^2+m_f^2)^2+\frac{1}{4}\Big[s^2+(s-4M^2)(s-4m_f^2)\cos^2\theta'\Big]-(M^2+m_f^2)s \tag{4.23}$$

and

$$u+t=2(M^2+m_f^2)-s \tag{4.24}$$

We can now compute $w(s)$ by injecting (4.23) and (4.24) in (4.18) and the resulting expression for $|\overline{\mathcal{M}}|^2 = \sum_f |\overline{\mathcal{M}}|_f^2$ in (4.8). Therefore we have

$$\begin{aligned} w(s) &= \sum_f \left(1 - \frac{4m_f^2}{s}\right)^{1/2} \int_{-1}^{1} d\cos\theta' \frac{4Q_f^2 e^2 g'^2}{64\pi(s-\Lambda^2)^2}\left[\frac{u^2+t^2}{2} - 2(u+t)(M^2+m_f^2)\right. \\ &\qquad \left. + 3(M^4+m_f^4) + 6M^2m_f^2\right] \\ &= \sum_f \left(1 - \frac{4m_f^2}{s}\right)^{1/2} \frac{Q_f^2 e^2 g'^2}{16\pi(s-\Lambda^2)^2} \\ &\quad \times \int_{-1}^{1} d\cos\theta' \left[(M^2+m_f^2)^2 + \frac{1}{4}\Big[s^2 + (s-4M^2)(s-4m_f^2)\cos^2\theta'\Big] - (M^2+m_f^2)s\right. \\ &\qquad \left. - 4(M^2+m_f^2)^2 + 2(M^2+m_f^2)s + 3(M^4+m_f^4) + 6M^2m_f^2\right] \\ &= \sum_f \left(1 - \frac{4m_f^2}{s}\right)^{1/2} \frac{Q_f^2 e^2 g'^2}{16\pi(s-\Lambda^2)^2}\frac{2}{3}\Big[s^2 + 2(M^2+m_f^2)s + 4M^2m_f^2\Big] \\ &= \sum_f \left(1 - \frac{4m_f^2}{s}\right)^{1/2} \frac{Q_f^2 e^2 g'^2}{24\pi}\frac{s^2 + 2(M^2+m_f^2)s + 4M^2m_f^2}{(s-\Lambda^2)^2} \end{aligned} \tag{4.25}$$

Then we make a Taylor expansion about $s = 4M^2$ of the last quotient of the latter equation up to order two and we obtain (see Appendix A)

$$w(s) = \sum_f \left(1 - \frac{4m_f^2}{s}\right)^{1/2} \left[C_{0f} + C_{1f}\frac{s}{4M^2} + C_{2f}\left(\frac{s}{4M^2}\right)^2\right] \tag{4.26}$$

with

$$C_{0f} = \frac{Q_f^2 e^2 g'^2}{24\pi}\frac{4\Lambda^4M^2m_f^2 + 128\Lambda^2M^6 - 64\Lambda^2M^4m_f^2 + 640M^8 + 768M^6m_f^2}{(4M^2-\Lambda^2)^4} \tag{4.27}$$

$$C_{1f} = \frac{Q_f^2 e^2 g'^2}{24\pi}4M^2\frac{2\Lambda^4(M^2+m_f^2) - 128\Lambda^2M^4 - 24\Lambda^2M^2m_f^2 - 96M^6 - 224M^4m_f^2}{(4M^2-\Lambda^2)^4} \tag{4.28}$$

$$C_{2f} = \frac{Q_f^2 e^2 g'^2}{24\pi}16M^4\frac{\Lambda^4 + 12\Lambda^2M^2 + 4\Lambda^2m_f^2 + 8M^4 + 20M^2m_f^2}{(4M^2-\Lambda^2)^4} \tag{4.29}$$

Now if we consider the mass of the dark photon to be rigorously zero (i.e. $\Lambda = 0$) as in the next section, the latter coefficients become

$$C_{0f} = \frac{Q_f^2 e^2 g'^2}{48\pi}\frac{5M^2 + 6m_f^2}{M^2} \tag{4.30}$$

$$C_{1f} = -\frac{Q_f^2 e^2 g'^2}{48\pi}\frac{3M^2 + 7m_f^2}{M^2} \tag{4.31}$$

$$C_{2f} = \frac{Q_f^2 e^2 g'^2}{96\pi}\frac{2M^2 + 5m_f^2}{M^2} \tag{4.32}$$

4.1.1 Results

We computed the thermally averaged annihilation cross section $\langle\sigma v_{\rm rel}\rangle$ in two ways. First, we calculated it using the approximation (3.72). Second, we determined it exactly numerically using (3.64). The integrals were computed numerically with a precision of 0.1% and via the Romberg method [1]. In the end, the relative errors between the approximation and the exact solution were about 0.7% (see Fig. 4.2). For this reason, in order to determine the different parameters which yield an abundance comprised between 5% and 15% of $\Omega_{\rm CDM}$ for the subdominant dark-matter component, we used, for convenience, the analytical formulation we have derived for $\langle\sigma v_{\rm rel}\rangle$. Indeed we make the different parameters vary in loops nested in other ones. Therefore, since at each iteration we have to compute [2] $\langle\sigma v_{\rm rel}\rangle_f$ which is then injected in (3.49), the simulation becomes very long if we want to compute the triple integral present in (3.64) with a sufficiently high precision *e.g.* 0.1%.

Actually, the $\langle\sigma v_{\rm rel}\rangle_f$ we have computed is not the one found in (3.72) because we did not sum over all possible final particles. In fact, in this toy model, whatever the mass of the final fermionic particles, we obtain the same result. Even for the top quark, which has the largest mass in the standard model, we obtain a $\langle\sigma v_{\rm rel}\rangle_f$ which is only different from that computed for the other fermions by a factor inferior to 1% (see Fig. 4.3). Therefore in this model, since $\langle\sigma v_{\rm rel}\rangle_f$ is approximately the same for all fermions ($\langle\sigma v_{\rm rel}\rangle_f = \langle\sigma v_{\rm rel}\rangle_0$) we have

$$\langle\sigma v_{\rm rel}\rangle = \sum_f \langle\sigma v_{\rm rel}\rangle_f \simeq \eta\langle\sigma v_{\rm rel}\rangle_0 \tag{4.33}$$

with η a constant multiplier.

In this model, since we have 3 charged leptons and 6 quarks with three possible colours, we find

$$\begin{aligned}\eta &= 3\left(Q_u^2 + Q_d^2 + Q_c^2 + Q_s^2 + Q_t^2 + Q_b^2\right) + Q_e^2 + Q_\mu^2 + Q_\tau^2 \\ &= 3\left(3\left(\frac{2}{3}\right)^2 + 3\left(\frac{1}{3}\right)^2\right) + 3 \\ &= 8\end{aligned} \tag{4.34}$$

Now the purpose is to constrain $\langle\sigma v_{\rm rel}\rangle$ in order to have the abundance of subdominant dark-matter particles, Ω_{χ_f} to be comprised between 5% and 15% of $\Omega_{\rm CDM}$. By varying the different parameters for this model, namely M, g' and x (we consider $\Lambda = 0$ since we work with a massless dark gauge boson) [3], we can obtain some information about the dependence of $\langle\sigma v_{\rm rel}\rangle$. Even though the value of the charge e changes with the energy scale and thus with the Universe temperature, we consider it as a constant equal to $\sqrt{\frac{4\pi}{137}}$, which is the present value, because it remains rather constant in the temperature range of interest.

1. See `https://people.sc.fsu.edu/~jburkardt/cpp_src/nintlib/nintlib.html`.
2. $\langle\sigma v_{\rm rel}\rangle \equiv \sum_f \langle\sigma v_{\rm rel}\rangle_f$.
3. Since the temperature $T = xM$ varies because of the variation of x and M, this also holds true for g_* and g_{*s}. Moreover, the presence of a massless dark photon should imply an increase of 2 supplementary relativistic degrees of freedom in g_* and g_{*s} but since the dark photon is coupled to the visible sector very weakly, its contribution to g_* and g_{*s} can be neglected.

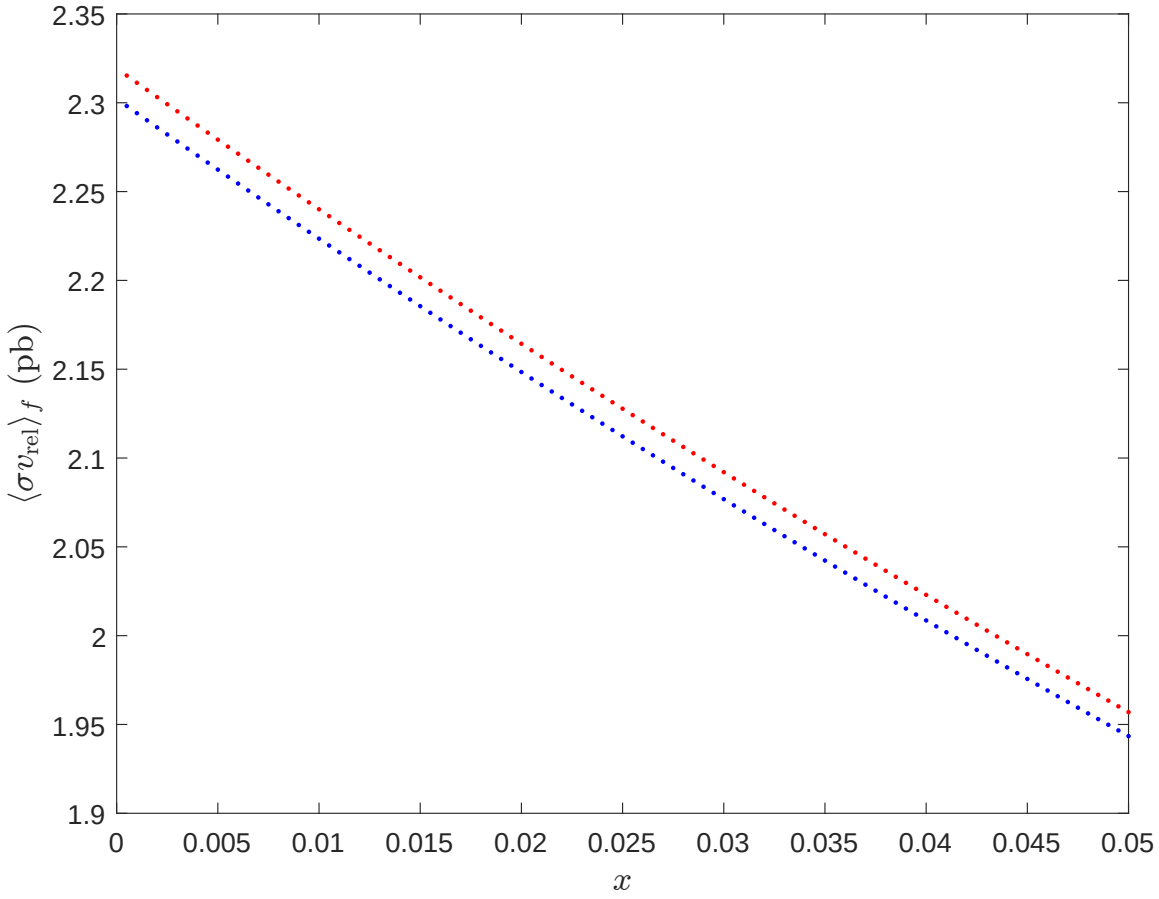

Figure 4.2 – Evolution of $\langle \sigma v_{\mathrm{rel}} \rangle_f$ as a function of x for $M = 500$ GeV, $m_f = m_e$, $e = \sqrt{\frac{4\pi}{137}}$ and $g' = 0.9$. The blue dotted curve refers to the approximate $\langle \sigma v_{\mathrm{rel}} \rangle_f$ obtained via (3.72) whereas the red one refers to the exact $\langle \sigma v_{\mathrm{rel}} \rangle_f$ obtained via (3.64). We can observe that both curves have the same trend and that the discrepancies between these curves is quite negligible which means that the analytical formulation of $\langle \sigma v_{\mathrm{rel}} \rangle_f$ is a very good approximation in this toy model.

We therefore obtain the following dependences for $\langle \sigma v_{\mathrm{rel}} \rangle$:

$$\text{if } g' \to a g', \text{ then } \langle \sigma v_{\mathrm{rel}} \rangle \to a^2 \langle \sigma v_{\mathrm{rel}} \rangle \tag{4.35}$$

with a a constant and where the others parameters are fixed.

The dependence on M is such that $\langle \sigma v_{\mathrm{rel}} \rangle$ rapidly decreases when M increases as shown in Fig. 4.4. As for the dependence of $\langle \sigma v_{\mathrm{rel}} \rangle$ on x, $\langle \sigma v_{\mathrm{rel}} \rangle$ decreases as a function of x (see Fig. 4.2) in a polynomial way as established in (3.72).

Given that the abundance is inversely proportional to $\langle \sigma v_{\mathrm{rel}} \rangle$ according to Eq. (3.49), in order not to have too high an abundance, the right abundance Ω_{χ_f} will therefore be favoured for low mass M, a strong coupling g' and low x. On the other hand, the more $T = xM$ increases, the more g_* and g_{*s} are susceptible to increase and thus to yield a

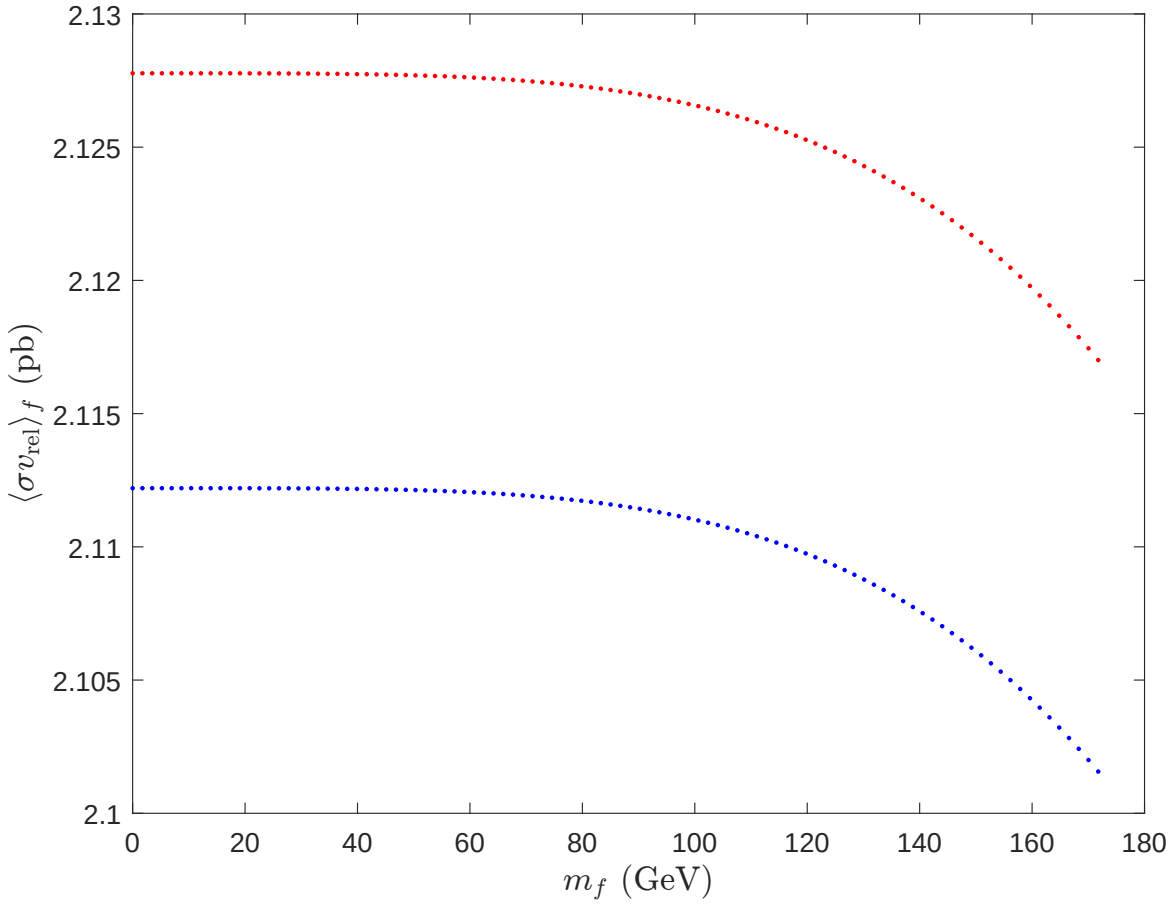

Figure 4.3 – Evolution of $\langle \sigma v_{\rm rel} \rangle_f$ as a function of m_f for $M = 500$ GeV, $x = 0.025$, $e = \sqrt{\frac{4\pi}{137}}$ and $g' = 0.9$. The blue dotted curve refers to the approximate $\langle \sigma v_{\rm rel} \rangle_f$ obtained via (3.72) whereas the red one refers to the exact $\langle \sigma v_{\rm rel} \rangle_f$ obtained via (3.64). The two curves display the same trend and are rather constant except at high fermion mass where they start to decrease but the discrepancies with respect to the beginning of the curve is negligible.

lower Ω_{χ_f} (see Appendix D for a complete inventory of the values of g_* and g_{*s}). Another important point to mention is that we should not forget that in the expression of Ω_{χ_f} (see Eq. 3.49), there is an x_f in the denominator. The x_f used in (3.49) is equal to the x that gives the value to the $\langle \sigma v_{\rm rel} \rangle$ we insert in Ω_{χ_f} in our simulations. Therefore, when only x is varying we have

$$\Omega_{\chi_f} \sim \frac{1}{x \langle \sigma v_{\rm rel} \rangle} \tag{4.36}$$

for an s-wave annihilation process.

Thereby it is no more obvious that small abundances will be favoured for small values of x. Actually it is even the converse since $\langle \sigma v_{\rm rel} \rangle$ varies more slowly than x when the latter varies. Indeed, Ω_{χ_f} decreases with x and small abundances are thus obtained for large values of x (see Fig. 4.5).

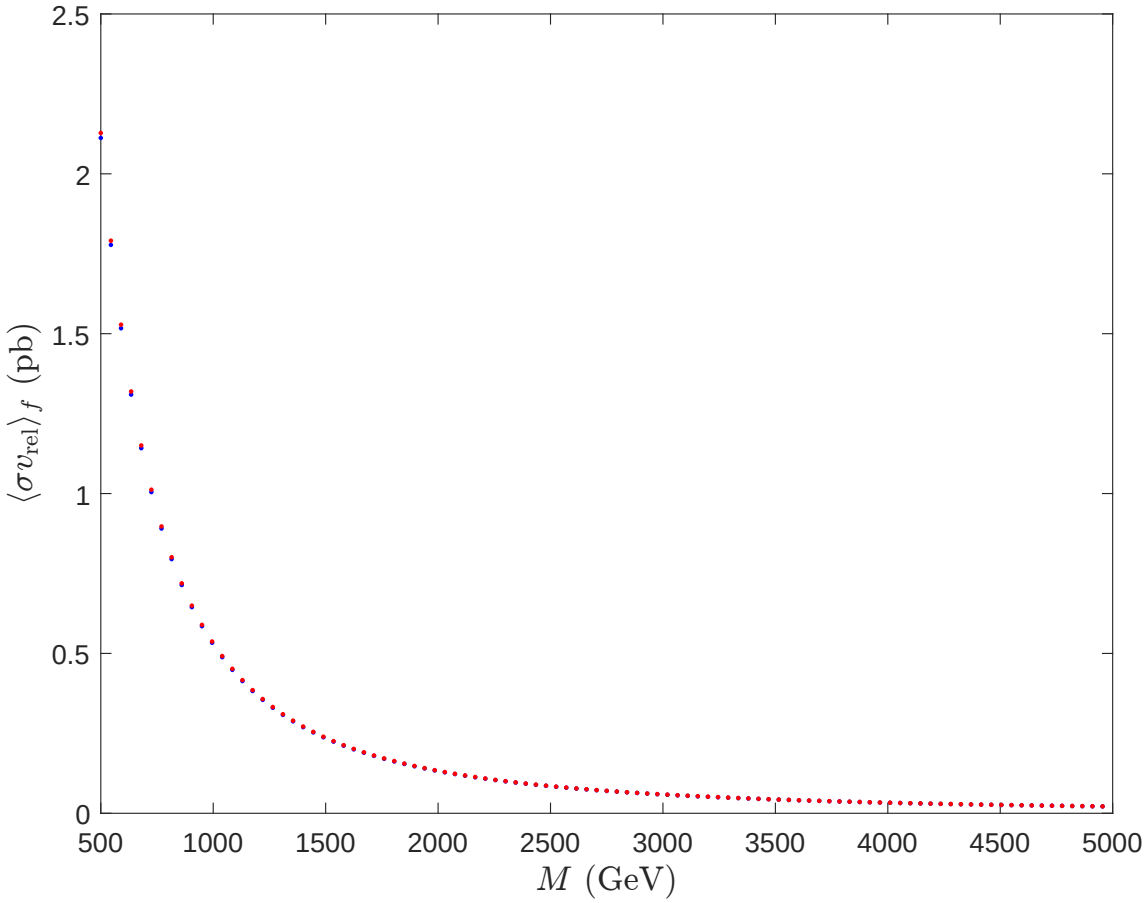

Figure 4.4 – Evolution of $\langle \sigma v_{\rm rel} \rangle_f$ as a function of M for $m_f = m_e$, $x = 0.025$, $e = \sqrt{\frac{4\pi}{137}}$ and $g' = 0.9$. The blue dotted curve refers to the approximate $\langle \sigma v_{\rm rel} \rangle_f$ obtained via (3.72) whereas the red one refers to the exact $\langle \sigma v_{\rm rel} \rangle_f$ obtained via (3.64). The two curves are coincident and decrease fast with M.

Our simulation yields hundreds of thousands of possible configurations for the parameters so that we obtain $5\%\ \Omega_{\rm CDM} \leq \Omega_{\chi_f} \leq 15\%\ \Omega_{\rm CDM}$ (or equivalently $1.29\% \leq \Omega_{\chi_f} \leq 3.88\%$). Therefore we only provide some values for these parameters (see Tab. 4.1) as well as the minimal and the maximal possible values we found (see Tab. 4.2).

We can note that given the obtained temperature range in Tab. 4.2, g_* and g_{*s} remain constant and are equal to 86.25. It should be noted that for the minimal value of M, we could have found a value lower than 500 GeV given what we said earlier but we start our simulation at $M = 500$ GeV in accordance with the various limits provided by LHC data.

Finally, given Tab 4.2, since $e = \sqrt{\frac{4\pi}{137}} \simeq 0.303$, we have $g'_{\rm min} = 0.47 = 1.54\ e$ and $g'_{\rm max} = 0.99 = 3.3\ e$. Therefore the subdominant dark-matter particles we have considered are clearly too charged since they are more charged than the electron, thereby the interaction between these dark-matter particles and *our* photon cannot be neglected

4. We ignore the variation of g_* and g_{*s} with the temperature.

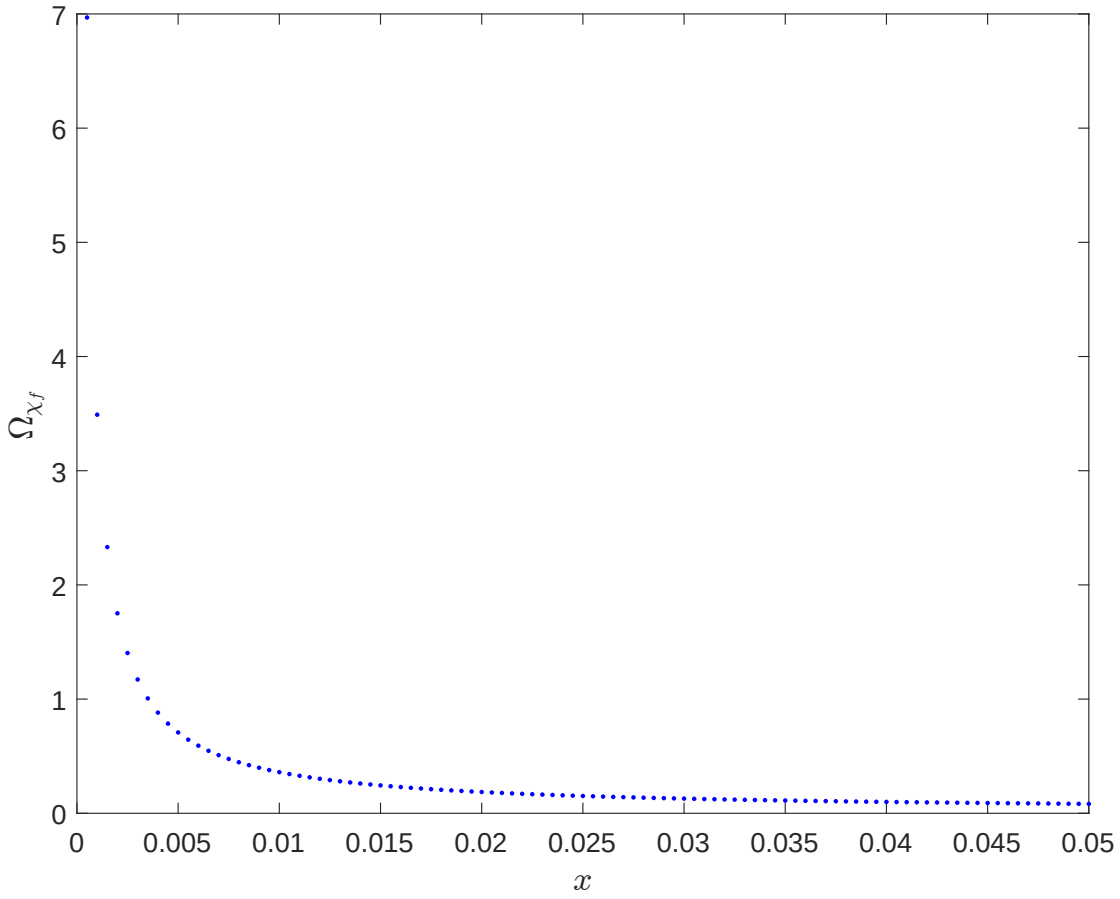

Figure 4.5 – Evolution of Ω_{χ_f} as a function of x for $M = 500$ GeV, $m_f = m_e$, $e = \sqrt{\frac{4\pi}{137}}$, $g' = 0.9$, $n = 0$ and [4] $g_* = g_{*s} = 86.25$. We see that even if $\langle \sigma v_{\text{rel}} \rangle$ decreases when x increases, it is not automatically the case for Ω_{χ_f} which shows a rather fast decrease with x.

anymore, which is absurd. Moreover, since in the definition of g' ($g' = \epsilon g_D$) the kinetic mixing parameter ϵ is such that $\epsilon \ll 1$ [63], it means that $\alpha_D = \frac{g_D^2}{4\pi}$ is larger than 1. In consequence, the annihilation process we considered is a non-perturbative one and therefore, the calculations we have made are not valid anymore. Moreover, the values of g' we obtained are excluded experimentally. However, if we take the annihilation of subdominant dark-matter particles into dark photons into account, the abundance will further decrease and so it could be possible to obtain reasonable parameters values leading to the right abundance.

x	M (GeV)	g'	T (GeV)	g_*	$\langle\sigma v_{\rm rel}\rangle$ (pb)	Ω_{χ_f} (%)
0.015	500	0.82	7.5	86.25	14.51	3.68
0.020	500	0.70	10	86.25	10.40	3.85
0.020	500	0.88	10	86.25	16.43	2.44
0.020	600	0.88	12	86.25	11.41	3.51
0.025	500	0.64	12.5	86.25	8.54	3.75
0.025	500	0.94	12.5	86.25	18.43	1.74
0.025	600	0.76	15	86.25	8.37	3.83
0.025	700	0.94	17.5	86.25	9.40	3.41
0.030	500	0.58	15	86.25	6.90	3.87
0.030	600	0.70	18	86.25	6.98	3.82
0.030	600	0.94	18	86.25	12.59	2.12
0.030	700	0.82	21	86.25	7.04	3.79
0.030	800	0.94	24	86.25	7.08	3.77
0.035	500	0.58	17.5	86.25	6.79	3.37
0.035	500	0.88	17.5	86.25	15.62	1.46
0.035	600	0.70	21	86.25	6.86	3.33
0.035	700	0.76	24.5	86.25	5.94	3.85
0.035	800	0.88	28	86.25	6.10	3.75
0.040	500	0.52	20	86.25	5.36	3.73
0.040	500	0.70	20	86.25	15.36	1.30
0.040	600	0.64	24	86.25	5.64	3.55
0.040	800	0.82	32	86.25	5.21	3.84
0.040	900	0.94	36	86.25	5.41	3.70
0.045	500	0.52	22.5	86.25	5.28	3.37
0.045	600	0.64	27	86.25	5.55	3.21
0.045	700	0.94	31.5	86.25	8.80	2.02
0.045	800	0.82	36	86.25	5.12	3.47
0.045	900	0.88	40.5	86.25	4.66	3.82
0.050	500	0.52	25	86.25	5.19	3.09
0.050	600	0.58	30	86.25	4.48	3.57
0.050	600	0.94	30	86.25	11.78	1.36
0.050	700	0.70	35	86.25	4.80	3.34
0.050	900	0.88	45	86.25	4.59	3.50
0.050	1000	0.94	50	86.25	4.24	3.78

Table 4.1 – A few values of the different parameters in order to have $1.29\% \leq \Omega_{\chi_f} \leq 3.88\%$.

	x	M (GeV)	g'	T (GeV)	g_*	$\langle\sigma v_{\rm rel}\rangle$ (pb)	Ω_{χ_f} (%)
min	0.0095	500	0.47	4.75	86.25	4.12	1.29
max	0.0500	1078	0.99	53.90	86.25	22	3.88

Table 4.2 – Minimal and maximal values of the different parameters in order to have $1.29\% \leq \Omega_{\chi_f} \leq 3.88\%$.

Conclusion

We derived a formalism based on the Boltzmann equation and with the latter we obtained an analytical expression for the relic density leading to compute the present abundance of dark-matter particles. This formula for the relic density required the calculation of the thermally averaged annihilation cross section. Therefore we derived an analytical expression for the latter.

Next we applied what we have derived to a specific case. We considered a PIDM model where dark matter is made of two components: one is made of non-dissipative (collisionless) traditional dark-matter particles like WIMPs whereas the other constituent is made of self-interacting dark-matter particles. However the particularity of this model is that the self-interacting part only accounts for 5% to 15% of the total amount of dark matter. In this thesis we considered a process involving fermionic dark-matter particles which interact with standard-model fermions. Even though dark matter does not interact with the standard photon since it is neutral, its interactions can be mediated via a dark photon. Then this dark photon can kinetically mixes with *our* photon which allows an interaction between the hidden and the visible sector other than the gravitation.

By computing the invariant amplitude of this annihilation process of dark-matter particles into standard fermions, we could then derive the thermally averaged annihilation cross section for one possible final state. We then calculated this cross section using the approximate formula we derived as well as by computing the integrals present in the exact formula numerically. We then compared both results and concluded the that the approximate expression for the thermally averaged annihilation cross section is actually very precise. Indeed, we found a relative error of about 0.7% between the exact and the approximate version of this cross section.

Then, we established the different dependences of the thermally averaged annihilation cross section as a function of its different parameters. From these, we noticed that our simulations for the other possible final states yield the same result as the first one within 1%. Therefore the total thermally averaged annihilation cross section is just the first one we computed but multiplied by a constant factor η (here we found $\eta = 8$). In the end, we obtained that $\langle \sigma v_{\text{rel}} \rangle_f$ decreases with x, m_f, M but increases with g'. Thus, given that the relic abundance is inversely proportional to $\langle \sigma v_{\text{rel}} \rangle$, we have the opposite dependences for Ω_{χ_f} except for its dependence in x where we showed that it decreased with it. As a consequence, since we searched abundances such that $5\%\ \Omega_{\text{CDM}} \leq \Omega_{\chi_f} \leq 15\%\ \Omega_{\text{CDM}}$, then, in order to obtain such low abundances, it could only be possible for relatively low-mass subdominant dark-matter particles (500 GeV$\leq M \leq$ 1078 GeV), interacting strongly with the visible sector ($0.47 \leq g' \leq 0.99$) and for subdominant dark-matter particles freezing out at a relatively high temperature (4.75 GeV $\leq T \leq$ 53.9 GeV).

We can further improve what has been done in this thesis by considering the following remarks. It is a well-known fact that the abundance of baryons computed with the Boltzmann equation is about 9 orders of magnitude lower than what is actually observed. This is because these calculations are made in a baryon-symmetric Universe, that is a Universe composed of as many baryons as antibaryons. However, nowadays we know that almost every antibaryons disappeared. The way we moved from a symmetric Universe where the baryon number was conserved to an asymmetric one where this baryon number is no longer conserved, is realized by means of the hypothetical baryogenesis process. Throughout this thesis, we considered a symmetric dark sector, that is to say our dark-matter model was made of as many particles χ as antiparticles $\bar{\chi}$. Nevertheless, contrary to the visible sector we have not yet determined the symmetric or asymmetric aspect of the dark sector. As a consequence, the abundances computed in this work are either right values (symmetric dark sector), or minimal values (asymmetric dark sector). Therefore, it might be interesting to consider an asymmetric treatment of dark matter applied to our case.

Furthermore, it should be noted that the abundance we computed only takes the annihilation process $\chi_f\bar{\chi}_f \to f\bar{f}$ into account. However, as already said, the annihilation in dark photons, $\chi_f\bar{\chi}_f \to \gamma'\gamma'$ should also be considered because the subdominant dark-matter abundance can further decrease through this process. Moreover, once this subdominant part is decoupled from the standard-model thermal bath, it evolves independently with its own sector but nothing indicates that it should evolve with the same temperature as the visible sector. Therefore, we could consider a two-temperature model in which, after the decoupling between the two worlds, both sectors have their own temperatures, one dictated by the photon temperature for the visible sector while the other one is ruled by the dark photon temperature. We could also consider a three-type dark matter model, along the same lines than the one used in this thesis, but which would differ from the latter by the fact that the subdominant part is composed of two different types of dark matter. The two subdominant components could interact with the same interaction but we could also consider a new dark force, the associated gauge group of which is different from $U(1)_{\mathrm{D}}$, for the new constituent. Therefore, with this two-type subdominant dark-matter model, the question of freeze-out is relevant. Indeed, the decoupling with the standard-model thermal bath and then with the dark thermal bath does not necessarily occur at the same time for the two subdominant dark-matter components.

In this thesis, for our application in Chapter 4, we considered a photon mixing but it might be interesting to study the case of fermionic dark matter interacting with the visible sector through a Higgs-boson mixing, that is a kinetic mixing between the Higgs boson H of the standard model and a Higgs boson H' belonging to the dark sector. Therefore, in this situation, we are no longer forced to choose fermionic dark matter and we could then consider annihilation processes involving other types of dark-matter particles such as scalar or gauge-boson particles. Nevertheless, considering this kind of kinetic mixing implies a non-zero mass for the propagators. The mass of the standard Higgs boson is fixed at about 125 GeV, thereby since we start to vary the initial mass at $M = 500$ GeV, there is no problem. However, for the mass Λ of the dark Higgs boson H', as for M, Λ is a free parameter and as a consequence we could encounter the situation where $2M \simeq \Lambda$. In this case, called resonance, the thermally averaged annihilation cross section would explode, which means that it would be easy to obtain low abundances comprised between

5% Ω_{CDM} and 15% Ω_{CDM}. Nonetheless, these values of abundance are obtained near a pole in the cross section and the case of resonance is not considered in this thesis. This is because according to [64], the Taylor expansion of the cross section in terms of v_{rel}^2 is not the appropriate treatment, thereby the obtained results should not be valid anymore; the approximate formula for the thermally averaged annihilation cross section breaks down in a presence of resonance.

As a last suggestion, since we treated the case of dark matter charged under a dark $U(1)_{\mathrm{D}}$ gauge group, we could contemplate the fact that this dark matter forms bound states like dark atoms, in the same manner as protons and electrons combine into hydrogen atoms. In this situation, we therefore need to deal with "dark electrons". We could even go further by considering molecules, and so on.

Appendix A

Explicit calculations

Liouville operator

In the absence of any perturbations, general relativity states that a particle follows a geodesic the equation of which is given by [22]

$$\frac{d^2x^\alpha}{d\tau^2} + \Gamma^\alpha_{\beta\gamma}\frac{dx^\beta}{d\tau}\frac{dx^\gamma}{d\tau} = 0 \tag{A.1}$$

where $\tau = \int_0^t dt'\sqrt{1-v^2}$ is the proper time of the particle and $\Gamma^\alpha_{\beta\gamma}$ is an affine connexion symbol also known as the Christoffel symbol.

This equation is equivalent to

$$\frac{dp^\alpha}{d\tau} + \frac{1}{m}\Gamma^\alpha_{\beta\gamma}p^\beta p^\gamma = 0 \tag{A.2}$$

since $p^\alpha = mU^\alpha = m\frac{dx^\alpha}{d\tau}$ with U^α the 4-velocity and m the rest mass.

The relativistic version of the Liouville operator is thus

$$\hat{\mathbf{L}}' = \frac{d}{d\tau} = \frac{\partial}{\partial x^\alpha}\frac{dx^\alpha}{d\tau} + \frac{\partial}{\partial p^\alpha}\frac{dp^\alpha}{d\tau} = \frac{1}{m}p^\alpha\frac{\partial}{\partial x^\alpha} - \frac{1}{m}\Gamma^\alpha_{\beta\gamma}p^\beta p^\gamma\frac{\partial}{\partial p^\alpha} \tag{A.3}$$

The latter expression can be extended in

$$\hat{\mathbf{L}} = m\hat{\mathbf{L}}' = p^\alpha\frac{\partial}{\partial x^\alpha} - \Gamma^\alpha_{\beta\gamma}p^\beta p^\gamma\frac{\partial}{\partial p^\alpha}. \tag{A.4}$$

In the FLRW metric we have

$$g_{\mu\nu} = \begin{pmatrix} 1 & 0 & 0 & 0 \\ 0 & \frac{-a^2}{1-kr^2} & 0 & 0 \\ 0 & 0 & -a^2r^2 & 0 \\ 0 & 0 & 0 & -a^2r^2\sin^2\theta \end{pmatrix} \tag{A.5}$$

and

$$g^{\mu\nu} = \begin{pmatrix} 1 & 0 & 0 & 0 \\ 0 & -\frac{1-kr^2}{a^2} & 0 & 0 \\ 0 & 0 & \frac{-1}{a^2 r^2} & 0 \\ 0 & 0 & 0 & \frac{-1}{a^2 r^2 \sin^2\theta} \end{pmatrix} \tag{A.6}$$

As in [22], let us define γ_{ij} and γ^{ij} such as

$$\gamma_{ij} = \begin{pmatrix} \frac{1}{1-kr^2} & 0 & 0 \\ 0 & r^2 & 0 \\ 0 & 0 & r^2 \sin^2\theta \end{pmatrix} \tag{A.7}$$

and

$$\gamma^{ij} = \begin{pmatrix} 1-kr^2 & 0 & 0 \\ 0 & \frac{1}{r^2} & 0 \\ 0 & 0 & \frac{1}{r^2 \sin^2\theta} \end{pmatrix} \tag{A.8}$$

We thus have $-a^2\gamma_{ij} = g_{ij}$ and $-\frac{1}{a^2}\gamma^{ij} = g^{ij}$.
Knowing that [22]

$$\Gamma^{\alpha}_{\beta\gamma} = \frac{1}{2} g^{\alpha\eta}(g_{\eta\beta,\gamma} + g_{\eta\gamma,\beta} - g_{\beta\gamma,\eta}) \tag{A.9}$$

where $g_{\alpha\beta,\gamma} \equiv \frac{\partial g_{\alpha\beta}}{\partial x^\gamma}$, we immediately have [1]

$$\Gamma^0_{00} = \Gamma^0_{i0} = \Gamma^i_{00} = 0 \tag{A.10}$$

As for Γ^0_{ij}, since the metric is diagonal $\eta = 0$. Thus we have

$$\begin{aligned} \Gamma^0_{ij} &= \frac{1}{2} g^{00}(g_{0i,j} + g_{0j,i} - g_{ij,0}) \\ &= -\frac{1}{2}\frac{\partial}{\partial t}(-a^2\gamma_{ij}) \\ &= a\dot{a}\gamma_{ij} \\ &= -\frac{\dot{a}}{a} g_{ij} \end{aligned} \tag{A.11}$$

Using (3.3) with $\alpha = 0$ we obtain

$$\begin{aligned} \hat{\mathbf{L}}[f(E,t)] &= p^0 \frac{\partial}{\partial x^0} f - \Gamma^0_{\beta\gamma} p^\beta p^\gamma \frac{\partial}{\partial p^0} f \\ &= p^0 \frac{\partial}{\partial x^0} f - (\Gamma^0_{00} p^0 p^0 + 2\Gamma^0_{i0} p^i p^0 + \Gamma^0_{ij} p^i p^j) \frac{\partial}{\partial p^0} f \\ &= p^0 \frac{\partial}{\partial x^0} f + \frac{\dot{a}}{a} g_{ij} p^i p^j \frac{\partial}{\partial p^0} f \\ &= E\frac{\partial f}{\partial E} - \frac{\dot{a}}{a} |\vec{p}|^2 \frac{\partial f}{\partial E}. \end{aligned} \tag{A.12}$$

where the last equality arises from $|\vec{p}|^2 \equiv -g_{ij} p^i p^j$.

1. The Christoffel symbol is symmetric with respect to its lower indices. Thus $\Gamma^{\alpha}_{\beta\gamma} = \Gamma^{\alpha}_{\gamma\beta}$.

Left-hand side of the Boltzmann equation

Combining (3.1) and (3.4), multiplying the result by $\frac{g}{E(2\pi)^3}$ and then integrating over d^3p, we obtain

$$\frac{g}{(2\pi)^3}\int\frac{d^3p}{E}\left(E\frac{\partial f}{\partial t}\right)-\frac{g}{(2\pi)^3}\int\frac{d^3p}{E}\left(\frac{\dot{a}}{a}|\vec{p}|^2\frac{\partial f}{\partial E}\right)=\frac{g}{(2\pi)^3}\int\frac{d^3p}{E}\mathbf{C}[f] \tag{A.13}$$

Knowing that $|\vec{p}|^2=E^2-m^2$, we have [2] $|\vec{p}|d|\vec{p}|=EdE$. Thus the left-hand side of (A.13), with the second term expressed in spherical coordinates ($d^3p=d|\vec{p}||\vec{p}|^2d\Omega$), becomes

$$\underbrace{\frac{g}{(2\pi)^3}\frac{\partial}{\partial t}\left(\int d^3p\ f\right)}_{=\frac{\partial n}{\partial t}}-\frac{g}{(2\pi)^3}\frac{\dot{a}}{a}\int dEd\Omega\ (E^2-m^2)^{3/2}\left(\frac{\partial f}{\partial E}\right) \tag{A.14}$$

Let us integrate the second term of (A.14) by part, we have [3]

$$\begin{aligned}&\frac{\partial n}{\partial t}-\frac{g}{(2\pi)^3}\frac{\dot{a}}{a}\Big\{\int d\Omega\Big[(E^2-m^2)^{3/2}f\Big]_{-\infty}^{+\infty}-\int dEd\Omega\ \frac{3}{2}(E^2-m^2)^{1/2}\ 2Ef\Big\}\\ =\ &\frac{\partial n}{\partial t}+\frac{g}{(2\pi)^3}\frac{\dot{a}}{a}3\int d^3p\ f\\ =\ &\frac{\partial n}{\partial t}+3\frac{\dot{a}}{a}n\end{aligned} \tag{A.15}$$

Therefore (3.1) is equivalent to

$$\frac{\partial n}{\partial t}+3\frac{\dot{a}}{a}n=\frac{g}{(2\pi)^3}\int\frac{d^3p}{E}\mathbf{C}[f]. \tag{A.16}$$

Taylor expansion of n_0

Let us start by expanding $f(x)\equiv(1+xy)(y+\frac{1}{2}xy^2)^{1/2}$ until the third order around $x=0$. We find

$$\frac{df}{dx}=y(y+\frac{1}{2}xy^2)^{1/2}+(1+xy)\frac{1}{2}(y+\frac{1}{2}xy^2)^{-1/2}\frac{y^2}{2} \tag{A.17}$$

$$\Rightarrow\frac{df}{dx}(0)=yy^{1/2}+\frac{1}{4}yy^{1/2}=\frac{5}{4}yy^{1/2} \tag{A.18}$$

$$\frac{d^2f}{dx^2}=\frac{1}{2}y(y+\frac{1}{2}xy^2)^{-1/2}\frac{y^2}{2}+\frac{y^3}{4}(y+\frac{1}{2}xy^2)^{-1/2}-\frac{1}{2}\frac{y^2}{4}(1+xy)(y+\frac{1}{2}xy^2)^{-3/2}\frac{y^2}{2} \tag{A.19}$$

2. Indeed $|\vec{p}|=\sqrt{E^2-p^2}$ thus $d|\vec{p}|=\frac{2EdE}{2\sqrt{E^2-p^2}}=\frac{EdE}{|\vec{p}|}$.

3. f vanishes at $\pm\infty$ since we assume that one cannot find a particle with an infinite energy.

$$\Rightarrow \frac{d^2f}{dx^2}(0) = \frac{1}{4}y^2y^{1/2} + \frac{1}{4}y^2y^{1/2} - \frac{1}{16}y^2y^{1/2} = \frac{7}{16}y^2y^{1/2} \tag{A.20}$$

$$\begin{aligned}\frac{d^3f}{dx^3} = &-\frac{1}{8}y^3(y+\frac{1}{2}xy^2)^{-3/2}\frac{y^2}{2} - \frac{1}{8}y^3(y+\frac{1}{2}xy^2)^{-3/2}\frac{y^2}{2} \\ &- \frac{1}{16}y^4y(y+\frac{1}{2}xy^2)^{-3/2} + \frac{3}{32}y^4(1+xy)(y+\frac{1}{2}xy^2)^{-5/2}\frac{y^2}{2}\end{aligned} \tag{A.21}$$

$$\Rightarrow \frac{d^3f}{dx^3}(0) = -\frac{1}{16}y^3y^{1/2} - \frac{1}{16}y^3y^{1/2} - \frac{1}{16}y^3y^{1/2} + \frac{3}{64}y^3y^{1/2} = -\frac{9}{64}y^3y^{1/2} \tag{A.22}$$

Thereby we obtain

$$\begin{aligned}f(x) &= f(0) + \frac{df}{dx}(0)x + \frac{1}{2}\frac{d^2f}{dx^2}(0)x^2 + \frac{1}{6}\frac{d^3f}{dx^3}(0)x^3 + \mathcal{O}(x^4) \\ &= y^{1/2} + \frac{5}{4}yy^{1/2}x + \frac{7}{32}y^2y^{1/2}x^2 - \frac{3}{128}y^3y^{1/2}x^3 + \mathcal{O}(x^4)\end{aligned} \tag{A.23}$$

and thus, in (3.63), we have

$$\int_0^\infty dy\ \left(y^{1/2} + \frac{5}{4}yy^{1/2}x + \frac{7}{32}y^2y^{1/2}x^2 - \frac{3}{128}y^3y^{1/2}x^3 + \mathcal{O}(x^4)\right)e^{-y} \tag{A.24}$$

Before going further we compute $\int_0^\infty dy\ y^{1/2}e^{-ay}$ with $r = y^{1/2}$ ($dy = 2rdr$) as a change of variable:

$$\int_0^\infty dy\ y^{1/2}e^{-ay} = 2\int_0^\infty dr\ r^2e^{-ar^2} = \frac{1}{2a}\left(\frac{\pi}{a}\right)^{1/2} \tag{A.25}$$

$$\Rightarrow \int_0^\infty dy\ y^{1/2}e^{-y} = \frac{1}{2}\pi^{1/2} \tag{A.26}$$

where the value of this integral is provided in Appendix B.

Moreover, we can remark that

$$-\frac{d}{da}\left(y^{1/2}e^{-ay}\right) = yy^{1/2}e^{-ay} \tag{A.27}$$

which means that we have

$$(-1)^n\frac{d^n}{da^n}\left(y^{1/2}e^{-ay}\right) = y^ny^{1/2}e^{-ay} \tag{A.28}$$

Now we compute the three integrals that are needed in (A.24):

$$\int_0^\infty dy\ yy^{1/2}e^{-ay} = -\frac{d}{da}\int_0^\infty dy\ y^{1/2}e^{-ay} = -\frac{d}{da}\left[\frac{1}{2a}\left(\frac{\pi}{a}\right)^{1/2}\right] = \frac{3}{4}\pi^{1/2}a^{-5/2} \tag{A.29}$$

$$\Rightarrow \int_0^\infty dy\ yy^{1/2}e^{-y} = \frac{3}{4}\pi^{1/2} \tag{A.30}$$

$$\int_0^\infty dy\ y^2 y^{1/2} e^{-ay} = -\frac{d}{da}\int_0^\infty dy\ y y^{1/2} e^{-ay} = -\frac{d}{da}\left(\frac{3}{4}\pi^{1/2}a^{-5/2}\right) = \frac{15}{8}\pi^{1/2}a^{-7/2} \tag{A.31}$$

$$\Rightarrow \int_0^\infty dy\ y^2 y^{1/2} e^{-y} = \frac{15}{8}\pi^{1/2} \tag{A.32}$$

$$\int_0^\infty dy\ y^3 y^{1/2} e^{-ay} = -\frac{d}{da}\int_0^\infty dy\ y^2 y^{1/2} e^{-ay} = -\frac{d}{da}\left(\frac{15}{8}\pi^{1/2}a^{-7/2}\right) = \frac{105}{16}\pi^{1/2}a^{-9/2} \tag{A.33}$$

$$\Rightarrow \int_0^\infty dy\ y^3 y^{1/2} e^{-y} = \frac{105}{16}\pi^{1/2} \tag{A.34}$$

Therefore (A.24) can be written as

$$\frac{\pi^{1/2}}{2}\left[1 + \frac{15}{8}x + \frac{105}{128}x^2 - \frac{315}{1024}x^3 + \mathcal{O}(x^4)\right] \tag{A.35}$$

and then (3.63) becomes

$$n_0 = \left[g(2\pi x)^{-3/2}T^3 e^{-1/x}\right]\left[1 + \frac{15}{8}x + \frac{105}{128}x^2 - \frac{315}{1024}x^3 + \mathcal{O}(x^4)\right] \tag{A.36}$$

$$\Rightarrow \frac{1}{n_0^2} = \frac{8\pi^3 e^{2/x}}{g^2 x^3 M^6}\left[1 + \frac{15}{8}x + \frac{105}{128}x^2 - \frac{315}{1024}x^3 + \mathcal{O}(x^4)\right]^{-2} \tag{A.37}$$

In order to compute the latter expression, we make an Taylor expansion of the polynomial within the brackets, namely $g(x) \equiv \left[1 + \frac{15}{8}x + \frac{105}{128}x^2 - \frac{315}{1024}x^3 + \mathcal{O}(x^4)\right]^{-2}$, around $x = 0$ and up to order three. We thus obtain

$$\frac{dg}{dx} = -2\left(1 + \frac{15}{8}x + \frac{105}{128}x^2 - \frac{315}{1024}x^3\right)^{-3}\left(\frac{15}{8} + \frac{105}{64}x - \frac{945}{1024}x^2\right) \tag{A.38}$$

$$\Rightarrow \frac{dg}{dx}(0) = -\frac{15}{4} \tag{A.39}$$

$$\begin{aligned}\frac{d^2g}{dx^2} = {} & 6\left(1 + \frac{15}{8}x + \frac{105}{128}x^2 - \frac{315}{1024}x^3\right)^{-4}\left(\frac{15}{8} + \frac{105}{64}x - \frac{945}{1024}x^2\right)^2 \\ & - 2\left(1 + \frac{15}{8}x + \frac{105}{128}x^2 - \frac{315}{1024}x^3\right)^{-3}\left(\frac{105}{64} - \frac{945}{512}x\right)\end{aligned} \tag{A.40}$$

$$\Rightarrow \frac{d^2g}{dx^2}(0) = 6\frac{225}{64} - 2\frac{105}{64} = \frac{675}{32} - \frac{105}{32} = \frac{570}{32} \tag{A.41}$$

$$\begin{aligned}\frac{d^3g}{dx^3} = {} & -24\left(1 + \frac{15}{8}x + \frac{105}{128}x^2 - \frac{315}{1024}x^3\right)^{-5}\left(\frac{15}{8} + \frac{105}{64}x - \frac{945}{1024}x^2\right)^3 \\ & + 6\left(1 + \frac{15}{8}x + \frac{105}{128}x^2 - \frac{315}{1024}x^3\right)^{-4} 2\left(\frac{15}{8} + \frac{105}{64}x - \frac{945}{1024}x^2\right)\left(\frac{105}{64} - \frac{945}{512}x\right) \\ & + 6\left(1 + \frac{15}{8}x + \frac{105}{128}x^2 - \frac{315}{1024}x^3\right)^{-4}\left(\frac{15}{8} + \frac{105}{64}x - \frac{945}{1024}x^2\right)\left(\frac{105}{64} - \frac{945}{512}x\right) \\ & + 2\left(1 + \frac{15}{8}x + \frac{105}{128}x^2 - \frac{315}{1024}x^3\right)^{-3}\frac{945}{512}\end{aligned} \tag{A.42}$$

$$\begin{aligned}\Rightarrow \frac{d^3g}{dx^3}(0) &= -24\frac{3375}{512} + 18\frac{15}{8}\frac{105}{64} + \frac{945}{256} \\ &= -\frac{40500}{256} + \frac{14175}{256} + \frac{945}{256} \\ &= -\frac{6345}{64}\end{aligned} \tag{A.43}$$

Thus we find

$$\begin{aligned}g(x) &= g(0) + \frac{dg}{dx}(0)x + \frac{1}{2}\frac{d^2g}{dx^2}(0)x^2 + \frac{1}{6}\frac{d^3g}{dx^3}(0)x^3 + \mathcal{O}(x^4) \\ &= 1 - \frac{15}{4}x + \frac{285}{32}x^2 - \frac{2115}{128}x^3 + \mathcal{O}(x^4)\end{aligned} \tag{A.44}$$

and so,

$$\frac{1}{n_0^2} = \frac{8\pi^3 e^{2/x}}{g^2x^3M^6}\left[1 - \frac{15}{4}x + \frac{285}{32}x^2 - \frac{2115}{128}x^3 + \mathcal{O}(x^4)\right] \tag{A.45}$$

Taylor expansion of $w(s)$

The Taylor expansion of $w(s)$ about $\frac{s}{4M^2} = 1$ up to order three is

$$\begin{aligned}w(s) \simeq\ & w(s)\Big|_{\frac{s}{4M^2}=1} + \frac{dw}{d\frac{s}{4M^2}}\Big|_{\frac{s}{4M^2}=1}\left(\frac{s}{4M^2} - 1\right) \\ & + \frac{1}{2}\frac{d^2w}{d\left(\frac{s}{4M^2}\right)^2}\Big|_{\frac{s}{4M^2}=1}\left(\frac{s}{4M^2} - 1\right)^2 + \frac{1}{6}\frac{d^3w}{d\left(\frac{s}{4M^2}\right)^3}\Big|_{\frac{s}{4M^2}=1}\left(\frac{s}{4M^2} - 1\right)^3 \\ =\ & w(s) + \frac{1}{4M^2}w'(s)\Big|_{\frac{s}{4M^2}=1}(s - 4M^2) + \frac{1}{2(4M^2)^2}w''(s)\Big|_{\frac{s}{4M^2}=1}(s - 4M^2)^2 \\ & + \frac{1}{6(4M^2)^3}w'''(s)\Big|_{\frac{s}{4M^2}=1}(s - 4M^2)^3\end{aligned} \tag{A.46}$$

where the prime refers to the derivative with respect to $\frac{s}{4M^2}$.
Thus, in (3.66), we have

$$\begin{aligned}\int_{-1}^{1} d\cos\theta\ \Bigg[& w(s) + \frac{1}{4M^2}w'(s)\Big|_{\frac{s}{4M^2}=1}(s - 4M^2) + \frac{1}{2(4M^2)^2}w''(s)\Big|_{\frac{s}{4M^2}=1}(s - 4M^2)^2 \\ & + \frac{1}{6(4M^2)^3}w'''(s)\Big|_{\frac{s}{4M^2}=1}(s - 4M^2)^3\Bigg]\end{aligned} \tag{A.47}$$

Thereby, for each term in the latter relation we have

$$\int_{-1}^{1} d\cos\theta\ w(s)\Big|_{\frac{s}{4M^2}=1} = w(s)\Big|_{\frac{s}{4M^2}=1}\int_{-1}^{1} d\cos\theta = 2w(s)\Big|_{\frac{s}{4M^2}=1} \tag{A.48}$$

$$
\begin{aligned}
&\int_{-1}^{1} d\cos\theta\ \frac{1}{4M^2} w'(s)\Big|_{\frac{s}{4M^2}=1} (s-4M^2) \\
&= \int_{-1}^{1} d\cos\theta\ w'(s)\Big|_{\frac{s}{4M^2}=1} \Big(\frac{1}{2}x(y_1+y_2) + \frac{1}{2}x^2 y_1 y_2 - x(y_1+\frac{1}{2}xy_1^2)^{1/2}(y_2+\frac{1}{2}xy_2^2)^{1/2}\cos\theta\Big) \\
&= w'(s)\Big|_{\frac{s}{4M^2}=1} \Big(x(y_1+y_2) + x^2 y_1 y_2 - x(y_1+\frac{1}{2}xy_1^2)^{1/2}(y_2+\frac{1}{2}xy_2^2)^{1/2}\int_{-1}^{1} d\cos\theta\ \cos\theta\Big) \\
&= w'(s)\Big|_{\frac{s}{4M^2}=1} \Big(x(y_1+y_2) + x^2 y_1 y_2\Big)
\end{aligned}
\tag{A.49}
$$

$$
\begin{aligned}
&\int_{-1}^{1} d\cos\theta\ \frac{1}{2(4M^2)^2} w''(s)\Big|_{\frac{s}{4M^2}=1} (s-4M^2)^2 \\
&= \int_{-1}^{1} d\cos\theta\ \frac{w''(s)}{2}\Big|_{\frac{s}{4M^2}=1} \Big(\frac{1}{2}x(y_1+y_2) + \frac{1}{2}x^2 y_1 y_2 - x(y_1+\frac{1}{2}xy_1^2)^{1/2}(y_2+\frac{1}{2}xy_2^2)^{1/2}\cos\theta\Big)^2 \\
&= \int_{-1}^{1} d\cos\theta\ \frac{w''(s)}{2}\Big|_{\frac{s}{4M^2}=1} \Big(\frac{1}{4}x^2(y_1+y_2)^2 + x^2(y_1+\frac{1}{2}xy_1^2)(y_2+\frac{1}{2}xy_2^2)\cos^2\theta \\
&\qquad + 2\frac{1}{4}x^3(y_1+y_2)y_1y_2 - 2\frac{x^2}{2}(y_1+y_2)(y_1+\frac{1}{2}xy_1^2)^{1/2}(y_2+\frac{1}{2}xy_2^2)^{1/2}\cos\theta \\
&\qquad - 2\frac{x^3}{2}y_1y_2(y_1+\frac{1}{2}xy_1^2)^{1/2}(y_2+\frac{1}{2}xy_2^2)^{1/2}\cos\theta + \mathcal{O}(x^4)\Big) \\
&= \frac{w''(s)}{2}\Big|_{\frac{s}{4M^2}=1} \Big(\frac{x^2}{2}(y_1+y_2)^2 + \frac{2}{3}x^2(y_1+\frac{1}{2}xy_1^2)(y_2+\frac{1}{2}xy_2^2) + x^3(y_1+y_2)y_1y_2 + \mathcal{O}(x^4)\Big)
\end{aligned}
\tag{A.50}
$$

$$
\begin{aligned}
&\int_{-1}^{1} d\cos\theta\ \frac{1}{6(4M^2)^3} w'''(s)\Big|_{\frac{s}{4M^2}=1} (s-4M^2)^3 \\
&= \int_{-1}^{1} d\cos\theta\ \frac{w'''(s)}{6}\Big|_{\frac{s}{4M^2}=1} \Big(\frac{1}{2}x(y_1+y_2) + \frac{1}{2}x^2 y_1 y_2 - x(y_1+\frac{1}{2}xy_1^2)^{1/2}(y_2+\frac{1}{2}xy_2^2)^{1/2}\cos\theta\Big)^3 \\
&= \int_{-1}^{1} d\cos\theta\ \frac{w'''(s)}{6}\Big|_{\frac{s}{4M^2}=1} \Big(\frac{1}{8}x^3(y_1+y_2)^3 - x^3(y_1+\frac{1}{2}xy_1^2)^{3/2}(y_2+\frac{1}{2}xy_2^2)^{3/2}\cos^3\theta \\
&\qquad - 3\frac{1}{4}x^3(y_1+y_2)^2(y_1+\frac{1}{2}xy_1^2)^{1/2}(y_2+\frac{1}{2}xy_2^2)^{1/2}\cos\theta \\
&\qquad + 3\frac{1}{2}x^3(y_1+y_2)(y_1+\frac{1}{2}xy_1^2)(y_2+\frac{1}{2}xy_2^2)\cos^2\theta + \mathcal{O}(x^4)\Big) \\
&= \frac{w'''(s)}{6}\Big|_{\frac{s}{4M^2}=1} \Big(\frac{x^3}{4}(y_1+y_2)^3 + x^3(y_1+y_2)(y_1+\frac{1}{2}xy_1^2)(y_2+\frac{1}{2}xy_2^2) + \mathcal{O}(x^4)\Big)
\end{aligned}
\tag{A.51}
$$

where we expressed $(s-4M^2)$ using (3.68).

One can therefore write $\langle\sigma v_{\rm rel}\rangle$ as

$$\langle\sigma v_{\rm rel}\rangle = \frac{2}{\pi M^2}\left[1-\frac{15}{4}x+\frac{285}{32}x^2-\frac{2115}{128}x^3\right]\int_0^\infty dy_1dy_2\ (y_1+\frac{1}{2}xy_1^2)^{1/2}(y_2+\frac{1}{2}xy_2^2)^{1/2}$$
$$\times e^{-y_1}e^{-y_2}\left[2w(s)+w'(s)\left(x(y_1+y_2)+x^2y_1y_2\right)+\frac{w''(s)}{2}\left(\frac{x^2}{2}(y_1+y_2)^2\right.\right.$$
$$\left.+\frac{2}{3}x^2(y_1+\frac{1}{2}xy_1^2)(y_2+\frac{1}{2}xy_2^2)+x^3(y_1+y_2)y_1y_2\right)+\frac{w'''(s)}{6}\left(\frac{x^3}{4}(y_1+y_2)^3\right.$$
$$\left.\left.+x^3(y_1+y_2)(y_1+\frac{1}{2}xy_1^2)(y_2+\frac{1}{2}xy_2^2)\right)+\mathcal{O}(x^4)\right]_{\frac{s}{4M^2}=1} \tag{A.52}$$

Integrals in the thermally averaged annihilation cross section

In order to compute

$$\int_0^\infty dy_1dy_2\ \left(y_1+\frac{1}{2}xy_1^2\right)^{1/2}\left(y_2+\frac{1}{2}xy_2^2\right)^{1/2}e^{-y_1}e^{-y_2}\left[2w(s)+w'(s)\left(x(y_1+y_2)+x^2y_1y_2\right)\right.$$
$$+\frac{w''(s)}{2}\left(\frac{x^2}{2}(y_1+y_2)^2+\frac{2}{3}x^2\left(y_1+\frac{1}{2}xy_1^2\right)\left(y_2+\frac{1}{2}xy_2^2\right)+x^3(y_1+y_2)y_1y_2\right)$$
$$\left.+\frac{w'''(s)}{6}\left(\frac{x^3}{4}(y_1+y_2)^3+x^3(y_1+y_2)\left(y_1+\frac{1}{2}xy_1^2\right)\left(y_2+\frac{1}{2}xy_2^2\right)\right)\right] \tag{A.53}$$

we have to make a Taylor expansion in x (around zero) of each integrand. Again we stop at the third order. Here, for the purpose of not being too cumbersome, we will use a prime for the derivative with respect to x, thereby, it is not related to the primes utilized for the derivatives of $w(s)$.

First integral

Let us compute

$$\int_0^\infty dy_1dy_2\ \left(y_1+\frac{1}{2}xy_1^2\right)^{1/2}\left(y_2+\frac{1}{2}xy_2^2\right)^{1/2}e^{-y_1}e^{-y_2} \tag{A.54}$$

We can define $h_1(x)\equiv\left(y_1+\frac{1}{2}xy_1^2\right)^{1/2}\left(y_2+\frac{1}{2}xy_2^2\right)^{1/2}$ and so we have

$$h_1'(x)=\frac{1}{2}\left(y_1+\frac{1}{2}xy_1^2\right)^{-1/2}\frac{y_1^2}{2}\left(y_2+\frac{1}{2}xy_2^2\right)^{1/2}$$
$$+\left(y_1+\frac{1}{2}xy_1^2\right)^{1/2}\frac{1}{2}\left(y_2+\frac{1}{2}xy_2^2\right)^{-1/2}\frac{y_2^2}{2} \tag{A.55}$$
$$\Rightarrow h_1'(0)=\frac{1}{4}y_1^{-1/2}y_1^2y_2^{1/2}+\frac{1}{4}y_1^{1/2}y_2^{-1/2}y_2^2=\frac{1}{4}(y_1+y_2)y_1^{1/2}y_2^{1/2} \tag{A.56}$$

$$
\begin{aligned}
h_1''(x) = &-\frac{y_1^2}{8}\left(y_1+\frac{1}{2}xy_1^2\right)^{-3/2}\frac{y_1^2}{2}\left(y_2+\frac{1}{2}xy_2^2\right)^{1/2}\\
&+\frac{y_1^2}{8}\left(y_1+\frac{1}{2}xy_1^2\right)^{-1/2}\left(y_2+\frac{1}{2}xy_2^2\right)^{-1/2}\frac{y_2^2}{2}\\
&+\frac{y_2^2}{8}\left(y_1+\frac{1}{2}xy_1^2\right)^{-1/2}\frac{y_1^2}{2}\left(y_2+\frac{1}{2}xy_2^2\right)^{-1/2}\\
&-\frac{y_2^2}{8}\left(y_1+\frac{1}{2}xy_1^2\right)^{1/2}\left(y_2+\frac{1}{2}xy_2^2\right)^{-3/2}\frac{y_2^2}{2} \qquad \text{(A.57)}\\
\Rightarrow h_1''(0) = &-\frac{y_1^4}{16}y_1^{-3/2}y_2^{1/2}+\frac{y_1^2}{16}y_2^2y_1^{-1/2}y_2^{-1/2}+\frac{y_2^2}{16}y_1^2y_1^{-1/2}y_2^{-1/2}-\frac{y_2^4}{16}y_1^{1/2}y_2^{-3/2}\\
= &-\frac{1}{16}\left(y_1^2-2y_1y_2+y_2^2\right)y_1^{1/2}y_2^{1/2} \qquad \text{(A.58)}\\
h_1'''(x) = &\frac{3y_1^4}{32}\left(y_1+\frac{1}{2}xy_1^2\right)^{-5/2}\frac{y_1^2}{2}\left(y_2+\frac{1}{2}xy_2^2\right)^{1/2}\\
&-\frac{y_1^4}{32}\left(y_1+\frac{1}{2}xy_1^2\right)^{-3/2}\left(y_2+\frac{1}{2}xy_2^2\right)^{-1/2}\frac{y_2^2}{2}\\
&-\frac{1}{16}y_1^2y_2^2\left(y_1+\frac{1}{2}xy_1^2\right)^{-3/2}\frac{y_1^2}{2}\left(y_2+\frac{1}{2}xy_2^2\right)^{-1/2}\\
&-\frac{1}{16}y_1^2y_2^2\left(y_1+\frac{1}{2}xy_1^2\right)^{-1/2}\left(y_2+\frac{1}{2}xy_2^2\right)^{-3/2}\frac{y_2^2}{2}\\
&-\frac{y_2^4}{32}\left(y_1+\frac{1}{2}xy_1^2\right)^{-1/2}\frac{y_1^2}{2}\left(y_2+\frac{1}{2}xy_2^2\right)^{-3/2}\\
&+\frac{3y_2^4}{32}\left(y_1+\frac{1}{2}xy_1^2\right)^{1/2}\left(y_2+\frac{1}{2}xy_2^2\right)^{-5/2}\frac{y_2^2}{2} \qquad \text{(A.59)}
\end{aligned}
$$

$$
\begin{aligned}
\Rightarrow h_1'''(0) = &\frac{3y_1^4}{64}y_1^{-5/2}y_1^2y_2^{1/2}-\frac{1}{64}y_1^4y_1^{-3/2}y_2^{-1/2}y_2^2-\frac{1}{32}y_1^2y_2^2y_1^{-3/2}y_1^2y_2^{-1/2}\\
&-\frac{1}{32}y_1^2y_2^2y_1^{-1/2}y_2^{-3/2}y_2^2-\frac{y_2^4}{64}y_1^{-1/2}y_1^2y_2^{-3/2}+\frac{3y_2^4}{64}y_1^{1/2}y_2^{-5/2}y_2^2\\
= &\frac{1}{64}\left(3y_1^3-y_1^2y_2-2y_1^2y_2-2y_1y_2^2-y_1y_2^2+3y_2^3\right)y_1^{1/2}y_2^{1/2}\\
= &\frac{3}{64}\left(y_1^3-y_1^2y_2-y_1y_2^2+y_2^3\right)y_1^{1/2}y_2^{1/2} \qquad \text{(A.60)}
\end{aligned}
$$

Thus

$$
\begin{aligned}
h_1(x) &= h_1(0)+h_1'(0)x+\frac{1}{2}h_1''(0)x^2+\frac{1}{6}h_1'''(0)x^3+\mathcal{O}(x^4)\\
&= y_1^{1/2}y_2^{1/2}+\frac{1}{4}y_1^{1/2}y_2^{1/2}(y_1+y_2)x-\frac{1}{32}y_1^{1/2}y_2^{1/2}\left(y_1^2-2y_1y_2+y_2^2\right)x^2\\
&\quad+\frac{1}{128}y_1^{1/2}y_2^{1/2}\left(y_1^3-y_1^2y_2-y_1y_2^2+y_2^3\right)x^3+\mathcal{O}(x^4) \qquad \text{(A.61)}
\end{aligned}
$$

and then (A.54) becomes

$$
\int_0^\infty dy_1\ y_1^{1/2}e^{-y_1}\int_0^\infty dy_2\ y_2^{1/2}e^{-y_2}+\frac{1}{4}\Bigg[\int_0^\infty dy_1\ y_1^{1/2}y_1e^{-y_1}\int_0^\infty dy_2\ y_2^{1/2}e^{-y_2}
$$

$$
\begin{aligned}
&+\int_0^\infty dy_1\; y_1^{1/2}e^{-y_1}\int_0^\infty dy_2\; y_2^{1/2}y_2e^{-y_2}\Bigg]x-\frac{1}{32}\Bigg[\int_0^\infty dy_1\; y_1^{1/2}y_1^2e^{-y_1}\int_0^\infty dy_2\; y_2^{1/2}e^{-y_2}\\
&-2\int_0^\infty dy_1\; y_1^{1/2}y_1e^{-y_1}\int_0^\infty dy_2\; y_2^{1/2}y_2e^{-y_2}+\int_0^\infty dy_1\; y_1^{1/2}e^{-y_1}\int_0^\infty dy_2\; y_2^{1/2}y_2^2e^{-y_2}\Bigg]x^2\\
&+\frac{1}{128}\Bigg[\int_0^\infty dy_1\; y_1^{1/2}y_1^3e^{-y_1}\int_0^\infty dy_2\; y_2^{1/2}e^{-y_2}-\int_0^\infty dy_1\; y_1^{1/2}y_1^2e^{-y_1}\int_0^\infty dy_2\; y_2^{1/2}y_2e^{-y_2}\\
&-\int_0^\infty dy_1\; y_1^{1/2}y_1e^{-y_1}\int_0^\infty dy_2\; y_2^{1/2}y_2^2e^{-y_2}+\int_0^\infty dy_1\; y_1^{1/2}e^{-y_1}\int_0^\infty dy_2\; y_2^{1/2}y_2^3e^{-y_2}\Bigg]x^3\\
&+\mathcal{O}(x^4)\\
=\;&\frac{\pi^{1/2}}{2}\frac{\pi^{1/2}}{2}+\frac{1}{4}\left[\frac{3\pi^{1/2}}{4}\frac{\pi^{1/2}}{2}+\frac{\pi^{1/2}}{2}\frac{3\pi^{1/2}}{4}\right]x-\frac{1}{32}\left[\frac{15\pi^{1/2}}{8}\frac{\pi^{1/2}}{2}-2\frac{3\pi^{1/2}}{4}\frac{3\pi^{1/2}}{4}\right.\\
&\left.+\frac{\pi^{1/2}}{2}\frac{15\pi^{1/2}}{8}\right]x^2+\frac{1}{128}\left[\frac{105\pi^{1/2}}{16}\frac{\pi^{1/2}}{2}-\frac{15\pi^{1/2}}{8}\frac{3\pi^{1/2}}{4}-\frac{3\pi^{1/2}}{4}\frac{15\pi^{1/2}}{8}+\frac{\pi^{1/2}}{2}\frac{105\pi^{1/2}}{16}\right]x^3\\
&+\mathcal{O}(x^4)\\
=\;&\frac{\pi}{4}\left(1+\frac{3}{4}x-\frac{3}{32}x^2+\frac{15}{128}x^3+\mathcal{O}(x^4)\right)
\end{aligned}
\tag{A.62}
$$

where we used (A.26), (A.30), (A.32) and (A.34).

Second integral

Now we calculate

$$
\int_0^\infty dy_1dy_2\;\left(y_1+\frac{1}{2}xy_1^2\right)^{1/2}\left(y_2+\frac{1}{2}xy_2^2\right)^{1/2}e^{-y_1}e^{-y_2}\left(x(y_1+y_2)+x^2y_1y_2\right) \tag{A.63}
$$

In order to do that, we can define $h_{2,1}(x)\equiv\left(y_1+\frac{1}{2}xy_1^2\right)^{1/2}\left(y_2+\frac{1}{2}xy_2^2\right)^{1/2}x(y_1+y_2)$ $=h_1(x)x(y_1+y_2)$. Thus, making a Taylor expansion, we obtain

$$
h'_{2,1}(x)=(y_1+y_2)\left[h'_1(x)x+h_1(x)\right] \tag{A.64}
$$

$$
\Rightarrow h'_{2,1}(0)=(y_1+y_2)h_1(0)=(y_1+y_2)y_1^{1/2}y_2^{1/2} \tag{A.65}
$$

$$
h''_{2,1}(x)=(y_1+y_2)\left[h''_1(x)x+h'_1(x)+h'_1(x)\right] \tag{A.66}
$$

$$
\Rightarrow h''_{2,1}(0)=(y_1+y_2)2h'_1(0)=\frac{1}{2}(y_1+y_2)^2y_1^{1/2}y_2^{1/2} \tag{A.67}
$$

$$
h'''_{2,1}(x)=(y_1+y_2)\left[h'''_1(x)x+h''_1(x)+2h''_1(x)\right] \tag{A.68}
$$

$$
\Rightarrow h'''_{2,1}(0)=(y_1+y_2)3h''_1(0)=(y_1+y_2)\left[-\frac{3}{16}\left(y_1^2-2y_1y_2+y_2^2\right)\right]y_1^{1/2}y_2^{1/2} \tag{A.69}
$$

Therefore

$$
h_{2,1}(x)=h_{2,1}(0)+h'_{2,1}(0)x+\frac{1}{2}h''_{2,1}(0)x^2+\frac{1}{6}h'''_{2,1}(0)x^3+\mathcal{O}(x^4)
$$

$$= y_1^{1/2} y_2^{1/2} (y_1 + y_2) \left[x + \frac{1}{4}(y_1 + y_2)x^2 - \frac{1}{32}\left(y_1^2 - 2y_1 y_2 + y_2^2\right) x^3 + \mathcal{O}(x^4) \right] \quad \text{(A.70)}$$

Then we define $h_{2,2}(x) \equiv \left(y_1 + \frac{1}{2}xy_1^2\right)^{1/2} \left(y_2 + \frac{1}{2}xy_2^2\right)^{1/2} x^2 y_1 y_2 = h_1(x)x^2 y_1 y_2$ and thereby we find

$$h'_{2,2}(x) = y_1 y_2 \left[h'_1(x)x^2 + 2xh_1(x) \right] \quad \text{(A.71)}$$

$$\Rightarrow h'_{2,2}(0) = 0 \quad \text{(A.72)}$$

$$h''_{2,2}(x) = y_1 y_2 \left[h''_1(x)x^2 + 2xh'_1(x) + 2h_1(x) + 2xh'_1(x) \right] \quad \text{(A.73)}$$

$$\Rightarrow h''_{2,2}(0) = y_1 y_2 2h_1(0) = 2y_1 y_2 y_1^{1/2} y_2^{1/2} \quad \text{(A.74)}$$

$$h'''_{2,2}(x) = y_1 y_2 \left[h'''_1(x)x^2 + 2xh''_1(x) + 4h'_1(x) + 4xh''_1(x) + 2h'_1(x) \right] \quad \text{(A.75)}$$

$$\Rightarrow h'''_{2,2}(0) = y_1 y_2 6h'_1(0) = \frac{3}{2} y_1 y_2 (y_1 + y_2) y_1^{1/2} y_2^{1/2} \quad \text{(A.76)}$$

So

$$\begin{aligned} h_{2,2}(x) &= h_{2,2}(0) + h'_{2,2}(0)x + \frac{1}{2}h''_{2,2}(0)x^2 + \frac{1}{6}h'''_{2,2}(0)x^3 + \mathcal{O}(x^4) \\ &= y_1^{1/2} y_2^{1/2} y_1 y_2 \left[x^2 + \frac{1}{4}(y_1 + y_2)x^3 + \mathcal{O}(x^4) \right] \end{aligned} \quad \text{(A.77)}$$

We thus obtain

$$\begin{aligned} h_2(x) &\equiv h_{2,1}(x) + h_{2,2}(x) \\ &= y_1^{1/2} y_2^{1/2} (y_1 + y_2)x + y_1^{1/2} y_2^{1/2} \frac{1}{4}\left(y_1^2 + 6y_1 y_2 + y_2^2\right) x^2 \\ &\quad - y_1^{1/2} y_2^{1/2} \frac{1}{32}\left(y_1^3 - 9y_1^2 y_2 - 9y_1 y_2^2 + y_2^3\right) x^3 + \mathcal{O}(x^4) \end{aligned} \quad \text{(A.78)}$$

Therefore, we can express (A.63) as

$$\begin{aligned} &\left[\int_0^\infty dy_1\ y_1^{1/2} y_1 e^{-y_1} \int_0^\infty dy_2\ y_2^{1/2} e^{-y_2} + \int_0^\infty dy_1\ y_1^{1/2} e^{-y_1} \int_0^\infty dy_2\ y_2^{1/2} y_2 e^{-y_2} \right] x \\ &+ \frac{1}{4}\left[\int_0^\infty dy_1\ y_1^{1/2} y_1^2 e^{-y_1} \int_0^\infty dy_2\ y_2^{1/2} e^{-y_2} + 6\int_0^\infty dy_1\ y_1^{1/2} y_1 e^{-y_1} \int_0^\infty dy_2\ y_2^{1/2} y_2 e^{-y_2} \right. \\ &\left. + \int_0^\infty dy_1\ y_1^{1/2} e^{-y_1} \int_0^\infty dy_2\ y_2^{1/2} y_2^2 e^{-y_2} \right] x^2 - \frac{1}{32}\left[\int_0^\infty dy_1\ y_1^{1/2} y_1^3 e^{-y_1} \int_0^\infty dy_2\ y_2^{1/2} e^{-y_2} \right. \\ &- 9\int_0^\infty dy_1\ y_1^{1/2} y_1^2 e^{-y_1} \int_0^\infty dy_2\ y_2^{1/2} y_2 e^{-y_2} - 9\int_0^\infty dy_1\ y_1^{1/2} y_1 e^{-y_1} \int_0^\infty dy_2\ y_2^{1/2} y_2^2 e^{-y_2} \\ &\left. + \int_0^\infty dy_1\ y_1^{1/2} e^{-y_1} \int_0^\infty dy_2\ y_2^{1/2} y_2^3 e^{-y_2} \right] x^3 + \mathcal{O}(x^4) \end{aligned}$$

$$= \left(\frac{3\pi^{1/2}}{4}\frac{\pi^{1/2}}{2} + \frac{\pi^{1/2}}{2}\frac{3\pi^{1/2}}{4}\right)x + \frac{1}{4}\left(\frac{15\pi^{1/2}}{8}\frac{\pi^{1/2}}{2} + 6\frac{3\pi^{1/2}}{4}\frac{3\pi^{1/2}}{4} + \frac{\pi^{1/2}}{2}\frac{15\pi^{1/2}}{8}\right)x^2$$
$$- \frac{1}{32}\left(\frac{105\pi^{1/2}}{16}\frac{\pi^{1/2}}{2} - 9\frac{15\pi^{1/2}}{8}\frac{3\pi^{1/2}}{4} - 9\frac{3\pi^{1/2}}{4}\frac{15\pi^{1/2}}{8} + \frac{\pi^{1/2}}{2}\frac{105\pi^{1/2}}{16}\right)x^3 + \mathcal{O}(x^4)$$
$$= \frac{3\pi}{128}\left(32x + 56x^2 + 25x^3 + \mathcal{O}(x^4)\right) \tag{A.79}$$

where we used (A.26), (A.30), (A.32) and (A.34).

Third integral

Here, the integral to compute is

$$\int_0^\infty dy_1 dy_2 \ \left(y_1 + \frac{1}{2}xy_1^2\right)^{1/2}\left(y_2 + \frac{1}{2}xy_2^2\right)^{1/2} e^{-y_1}e^{-y_2}$$
$$\times \left(\frac{x^2}{2}(y_1+y_2)^2 + \frac{2}{3}x^2\left(y_1 + \frac{1}{2}xy_1^2\right)\left(y_2 + \frac{1}{2}xy_2^2\right) + x^3(y_1+y_2)y_1y_2\right) \tag{A.80}$$

In the same manner as in the calculation of the second integral, we can define $h_{3,1}(x) \equiv \left(y_1 + \frac{1}{2}xy_1^2\right)^{1/2}\left(y_2 + \frac{1}{2}xy_2^2\right)^{1/2}\frac{x^2}{2}(y_1+y_2)^2 = h_1(x)\frac{x^2}{2}(y_1+y_2)^2$ and then we derive what follows:

$$h'_{3,1}(x) = \frac{1}{2}(y_1+y_2)^2\left[h'_1(x)x^2 + 2xh_1(x)\right] \tag{A.81}$$
$$\Rightarrow h'_{3,1}(0) = 0 \tag{A.82}$$

$$h''_{3,1}(x) = \frac{1}{2}(y_1+y_2)^2\left[h''_1(x)x^2 + 2xh'_1(x) + 2h_1(x) + 2xh'_1(x)\right] \tag{A.83}$$
$$\Rightarrow h''_{3,1}(0) = \frac{1}{2}(y_1+y_2)^2 2h_1(0) = (y_1+y_2)^2 y_1^{1/2}y_2^{1/2} \tag{A.84}$$

$$h'''_{3,1}(x) = \frac{1}{2}(y_1+y_2)^2\left[h'''_1(x)x^2 + 2xh''_1(x) + 4h'_1(x) + 4xh''_1(x) + 2h'_1(x)\right] \tag{A.85}$$
$$\Rightarrow h'''_{3,1}(0) = \frac{1}{2}(y_1+y_2)^2 6h'_1(0) = \frac{3}{4}(y_1+y_2)^3 y_1^{1/2}y_2^{1/2} \tag{A.86}$$

which implies that

$$h_{3,1}(x) = h_{3,1}(0) + h'_{3,1}(0)x + \frac{1}{2}h''_{3,1}(0)x^2 + \frac{1}{6}h'''_{3,1}(0)x^3 + \mathcal{O}(x^4)$$
$$= y_1^{1/2}y_2^{1/2}(y_1+y_2)^2\left[\frac{1}{2}x^2 + \frac{1}{8}(y_1+y_2)x^3 + \mathcal{O}(x^4)\right] \tag{A.87}$$

Next we define $h_{3,2}(x) \equiv \left(y_1 + \frac{1}{2}xy_1^2\right)^{1/2}\left(y_2 + \frac{1}{2}xy_2^2\right)^{1/2}\frac{2}{3}x^2\left(y_1 + \frac{1}{2}xy_1^2\right)\left(y_2 + \frac{1}{2}xy_2^2\right) = h_1^3(x)\frac{2}{3}x^2$ and compute its derivatives:

$$h'_{3,2}(x) = 3h_1^2(x)h'_1(x)\frac{2}{3}x^2 + h_1^3(x)\frac{4}{3}x \tag{A.88}$$
$$\Rightarrow h'_{3,2}(0) = 0 \tag{A.89}$$

$$h''_{3,2}(x) = 4h_1(x)(h'_1)^2(x)x^2 + 2h_1^2(x)h''_1(x)x^2 + 4h_1^2(x)h'_1(x)x + 4h_1^2(x)h'_1(x)x + \frac{4}{3}h_1^3(x) \tag{A.90}$$
$$\Rightarrow h''_{3,2}(0) = \frac{4}{3}h_1^3(0) = \frac{4}{3}y_1y_2y_1^{1/2}y_2^{1/2} \tag{A.91}$$

$$\begin{aligned} h'''_{3,2}(x) = {} & 4(h'_1)^3(x)x^2 + 8h_1(x)h'_1(x)h''_1(x)x^2 + 8h_1(x)(h'_1)^2(x)x + 4h_1(x)h'_1(x)h''_1(x)x^2 \\ & + 2h_1^2(x)h'''_1(x)x^2 + 4h_1^2(x)h''_1(x)x + 16h_1(x)(h'_1)^2(x)x + 8h_1^2(x)h''_1(x)x \\ & + 8h_1^2(x)h'_1(x) + 4h_1^2(x)h'_1(x) \end{aligned} \tag{A.92}$$
$$\Rightarrow h'''_{3,2}(0) = 12h_1^2(0)h'_1(0) = 3y_1y_2(y_1+y_2)y_1^{1/2}y_2^{1/2} \tag{A.93}$$

and thus

$$\begin{aligned} h_{3,2}(x) &= h_{3,2}(0) + h'_{3,2}(0)x + \frac{1}{2}h''_{3,2}(0)x^2 + \frac{1}{6}h'''_{3,2}(0)x^3 + \mathcal{O}(x^4) \\ &= y_1^{1/2}y_2^{1/2}y_1y_2\left[\frac{2}{3}x^2 + \frac{1}{2}(y_1+y_2)x^3 + \mathcal{O}(x^4)\right] \end{aligned} \tag{A.94}$$

We can then define $h_{3,3}(x) \equiv \left(y_1 + \frac{1}{2}xy_1^2\right)^{1/2}\left(y_2 + \frac{1}{2}xy_2^2\right)^{1/2}x^3(y_1+y_2)y_1y_2 = h_1(x)x^3(y_1+y_2)y_1y_2$ and so we have

$$h'_{3,3}(x) = (y_1+y_2)y_1y_2\left[h'_1(x)x^3 + h_1(x)3x^2\right] \tag{A.95}$$
$$\Rightarrow h'_{3,3}(0) = 0 \tag{A.96}$$

$$h''_{3,3}(x) = (y_1+y_2)y_1y_2\left[h''_1(x)x^3 + h'_1(x)3x^2 + h'_1(x)3x^2 + h_1(x)6x\right] \tag{A.97}$$
$$\Rightarrow h''_{3,3}(0) = 0 \tag{A.98}$$

$$\begin{aligned} h'''_{3,3}(x) = {} & (y_1+y_2)y_1y_2\Big[h'''_1(x)x^3 + h''_1(x)3x^2 + 2h''_1(x)3x^2 + 2h'_1(x)6x \\ & + h'_1(x)6x + 6h_1(x)\Big] \end{aligned} \tag{A.99}$$
$$\Rightarrow h'''_{3,3}(0) = (y_1+y_2)y_1y_2 6h_1(0) = 6(y_1+y_2)y_1y_2y_1^{1/2}y_2^{1/2} \tag{A.100}$$

Thus

$$\begin{aligned} h_{3,3}(x) &= h_{3,3}(0) + h'_{3,3}(0)x + \frac{1}{2}h''_{3,3}(0)x^2 + \frac{1}{6}h'''_{3,3}(0)x^3 + \mathcal{O}(x^4) \\ &= y_1^{1/2}y_2^{1/2}(y_1+y_2)y_1y_2x^3 + \mathcal{O}(x^4) \end{aligned} \tag{A.101}$$

and then

$$\begin{aligned} h_3(x) &\equiv h_{3,1}(x) + h_{3,2}(x) + h_{3,3}(x) \\ &= y_1^{1/2} y_2^{1/2} \frac{1}{6} \left(3y_1^2 + 10y_1y_2 + 3y_2^2\right) x^2 \\ &\quad + y_1^{1/2} y_2^{1/2} \frac{1}{8} \left(y_1^3 + 15y_1^2y_2 + 15y_1y_2^2 + y_2^3\right) x^3 + \mathcal{O}(x^4) \end{aligned} \tag{A.102}$$

It follows that (A.80) can be written as

$$\begin{aligned} &\frac{1}{6}\Bigg[3\int_0^\infty dy_1\ y_1^{1/2}y_1^2e^{-y_1}\int_0^\infty dy_2\ y_2^{1/2}e^{-y_2} + 10\int_0^\infty dy_1\ y_1^{1/2}y_1e^{-y_1}\int_0^\infty dy_2\ y_2^{1/2}y_2e^{-y_2} \\ &+ 3\int_0^\infty dy_1\ y_1^{1/2}e^{-y_1}\int_0^\infty dy_2\ y_2^{1/2}y_2^2e^{-y_2}\Bigg]x^2 + \frac{1}{8}\Bigg[\int_0^\infty dy_1\ y_1^{1/2}y_1^3e^{-y_1}\int_0^\infty dy_2\ y_2^{1/2}e^{-y_2} \\ &+ 15\int_0^\infty dy_1\ y_1^{1/2}y_1^2e^{-y_1}\int_0^\infty dy_2\ y_2^{1/2}y_2e^{-y_2} + 15\int_0^\infty dy_1\ y_1^{1/2}y_1e^{-y_1}\int_0^\infty dy_2\ y_2^{1/2}y_2^2e^{-y_2} \\ &+ \int_0^\infty dy_1\ y_1^{1/2}e^{-y_1}\int_0^\infty dy_2\ y_2^{1/2}y_2^3e^{-y_2}\Bigg]x^3 + \mathcal{O}(x^4) \\ &= \frac{1}{6}\left(3\frac{15\pi^{1/2}}{8}\frac{\pi^{1/2}}{2} + 10\frac{3\pi^{1/2}}{4}\frac{3\pi^{1/2}}{4} + 3\frac{\pi^{1/2}}{2}\frac{15\pi^{1/2}}{8}\right)x^2 \\ &\quad + \frac{1}{8}\left(\frac{105\pi^{1/2}}{16}\frac{\pi^{1/2}}{2} + 15\frac{15\pi^{1/2}}{8}\frac{3\pi^{1/2}}{4} + 15\frac{3\pi^{1/2}}{4}\frac{15\pi^{1/2}}{8} + \frac{\pi^{1/2}}{2}\frac{105\pi^{1/2}}{16}\right)x^3 + \mathcal{O}(x^4) \\ &= \frac{15\pi}{32}\left(4x^2 + 13x^3 + \mathcal{O}(x^4)\right) \end{aligned} \tag{A.103}$$

where we used (A.26), (A.30), (A.32) and (A.34).

Fourth integral

Finally, we deal with the last part of (A.53), namely

$$\begin{aligned} &\int_0^\infty dy_1dy_2\ \left(y_1 + \frac{1}{2}xy_1^2\right)^{1/2}\left(y_2 + \frac{1}{2}xy_2^2\right)^{1/2} e^{-y_1}e^{-y_2} \\ &\qquad \times \left(\frac{x^3}{4}(y_1+y_2)^3 + x^3(y_1+y_2)\left(y_1 + \frac{1}{2}xy_1^2\right)\left(y_2 + \frac{1}{2}xy_2^2\right)\right) \end{aligned} \tag{A.104}$$

To calculate this integral, we define $h_{4,1} \equiv \left(y_1 + \frac{1}{2}xy_1^2\right)^{1/2}\left(y_2 + \frac{1}{2}xy_2^2\right)^{1/2}\frac{x^3}{4}(y_1+y_2)^3$ $= h_1(x)\frac{x^3}{4}(y_1+y_2)^3$. We then obtain

$$h'_{4,1}(x) = \frac{1}{4}(y_1+y_2)^3\left[h'_1(x)x^3 + h_1(x)3x^2\right] \tag{A.105}$$

$$\Rightarrow h'_{4,1}(0) = 0 \tag{A.106}$$

$$h''_{4,1}(x) = \frac{1}{4}(y_1+y_2)^3\left[h''_1(x)x^3 + h'_1(x)3x^2 + h'_1(x)3x^2 + h_1(x)6x\right] \tag{A.107}$$
$$\Rightarrow h''_{4,1}(0) = 0 \tag{A.108}$$

$$h'''_{4,1}(x) = \frac{1}{4}(y_1+y_2)^3\Big[h'''_1(x)x^3 + h''_1(x)3x^2 + 2h''_1(x)3x^2 + 2h'_1(x)6x + h'_1(x)6x + 6h_1(x)\Big] \tag{A.109}$$
$$\Rightarrow h'''_{4,1}(0) = \frac{3}{2}(y_1+y_2)^3 h_1(0) = \frac{3}{2}(y_1+y_2)^3 y_1^{1/2} y_2^{1/2} \tag{A.110}$$

Thus

$$\begin{aligned} h_{4,1}(x) &= h_{4,1}(0) + h'_{4,1}(0)x + \frac{1}{2}h''_{4,1}(0)x^2 + \frac{1}{6}h'''_{4,1}(0)x^3 + \mathcal{O}(x^4) \\ &= y_1^{1/2}y_2^{1/2}\frac{1}{4}(y_1+y_2)^3x^3 + \mathcal{O}(x^4) \end{aligned} \tag{A.111}$$

We now define $h_{4,2} \equiv \left(y_1 + \frac{1}{2}xy_1^2\right)^{1/2}\left(y_2 + \frac{1}{2}xy_2^2\right)^{1/2} x^3(y_1+y_2)\left(y_1+\frac{1}{2}xy_1^2\right)\left(y_2+\frac{1}{2}xy_2^2\right)$ $= h_1^3(x)x^3(y_1+y_2)$ that we derive:

$$h'_{4,2}(x) = (y_1+y_2)\left[3h_1^2(x)h'_1(x)x^3 + h_1^3(x)3x^2\right] \tag{A.112}$$
$$\Rightarrow h'_{4,2}(0) = 0 \tag{A.113}$$

$$\begin{aligned} h''_{4,2}(x) = (y_1+y_2)\Big[&6h_1(x)(h'_1)^2(x)x^3 + 3h_1^2(x)h''_1(x)x^3 + 3h_1^2(x)h'_1(x)3x^2 \\ &+ 3h_1^2(x)h'_1(x)3x^2 + h_1^3(x)6x\Big] \end{aligned} \tag{A.114}$$
$$\Rightarrow h''_{4,2}(0) = 0 \tag{A.115}$$

$$\begin{aligned} h'''_{4,2}(x) = (y_1+y_2)\Big[&6(h'_1)^3(x)x^3 + 12h_1(x)h'_1(x)h''_1(x)x^3 + 6h_1(x)(h'_1)^2(x)3x^2 \\ &+ 6h_1(x)h'_1(x)h''_1(x)x^3 + 3h_1^2(x)h'''_1(x)x^3 + 3h_1^2(x)h''_1(x)3x^2 \\ &+ 12h_1(x)(h'_1)^2(x)3x^2 + 6h_1^2(x)h''_1(x)3x^2 + 6h_1^2(x)h'_1(x)6x \\ &+ 3h_1^2(x)h'_1(x)6x + 6h_1^3(x)\Big] \end{aligned} \tag{A.116}$$
$$\Rightarrow h'''_{4,2}(0) = 6(y_1+y_2)h_1^3(0) = 6(y_1+y_2)y_1y_2y_1^{1/2}y_2^{1/2} \tag{A.117}$$

Thereby

$$\begin{aligned} h_{4,2}(x) &= h_{4,2}(0) + h'_{4,2}(0)x + \frac{1}{2}h''_{4,2}(0)x^2 + \frac{1}{6}h'''_{4,2}(0)x^3 + \mathcal{O}(x^4) \\ &= y_1^{1/2}y_2^{1/2}y_1y_2(y_1+y_2)x^3 + \mathcal{O}(x^4) \end{aligned} \tag{A.118}$$

At the end, we find

$$h_4(x) \equiv h_{4,1}(x) + h_{4,2}(x) = \frac{1}{4}y_1^{1/2}y_2^{1/2}\left(y_1^3 + 7y_1^2y_2 + 7y_1y_2^2 + y_2^3\right)x^3 + \mathcal{O}(x^4) \tag{A.119}$$

Therefore (A.104) can be expressed as

$$\frac{1}{4}\Bigg[\int_0^\infty dy_1\ y_1^{1/2}y_1^3e^{-y_1}\int_0^\infty dy_2\ y_2^{1/2}e^{-y_2}+7\int_0^\infty dy_1\ y_1^{1/2}y_1^2e^{-y_1}\int_0^\infty dy_2\ y_2^{1/2}y_2e^{-y_2}$$
$$+7\int_0^\infty dy_1\ y_1^{1/2}y_1e^{-y_1}\int_0^\infty dy_2\ y_2^{1/2}y_2^2e^{-y_2}+\int_0^\infty dy_1\ y_1^{1/2}e^{-y_1}\int_0^\infty dy_2\ y_2^{1/2}y_2^3e^{-y_2}\Bigg]x^3$$
$$+\mathcal{O}(x^4) \tag{A.120}$$
$$=\frac{1}{4}\left(\frac{105\pi^{1/2}}{16}\frac{\pi^{1/2}}{2}+7\frac{15\pi^{1/2}}{8}\frac{3\pi^{1/2}}{4}+7\frac{3\pi^{1/2}}{4}\frac{15\pi^{1/2}}{8}+\frac{\pi^{1/2}}{2}\frac{105\pi^{1/2}}{16}\right)x^3+\mathcal{O}(x^4) \tag{A.121}$$
$$=\frac{105\pi}{16}x^3+\mathcal{O}(x^4) \tag{A.122}$$

where (A.26), (A.30), (A.32) and (A.34) were used.
We can eventually compute (A.53):

$$\Bigg[2w(s)\frac{\pi}{4}\left(1+\frac{3}{4}x-\frac{3}{32}x^2+\frac{15}{128}x^3\right)+w'(s)\frac{3\pi}{128}\left(32x+56x^2+25x^3\right)+$$
$$\frac{w''(s)}{2}\frac{15\pi}{32}(4x^2+13x^3)+\frac{w'''(s)}{6}\frac{105\pi}{16}x^3+\mathcal{O}(x^4)\Bigg] \tag{A.123}$$

Thus, injecting the latter result in (3.69) we obtain

$$\begin{aligned}\langle\sigma v_{\rm rel}\rangle =&\frac{2}{\pi M^2}\left[1-\frac{15}{4}x+\frac{285}{32}x^2-\frac{2115}{128}x^3\right]\Bigg[2w(s)\frac{\pi}{4}\left(1+\frac{3}{4}x-\frac{3}{32}x^2+\frac{15}{128}x^3\right)\\
&+w'(s)\frac{3\pi}{128}\left(32x+56x^2+25x^3\right)+\frac{w''(s)}{2}\frac{15\pi}{32}(4x^2+13x^3)+\frac{w'''(s)}{6}\frac{105\pi}{16}x^3\\
&+\mathcal{O}(x^4)\Bigg]_{\frac{s}{4M^2}=1}\\
=&\frac{1}{M^2}\Bigg[\left(1+\frac{3}{4}x-\frac{3}{32}x^2+\frac{15}{128}x^3-\frac{15}{4}x-\frac{45}{16}x^2+\frac{45}{128}x^3+\frac{285}{32}x^2+\frac{855}{128}x^3\right.\\
&\left.-\frac{2115}{128}x^3\right)w(s)+\left(\frac{96}{64}x+\frac{168}{64}x^2+\frac{75}{64}x^3-\frac{1440}{256}x^2-\frac{2520}{256}x^3+\frac{855}{64}x^3\right)w'(s)\\
&+\left(\frac{60}{32}x^2+\frac{195}{32}x^3-\frac{900}{128}x^3\right)w''(s)+\frac{35}{16}x^3w'''(s)+\mathcal{O}(x^4)\Bigg]_{\frac{s}{4M^2}=1}\\
=&\frac{1}{M^2}\Bigg[w(s)+\left(-3w(s)+\frac{3}{2}w'(s)\right)x+\left(6w(s)-3w'(s)+\frac{15}{8}w''(s)\right)x^2\\
&+\Big(-\frac{75}{8}w(s)+\frac{75}{16}w'(s)-\frac{15}{16}w''(s)+\frac{35}{16}w'''(s)\Big)x^3+\mathcal{O}(x^4)\Bigg]_{\frac{s}{4M^2}=1}\end{aligned}$$

$$=\frac{1}{M^2}\Big[w(s)-\frac{3}{2}\left(2w(s)-w'(s)\right)x+\frac{3}{8}\left(16w(s)-8w'(s)+5w''(s)\right)$$
$$-\frac{5}{16}(30w(s)-15w'(s)+3w''(s)-7w'''(s))+\mathcal{O}(x^4)\Big]_{\frac{s}{4M^2}=1} \tag{A.124}$$

Final form of the thermally averaged annihilation cross section

Let us compute the derivatives of

$$w(s)=\sum_f\left(1-\frac{4m_f^2}{s}\right)^{1/2}\left[C_{0f}+C_{1f}\frac{s}{4M^2}+C_{2f}\left(\frac{s}{4M^2}\right)^2\right] \tag{A.125}$$

First of all we have

$$\begin{aligned} w(s)\Big|_{\frac{s}{4M^2}=1} &= \sum_f\left(1-\frac{m_f^2}{M^2}\right)^{1/2}\left(C_{0f}+C_{1f}+C_{2f}\right) \\ &= \sum_f K_f\left(C_{0f}+C_{1f}+C_{2f}\right) \\ &= \sum_f K_f a_f \end{aligned} \tag{A.126}$$

where we have defined $K_f\equiv\left(1-\frac{m_f^2}{M^2}\right)^{1/2}$ for convenience.

First derivative

Here we calculate the three first derivatives of (A.125):

$$\begin{aligned} \left[\frac{d}{d\frac{s}{4M^2}}\left(1-\frac{4m_f^2}{s}\right)^{1/2}\right]_{\frac{s}{4M^2}=1} &= 4M^2\frac{1}{2}\frac{4m_f^2}{s^2}\left(1-\frac{4m_f^2}{s}\right)^{-1/2}\Bigg|_{\frac{s}{4M^2}=1} \\ &= K_f\frac{1}{2}\frac{m_f^2}{M^2}\left(1-\frac{m_f^2}{M^2}\right)^{-1} \\ &= K_f\frac{m_f^2}{2\left(M^2-m_f^2\right)} \end{aligned} \tag{A.127}$$

$$\begin{aligned} \left[\frac{d}{d\frac{s}{4M^2}}\left(\left(1-\frac{4m_f^2}{s}\right)^{1/2}\frac{s}{4M^2}\right)\right]_{\frac{s}{4M^2}=1} &= K_f\frac{m_f^2}{2\left(M^2-m_f^2\right)}+K_f \\ &= K_f\left(\frac{m_f^2}{2\left(M^2-m_f^2\right)}+1\right) \end{aligned} \tag{A.128}$$

$$\left[\frac{d}{d\frac{s}{4M^2}}\left(\left(1-\frac{4m_f^2}{s}\right)^{1/2}\left(\frac{s}{4M^2}\right)^2\right)\right]_{\frac{s}{4M^2}=1} = K_f\frac{m_f^2}{2\left(M^2-m_f^2\right)}+2K_f$$
$$= K_f\left(\frac{m_f^2}{2\left(M^2-m_f^2\right)}+2\right) \tag{A.129}$$

Therefore

$$w'(s)\Big|_{\frac{s}{4M^2}=1} = \sum_f K_f\left[\frac{m_f^2}{2\left(M^2-m_f^2\right)}C_{0f}+\left(\frac{m_f^2}{2\left(M^2-m_f^2\right)}+1\right)C_{1f}\right.$$
$$\left.+\left(\frac{m_f^2}{2\left(M^2-m_f^2\right)}+2\right)C_{2f}\right]$$
$$= \sum_f K_f\left[\frac{\beta_f}{2}C_{0f}+\left(\frac{\beta_f}{2}+1\right)C_{1f}+\left(\frac{\beta_f}{2}+2\right)C_{2f}\right] \tag{A.130}$$

with $\beta_f \equiv \frac{m_f^2}{M^2-m_f^2}$.

Second derivative

Now we can compute the three second derivatives of (A.125):

$$\left[\frac{d^2}{d\left(\frac{s}{4M^2}\right)^2}\left(1-\frac{4m_f^2}{s}\right)^{1/2}\right]_{\frac{s}{4M^2}=1}$$
$$= \left[\frac{\left(4M^2\right)^2 4m_f^2}{2}\left(1-\frac{4m_f^2}{s}\right)^{-1/2}\frac{-2}{s^3}+\frac{\left(4M^2\right)^2 4m_f^2}{2s^2}\frac{-1}{2}\frac{4m_f^2}{s^2}\left(1-\frac{4m_f^2}{s}\right)^{-3/2}\right]_{\frac{s}{4M^2}=1}$$
$$= K_f\left[-\frac{\left(4M^2\right)^2 4m_f^2}{\left(4M^2\right)^3}\left(1-\frac{m_f^2}{M^2}\right)^{-1}-\frac{1}{4}\frac{\left(4M^2\right)^2\left(4m_f^2\right)^2}{\left(4M^2\right)^2\left(4M^2\right)^2}\left(1-\frac{m_f^2}{M^2}\right)^{-2}\right]$$
$$= K_f\frac{-m_f^2}{M^2}\left(1-\frac{m_f^2}{M^2}\right)^{-1}\left[1+\frac{m_f^2}{4M^2}\left(1-\frac{m_f^2}{M^2}\right)^{-1}\right]$$
$$= K_f\frac{-m_f^2}{\left(M^2-m_f^2\right)}\left[1+\frac{m_f^2}{4\left(M^2-m_f^2\right)}\right] \tag{A.131}$$

Then, using

$$\frac{d^n}{dx^n}(fg)(x) = \sum_{k=0}^{n}\frac{n!}{k!(n-k)!}\frac{d^{n-k}f}{dx^{n-k}}\frac{d^k g}{dx^k}, \tag{A.132}$$

we obtain

$$\begin{aligned}
&\left[\frac{d^2}{d\left(\frac{s}{4M^2}\right)^2}\left(\left(1-\frac{4m_f^2}{s}\right)^{1/2}\frac{s}{4M^2}\right)\right]_{\frac{s}{4M^2}=1}\\
&=\left[\frac{d^2}{d\left(\frac{s}{4M^2}\right)^2}\left(\left(1-\frac{4m_f^2}{s}\right)^{1/2}\right)\frac{s}{4M^2}\right]_{\frac{s}{4M^2}=1}\\
&\quad+2\left[\frac{d}{d\frac{s}{4M^2}}\left(\left(1-\frac{4m_f^2}{s}\right)^{1/2}\right)\frac{d}{d\frac{s}{4M^2}}\left(\frac{s}{4M^2}\right)\right]_{\frac{s}{4M^2}=1}\\
&=K_f\frac{-m_f^2}{\left(M^2-m_f^2\right)}\left[1+\frac{m_f^2}{4\left(M^2-m_f^2\right)}\right]+2K_f\left(\frac{m_f^2}{2\left(M^2-m_f^2\right)}\right)\\
&=K_f\left[-\frac{m_f^2}{M^2-m_f^2}\frac{m_f^2}{4\left(M^2-m_f^2\right)}\right]
\end{aligned}\tag{A.133}$$

and

$$\begin{aligned}
&\left[\frac{d^2}{d\left(\frac{s}{4M^2}\right)^2}\left(\left(1-\frac{4m_f^2}{s}\right)^{1/2}\left(\frac{s}{4M^2}\right)^2\right)\right]_{\frac{s}{4M^2}=1}\\
&=\left[\frac{d^2}{d\left(\frac{s}{4M^2}\right)^2}\left(\left(1-\frac{4m_f^2}{s}\right)^{1/2}\frac{s}{4M^2}\right)\frac{s}{4M^2}\right]_{\frac{s}{4M^2}=1}\\
&\quad+2\left[\frac{d}{d\frac{s}{4M^2}}\left(\left(1-\frac{4m_f^2}{s}\right)^{1/2}\frac{s}{4M^2}\right)\frac{d}{d\frac{s}{4M^2}}\left(\frac{s}{4M^2}\right)\right]_{\frac{s}{4M^2}=1}\\
&=K_f\left[-\frac{m_f^2}{M^2-m_f^2}\frac{m_f^2}{4\left(M^2-m_f^2\right)}\right]+2K_f\left(\frac{m_f^2}{2\left(M^2-m_f^2\right)}+1\right)\\
&=K_f\left[2-\frac{m_f^2}{M^2-m_f^2}\left(-1+\frac{m_f^2}{4\left(M^2-m_f^2\right)}\right)\right]
\end{aligned}\tag{A.134}$$

Thus we have

$$\begin{aligned}
w''(s)\Big|_{\frac{s}{4M^2}=1}&=\sum_f K_f\left[\frac{-m_f^2}{M^2-m_f^2}\left[1+\frac{m_f^2}{4\left(M^2-m_f^2\right)}\right]C_{0f}-\frac{1}{4}\left(\frac{m_f^2}{M^2-m_f^2}\right)^2C_{1f}\right.\\
&\qquad\left.+\left(2-\frac{m_f^2}{M^2-m_f^2}\left(-1+\frac{m_f^2}{4\left(M^2-m_f^2\right)}\right)\right)C_{2f}\right]\\
&=\sum_f K_f\left[-\beta_f\left(1+\frac{\beta_f}{4}\right)C_{0f}-\frac{\beta_f^2}{4}C_{1f}+\left(2-\beta_f\left(-1+\frac{\beta_f}{4}\right)\right)C_{2f}\right]
\end{aligned}\tag{A.135}$$

Third derivative

In this part we deal with the last set of three derivatives:

$$
\begin{aligned}
&\left[\frac{d^3}{d\left(\frac{s}{4M^2}\right)^3}\left(1-\frac{4m_f^2}{s}\right)^{1/2}\right]_{\frac{s}{4M^2}=1}\\
&=\left[\left(4M^2\right)^3 4m_f^2\left(1-\frac{4m_f^2}{s}\right)^{-1/2}\frac{3}{s^4}+\frac{\left(4M^2\right)^3 4m_f^2}{s^3}\frac{1}{2}\left(1-\frac{4m_f^2}{s}\right)^{-3/2}\frac{4m_f^2}{s^2}\right.\\
&\quad\left.+\frac{\left(4M^2\right)^3\left(4m_f^2\right)^2}{4}\left(1-\frac{4m_f^2}{s}\right)^{-3/2}\frac{4}{s^5}+\frac{\left(4M^2\right)^3\left(4m_f^2\right)^2}{4s^4}\frac{3}{2}\left(1-\frac{4m_f^2}{s}\right)^{-5/2}\frac{4m_f^2}{s^2}\right]_{\frac{s}{4M^2}=1}\\
&=\frac{\left(4M^2\right)^3 12m_f^2}{\left(4M^2\right)^4}\left(1-\frac{m_f^2}{M^2}\right)^{-1/2}+\frac{\left(4M^2\right)^3 8m_f^4}{\left(4M^2\right)^5}\left(1-\frac{m_f^2}{M^2}\right)^{-3/2}\\
&\quad+\frac{\left(4M^2\right)^3 16m_f^4}{\left(4M^2\right)^5}\left(1-\frac{m_f^2}{M^2}\right)^{-3/2}+\frac{\left(4M^2\right)^3 24m_f^6}{\left(4M^2\right)^6}\left(1-\frac{m_f^2}{M^2}\right)^{-5/2}\\
&=K_f\left(\frac{3m_f^2}{M^2-m^2}+\frac{3m_f^4}{2\left(M^2-m^2\right)^2}+\frac{3m_f^6}{8\left(M^2-m^2\right)^3}\right)
\end{aligned}
\tag{A.136}
$$

$$
\begin{aligned}
&\left[\frac{d^3}{d\left(\frac{s}{4M^2}\right)^3}\left(\left(1-\frac{4m_f^2}{s}\right)^{1/2}\frac{s}{4M^2}\right)\right]_{\frac{s}{4M^2}=1}\\
&=\left[\frac{d^3}{d\left(\frac{s}{4M^2}\right)^3}\left(\left(1-\frac{4m_f^2}{s}\right)^{1/2}\right)\frac{s}{4M^2}\right]_{\frac{s}{4M^2}=1}\\
&\quad+3\left[\frac{d^2}{d\left(\frac{s}{4M^2}\right)^2}\left(\left(1-\frac{4m_f^2}{s}\right)^{1/2}\right)\frac{d}{d\frac{s}{4M^2}}\left(\frac{s}{4M^2}\right)\right]_{\frac{s}{4M^2}=1}\\
&=K_f\frac{3m_f^2}{M^2-m_f^2}\left(1+\frac{m_f^2}{2\left(M^2-m_f^2\right)}+\frac{m_f^4}{8\left(M^2-m_f^2\right)^2}\right)\\
&\quad-3K_f\frac{m_f^2}{M^2-m_f^2}\left(1+\frac{m_f^2}{4\left(M^2-m_f^2\right)}\right)\\
&=K_f\frac{3m_f^2}{M^2-m_f^2}\left(\frac{m_f^2}{4\left(M^2-m_f^2\right)}+\frac{m_f^4}{8\left(M^2-m_f^2\right)^2}\right)
\end{aligned}
\tag{A.137}
$$

$$
\left[\frac{d^3}{d\left(\frac{s}{4M^2}\right)^3}\left(\left(1-\frac{4m_f^2}{s}\right)^{1/2}\left(\frac{s}{4M^2}\right)^2\right)\right]_{\frac{s}{4M^2}=1}
$$

$$
\begin{aligned}
&= \left[\frac{d^3}{d\left(\frac{s}{4M^2}\right)^3}\left(\left(1-\frac{4m_f^2}{s}\right)^{1/2}\frac{s}{4M^2}\right)\frac{s}{4M^2}\right]_{\frac{s}{4M^2}=1} \\
&\quad + 3\left[\frac{d^2}{d\left(\frac{s}{4M^2}\right)^2}\left(\left(1-\frac{4m_f^2}{s}\right)^{1/2}\frac{s}{4M^2}\right)\frac{d}{d\frac{s}{4M^2}}\left(\frac{s}{4M^2}\right)\right]_{\frac{s}{4M^2}=1} \\
&= K_f\frac{3m_f^2}{M^2-m_f^2}\left(\frac{m_f^2}{4\left(M^2-m_f^2\right)}+\frac{m_f^4}{8\left(M^2-m_f^2\right)^2}\right)-3K_f\frac{m_f^4}{4\left(M^2-m_f^2\right)^2} \\
&= K_f\frac{3m_f^2}{M^2-m_f^2}\left(\frac{m_f^4}{8\left(M^2-m_f^2\right)^2}\right)
\end{aligned}
\tag{A.138}
$$

Thereby, we have

$$
\begin{aligned}
w'''(s)\Big|_{\frac{s}{4M^2}=1} &= \sum_f K_f\left[\frac{3m_f^2}{M^2-m_f^2}\left(1+\frac{m_f^2}{2\left(M^2-m_f^2\right)}+\frac{m_f^4}{8\left(M^2-m_f^2\right)^2}\right)C_{0f}\right. \\
&\qquad + \frac{3m_f^2}{M^2-m_f^2}\left(\frac{m_f^2}{4\left(M^2-m_f^2\right)}+\frac{m_f^4}{8\left(M^2-m_f^2\right)^2}\right)C_{1f} \\
&\qquad \left. + \frac{3m_f^2}{M^2-m_f^2}\left(\frac{m_f^4}{8\left(M^2-m_f^2\right)^2}\right)C_{2f}\right] \\
&= \sum_f K_f\left[3\beta_f\left(1+\frac{\beta_f}{2}+\frac{\beta_f^2}{8}\right)C_{0f}+3\beta_f\left(\frac{\beta_f}{4}+\frac{\beta_f^2}{8}\right)C_{1f}+3\beta_f\frac{\beta_f^2}{8}C_{2f}\right]
\end{aligned}
\tag{A.139}
$$

Finally, by injecting (A.126), (A.130), (A.135) and (A.139) in

$$
\begin{aligned}
\frac{1}{M^2}\Big[&w(s)-\frac{3}{2}\left(2w(s)-w'(s)\right)x+\frac{3}{8}\left(16w(s)-8w'(s)+5w''(s)\right)x^2 \\
&-\frac{5}{16}(30w(s)-15w'(s)+3w''(s)-7w'''(s))x^3\Big]_{\frac{s}{4M^2}=1}
\end{aligned}
\tag{A.140}
$$

we obtain

$$
\begin{aligned}
-\frac{3}{2}(2w(s)-w'(s)) &= -\frac{3}{2}\sum_f K_f\left[2C_{0f}+2C_{1f}+2C_{2f}-\frac{\beta_f}{2}C_{0f}-\frac{\beta_f}{2}C_{1f}-C_{1f}\right. \\
&\qquad \left. -\frac{\beta_f}{2}C_{2f}-2C_{2f}\right] \\
&= \sum_f K_f\left[-\frac{3}{2}(2C_{0f}+C_{1f})+\frac{3}{4}\beta_f(C_{0f}+C_{1f}+C_{2f})\right] \\
&= \sum_f K_f b_f
\end{aligned}
\tag{A.141}
$$

$$\begin{aligned}\frac{3}{8}(16w(s)-8w'(s)+5w''(s)) &= \frac{3}{8}\sum_f K_f\Bigg(16C_{0f}+16C_{1f}+16C_{2f}-4\beta_f C_{0f}-4\beta_f C_{1f}\\ &\qquad -8C_{1f}-4\beta_f C_{2f}-16C_{2f}-5\beta_f C_{0f}-\frac{5}{4}\beta_f^2 C_{0f}\\ &\qquad -\frac{5}{4}\beta_f^2 C_{1f}+10C_{2f}+5\beta_f C_{2f}-\frac{5}{4}\beta_f^2 C_{2f}\Bigg)\\ &= \sum_f K_f\Bigg[\frac{3}{4}(8C_{0f}+4C_{1f}+5C_{2f})\\ &\qquad -\frac{3}{8}\beta_f(9C_{0f}+4C_{1f}-C_{2f})\\ &\qquad -\frac{15}{32}\beta_f^2(C_{0f}+C_{1f}+C_{2f})\Bigg]\\ &= \sum_f K_f c_f \end{aligned} \tag{A.142}$$

$$\begin{aligned}&-\frac{5}{16}(30w(s)-15w'(s)+3w''(s)-7w'''(s))\\ &= -\frac{5}{16}\sum_f K_f\Bigg(30C_{0f}+30C_{1f}+30C_{2f}-\frac{15}{2}\beta_f C_{0f}-\frac{15}{2}\beta_f C_{1f}-15C_{1f}-\frac{15}{2}\beta_f C_{2f}\\ &\qquad -30C_{2f}-3\beta_f C_{0f}-\frac{3}{4}\beta_f^2 C_{0f}-\frac{3}{4}\beta_f^2 C_{1f}+6C_{2f}+3\beta_f C_{2f}-\frac{3}{4}\beta_f^2 C_{2f}\\ &\qquad -21\beta_f C_{0f}-\frac{21}{2}\beta_f^2 C_{0f}-\frac{21}{8}\beta_f^3 C_{0f}-\frac{21}{4}\beta_f^2 C_{1f}-\frac{21}{8}\beta_f^3 C_{1f}-\frac{21}{8}\beta_f^3 C_{2f}\Bigg)\\ &= \sum_f K_f\Bigg[-\frac{15}{16}(10C_{0f}+5C_{1f}+2C_{2f})+\frac{15}{32}\beta_f(21C_{0f}+5C_{1f}+3C_{2f})\\ &\qquad +\frac{15}{64}\beta_f^2(15C_{0f}+8C_{1f}+C_{2f})+\frac{105}{128}\beta_f^3(C_{0f}+C_{1f}+C_{2f})\Bigg]\\ &= \sum_f K_f d_f \end{aligned} \tag{A.143}$$

Expression of the coefficients in $w(s)$

In this section, we will compute the coefficients C_{0f}, C_{1f} and C_{2f} of the $\chi_f\bar{\chi}_f \to \gamma'\gamma \to f\bar{f}$ process.

Let us start with

$$\begin{aligned} w(s) &= \sum_f \left(1-\frac{4m_f^2}{s}\right)^{1/2}\frac{Q_f^2e^2g'^2}{24\pi}\frac{s^2+2(M^2+m_f^2)s+4M^2m_f^2}{(s-\Lambda^2)^2}\\ &= \sum_f \left(1-\frac{4m_f^2}{s}\right)^{1/2}\frac{Q_f^2e^2g'^2}{24\pi}f_1(s) \end{aligned} \tag{A.144}$$

Then we expand $f_1(s)$ about $s = 4M^2$ up to order two:

$$f_1(4M^2) = \frac{16M^4 + 8M^4 + 8M^2m_f^2 + 4M^2m_f^2}{(4M^2 - \Lambda^2)^2} = 12\frac{2M^4 + M^2m_f^2}{(4M^2 - \Lambda^2)^2} \tag{A.145}$$

$$\frac{df_1}{ds}(s) = \frac{2s + 2(M^2 + m_f^2)}{(s - \Lambda^2)^2} - 2\frac{s^2 + 2(M^2 + m_f^2)s + 4M^2m_f^2}{(s - \Lambda^2)^3} \tag{A.146}$$

$$\begin{aligned}
\Rightarrow \frac{df_1}{ds}(4M^2) &= \frac{8M^2 + 2M^2 + 2m_f^2}{(4M^2 - \Lambda^2)^3}(4M^2 - \Lambda^2) - 2\frac{16M^4 + 8M^4 + 8M^2m_f^2 + 4M^2m_f^2}{(4M^2 - \Lambda^2)^3} \\
&= \frac{40M^4 + 8M^2m_f^2 - 10\Lambda^2M^2 - 2\Lambda^2m_f^2 - 48M^4 - 24M^2m_f^2}{(4M^2 - \Lambda^2)^3} \\
&= -2\frac{(5M^2 + m_f^2)\Lambda^2 + 4M^4 + 8M^2m_f^2}{(4M^2 - \Lambda^2)^3}
\end{aligned} \tag{A.147}$$

$$\begin{aligned}
\frac{d^2f_1}{ds^2}(s) &= \frac{2}{(s - \Lambda^2)^2} - 2\frac{2s + 2(M^2 + m_f^2)}{(s - \Lambda^2)^3} - 2\frac{2s + 2(M^2 + m_f^2)}{(s - \Lambda^2)^3} \\
&\quad + 6\frac{s^2 + 2(M^2 + m_f^2)s + 4M^2m_f^2}{(s - \Lambda^2)^4} \\
\Rightarrow \frac{d^2f_1}{ds^2}(4M^2) &= \frac{2(4M^2 - \Lambda^2)^2 - 4(8M^2 + 2M^2 + 2m_f^2)(4M^2 - \Lambda^2)}{(4M^2 - \Lambda^2)^4} \\
&\quad + \frac{6(16M^4 + 8M^4 + 8M^2m_f^2 + 4M^2m_f^2)}{(4M^2 - \Lambda^2)^4} \\
&= \frac{32M^4 + 2\Lambda^4 - 16\Lambda^2M^2 - 160M^4 + 40\Lambda^2M^2}{(4M^2 - \Lambda^2)^4} \\
&\quad + \frac{-32M^2m_f^2 + 8\Lambda^2m_f^2 + 144M^4 + 72M^2m_f^2}{(4M^2 - \Lambda^2)^4} \\
&= 2\frac{\Lambda^4 + 4(3M^2 + m_f^2)\Lambda^2 + 8M^4 + 20M^2m_f^2}{(4M^2 - \Lambda^2)^4}
\end{aligned} \tag{A.148}$$

Therefore we have

$$\begin{aligned}
f_1(s) &= f_1(4M^2) + \frac{df_1}{ds}(4M^2)(s - 4M^2) + \frac{1}{2}\frac{d^2f_1}{ds^2}(4M^2)(s - 4M^2)^2 + \mathcal{O}(s^3) \\
&= 12\frac{2M^4 + M^2m_f^2}{(4M^2 - \Lambda^2)^2} - 2\frac{(5M^2 + m_f^2)\Lambda^2 + 4M^4 + 8M^2m_f^2}{(4M^2 - \Lambda^2)^3}(s - 4M^2) \\
&\quad + \frac{\Lambda^4 + 4(3M^2 + m_f^2)\Lambda^2 + 8M^4 + 20M^2m_f^2}{(4M^2 - \Lambda^2)^4}(s - 4M^2)^2 + \mathcal{O}(s^3) \\
&= \frac{384M^8 + 24\Lambda^4M^4 - 192\Lambda^2M^6 + 192M^6m_f^2 + 12\Lambda^4M^2m_f^2 - 96\Lambda^2M^4m_f^2}{(4M^2 - \Lambda^2)^4} \\
&\quad + \frac{-40\Lambda^2M^4s + 10\Lambda^4M^2s - 8\Lambda^2M^2m_f^2s + 2\Lambda^4m_f^2s - 32M^6s + 8\Lambda^2M^4s}{(4M^2 - \Lambda^2)^4} \\
&\quad + \frac{-64M^4m_f^2s + 16\Lambda^2M^2m_f^2s + 160\Lambda^2M^6 - 40\Lambda^4M^4 + 32\Lambda^2M^4m_f^2}{(4M^2 - \Lambda^2)^4}
\end{aligned}$$

$$
\begin{aligned}
&+\frac{-8\Lambda^4M^2m_f^2+128M^8-32\Lambda^2M^6+256M^6m_f^2-64\Lambda^2M^4m_f^2}{(4M^2-\Lambda^2)^4}\\
&+\frac{\Lambda^4s^2+12\Lambda^2M^2s^2+4\Lambda^2m_f^2s^2+8M^4s^2+20M^2m_f^2s^2+16\Lambda^4M^4}{(4M^2-\Lambda^2)^4}\\
&+\frac{192\Lambda^2M^6+64\Lambda^2M^4m_f^2+128M^8+320M^6m_f^2-8\Lambda^4M^2s}{(4M^2-\Lambda^2)^4}\\
&+\frac{-96\Lambda^2M^4s-32\Lambda^2M^2m_f^2s-64M^6s-160M^4m_f^2s}{(4M^2-\Lambda^2)^4}+\mathcal{O}(s^3)\\
=&\frac{4\Lambda^4M^2m_f^2+128\Lambda^2M^6-64\Lambda^2M^4m_f^2+640M^8+768M^6m_f^2}{(4M^2-\Lambda^2)^4}\\
&+\frac{s}{4M^2}4M^2\frac{2\Lambda^4(M^2+m_f^2)-128\Lambda^2M^4-24\Lambda^2M^2m_f^2-96M^6-224M^4m_f^2}{(4M^2-\Lambda^2)^4}\\
&+\left(\frac{s}{4M^2}\right)^2 16M^4\frac{\Lambda^4+12\Lambda^2M^2+4\Lambda^2m_f^2+8M^4+20M^2m_f^2}{(4M^2-\Lambda^2)^4}+\mathcal{O}(s^3)\\
=&\,A_{0f}+A_{1f}\frac{s}{4M^2}+A_{2f}\left(\frac{s}{4M^2}\right)^2+\mathcal{O}(s^3)
\end{aligned}
\tag{A.149}
$$

Thus, we finally obtain

$$
\begin{aligned}
w(s)&=\sum_f\left(1-\frac{4m_f^2}{s}\right)^{1/2}\frac{Q_f^2e^2g'^2}{24\pi}\left(A_{0f}+A_{1f}\frac{s}{4M^2}+A_{2f}\left(\frac{s}{4M^2}\right)^2+\mathcal{O}(s^3)\right)\\
&=\sum_f\left(1-\frac{4m_f^2}{s}\right)^{1/2}\left(C_{0f}+C_{1f}\frac{s}{4M^2}+C_{2f}\left(\frac{s}{4M^2}\right)^2+\mathcal{O}(s^3)\right)
\end{aligned}
\tag{A.150}
$$

with

$$
\begin{aligned}
C_{0f}&=\frac{Q_f^2e^2g'^2}{24\pi}A_{0f}\\
&=\frac{Q_f^2e^2g'^2}{24\pi}\frac{4\Lambda^4M^2m_f^2+128\Lambda^2M^6-64\Lambda^2M^4m_f^2+640M^8+768M^6m_f^2}{(4M^2-\Lambda^2)^4}
\end{aligned}
\tag{A.151}
$$

$$
\begin{aligned}
C_{1f}&=\frac{Q_f^2e^2g'^2}{24\pi}A_{1f}\\
&=\frac{Q_f^2e^2g'^2}{24\pi}4M^2\frac{2\Lambda^4(M^2+m_f^2)-128\Lambda^2M^4-24\Lambda^2M^2m_f^2-96M^6-224M^4m_f^2}{(4M^2-\Lambda^2)^4}
\end{aligned}
\tag{A.152}
$$

$$
\begin{aligned}
C_{2f}&=\frac{Q_f^2e^2g'^2}{24\pi}A_{2f}\\
&=\frac{Q_f^2e^2g'^2}{24\pi}16M^4\frac{\Lambda^4+12\Lambda^2M^2+4\Lambda^2m_f^2+8M^4+20M^2m_f^2}{(4M^2-\Lambda^2)^4}
\end{aligned}
\tag{A.153}
$$

Appendix B

Useful integrals

Let us derive the general way to compute integrals of the following form [65]:

$$I_n = \int_0^\infty x^n e^{-\alpha x^2} dx \tag{B.1}$$

We note that

$$\frac{\partial}{\partial \alpha} \int_0^\infty x^n e^{-\alpha x^2} dx = \int_0^\infty x^n \frac{\partial}{\partial \alpha} e^{-\alpha x^2} dx = -\int_0^\infty x^{n+2} e^{-\alpha x^2} dx = -I_{n+2} \tag{B.2}$$

$$\Rightarrow \quad I_{n+2} = -\frac{\partial}{\partial \alpha} I_n \tag{B.3}$$

We therefore need to compute I_0 and I_1. For I_0 we know that it is equal to half the Gaussian integral, that is

$$I_0 = \frac{1}{2} \int_{-\infty}^{+\infty} e^{-\alpha x^2} dx = \frac{1}{2} \sqrt{\frac{\pi}{\alpha}} \tag{B.4}$$

As for I_1 we have

$$I_1 = \int_0^\infty x e^{-\alpha x^2} dx = -\frac{1}{2\alpha} \int_0^\infty \frac{d}{dx} e^{-\alpha x^2} dx = -\frac{1}{2\alpha} \left[e^{-\alpha x^2} \right]_0^\infty = \frac{1}{2\alpha} \tag{B.5}$$

Using (B.3), we can easily compute the next I_n by induction and we obtain

$$I_2 = \frac{1}{4\alpha} \sqrt{\frac{\pi}{\alpha}}, \; I_3 = \frac{1}{2\alpha^2}, \; I_4 = \frac{3}{8\alpha^2} \sqrt{\frac{\pi}{\alpha}}, \; I_5 = \frac{1}{\alpha^3}, \; I_6 = \frac{15}{16\alpha^3} \sqrt{\frac{\pi}{\alpha}} \tag{B.6}$$

Thus we can now compute $\langle v \rangle$, $\langle v^2 \rangle$ and $\langle v^4 \rangle$. It can be shown that [65]

$$\langle v \rangle = \frac{1}{\rho} \int_0^\infty v g(v) dv = 4\pi \left(\frac{m}{2\pi T} \right)^{3/2} \int_0^\infty v^3 e^{-\frac{mv^2}{2T}} dv \tag{B.7}$$

where ρ is the particle number density and $g(v)dv$ is the number of particles the magnitude of the velocity of which is comprised between v and $v + dv$. The latter is such that

$$g(v)dv = 4\pi\rho \left(\frac{m}{2\pi T} \right)^{3/2} v^2 e^{-\frac{mv^2}{2T}} dv \;\; \text{and} \;\; \int_0^\infty g(v) dv = \rho \tag{B.8}$$

Therefore we have

$$\langle v \rangle = 4\pi \left(\frac{m}{2\pi T}\right)^{3/2} \frac{1}{2} \left(\frac{2T}{m}\right)^2 = \sqrt{\frac{8T}{\pi m}}, \tag{B.9}$$

$$\begin{aligned} \langle v^2 \rangle &= 4\pi \left(\frac{m}{2\pi T}\right)^{3/2} \int_0^\infty v^4 e^{-\frac{mv^2}{2T}} dv \\ &= 4\pi \left(\frac{m}{2\pi T}\right)^{3/2} \frac{3}{8} \left(\frac{2T}{m}\right)^2 \sqrt{\frac{2\pi T}{m}} \\ &= 3\frac{T}{m} \end{aligned} \tag{B.10}$$

and

$$\begin{aligned} \langle v^4 \rangle &= 4\pi \left(\frac{m}{2\pi T}\right)^{3/2} \int_0^\infty v^6 e^{-\frac{mv^2}{2T}} dv \\ &= 4\pi \left(\frac{m}{2\pi T}\right)^{3/2} \frac{15}{16} \left(\frac{2T}{m}\right)^3 \sqrt{\frac{2\pi T}{m}} \\ &= 15 \left(\frac{T}{m}\right)^2. \end{aligned} \tag{B.11}$$

Appendix C

Feynman diagrams

Mandelstam variables

Let us consider the following $2 \to 2$ scattering process:

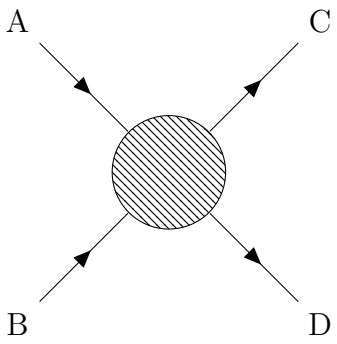

The Mandelstam variables s, t and u defined as

$$s = (p_A + p_B)^2 = (p_C + p_D)^2 \tag{C.1}$$

$$t = (p_A - p_C)^2 = (p_B - p_D)^2 \tag{C.2}$$

$$u = (p_A - p_D)^2 = (p_B - p_C)^2 \tag{C.3}$$

are Lorentz-invariant.

Moreover, s is the square of the center-of-mass energy and t the square of the 4-momentum transfer. If all the four 4-momenta were oriented inward, then p_C and p_D will gain a minus sign and so, there will be only plus signs in the three definitions above.

We can derive the following relation between these three variables, using the conservation of 4-momentum ($p_A + p_B = p_C + p_D$) and knowing that $p^2 = m^2$:

$$\begin{aligned} s + t + u &= p_A^2 + p_B^2 + 2p_A p_B + p_A^2 + p_C^2 - 2p_A p_C + p_A^2 + p_D^2 - 2p_A p_D \\ &= 3p_A^2 + p_B^2 + p_C^2 + p_D^2 - 2p_A(-p_B + p_C + p_D) \end{aligned}$$

$$
\begin{aligned}
&= 3p_A^2 + p_B^2 + p_C^2 + p_D^2 - 2p_A^2 \\
&= p_A^2 + p_B^2 + p_C^2 + p_D^2 \\
&= m_A^2 + m_B^2 + m_C^2 + m_D^2 \\
&= \sum m_{ext}^2
\end{aligned} \tag{C.4}
$$

with m_{ext} the mass attached to an external line of a Feynman diagram.

Gamma matrices

The gamma matrices γ^μ are defined as [60]

$$
\begin{aligned}
\gamma^0 &= \begin{pmatrix} 0 & 0 & 0 & 1 \\ 0 & 0 & 1 & 0 \\ 0 & 1 & 0 & 0 \\ 1 & 0 & 0 & 0 \end{pmatrix}, \quad \gamma^1 = \begin{pmatrix} 0 & 0 & 0 & 1 \\ 0 & 0 & 1 & 0 \\ 0 & -1 & 0 & 0 \\ -1 & 0 & 0 & 0 \end{pmatrix}, \\
\gamma^2 &= \begin{pmatrix} 0 & 0 & 0 & -i \\ 0 & 0 & i & 0 \\ 0 & i & 0 & 0 \\ -i & 0 & 0 & 0 \end{pmatrix}, \quad \gamma^3 = \begin{pmatrix} 0 & 0 & -1 & 0 \\ 0 & 0 & 0 & 1 \\ 1 & 0 & 0 & 0 \\ 0 & -1 & 0 & 0 \end{pmatrix}
\end{aligned} \tag{C.5}
$$

in the Weyl representation.

Let us state some results of trace computations [60]:

$$\mathrm{Tr}\left[\text{odd number of } \gamma\right] = 0 \tag{C.6}$$

$$\mathrm{Tr}\left[\gamma^\mu \gamma^\nu\right] = 4g^{\mu\nu} \tag{C.7}$$

$$\mathrm{Tr}\left[\gamma^\mu \gamma^\nu \gamma^\rho \gamma^\sigma\right] = 4\left(g^{\mu\nu} g^{\rho\sigma} - g^{\mu\rho} g^{\nu\sigma} + g^{\mu\sigma} g^{\nu\rho}\right) \tag{C.8}$$

Vertices

The vertices in the Feynman diagram presented in Chapter 4 correspond to the interaction between two standard-model fermions f and $\bar{f}$ and a photon γ and to the interaction between two fermionic dark-matter particles χ_f and $\bar{\chi}_f$ and a dark photon γ'. These vertices are depicted in Fig. C.1 and in Fig. C.2.

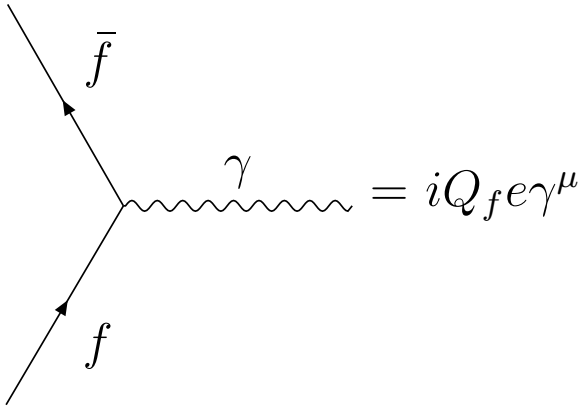

Figure C.1 – $ff\gamma$ vertex.

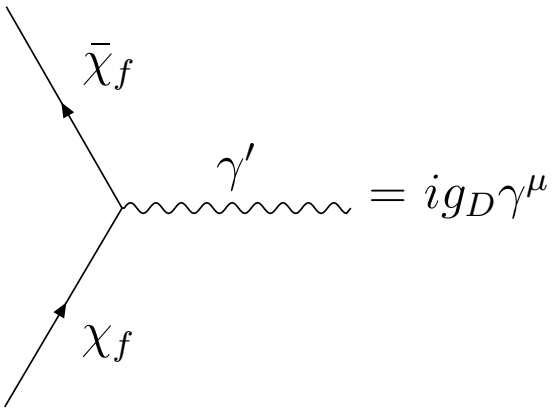

Figure C.2 – $\chi_f\bar{\chi}_f\gamma'$ vertex.

Appendix D

Complements about degrees of freedom

The degrees of freedom of the standard-model particles are given in Tab. D.1.

Bosons	Fermions
$g_\gamma = 2$	$g_{t\bar{t}} = g_{b\bar{b}} = g_{c\bar{c}} = g_{s\bar{s}} = g_{u\bar{u}} = g_{d\bar{d}} = 2 \times 2 \times 3$
$g_g = 2 \times 8 = 16$	$\Rightarrow g_q = 2 \times 2 \times 3 \times 6 = 72$
$g_{W^+W^-} = 3 \times 2 = 6$	$g_{\tau^-\tau^+} = g_{\mu^-\mu+} = g_{e^-e^+} = 2 \times 2$
$g_{Z^0} = 3$	$\Rightarrow g_l = 2 \times 2 \times 3 = 12$
$g_{H^0} = 1$	$g_{\nu_\tau\bar{\nu_\tau}} = g_{\nu_\mu\bar{\nu_\mu}} = g_{\nu_e\bar{\nu_e}} = 2 \times 2$
$g_{\pi^+\pi^-} = 1 \times 2$	$\Rightarrow g_\nu = 2 \times 1 \times 3 = 6$
$g_{\pi^0} = 1$	
$g_b = 28$	$g_f = 90$

Table D.1 – Degrees of freedom.

with

$$g_q = \underbrace{2}_{\text{spin}} \times \underbrace{2}_{\text{antiparticle}} \times \underbrace{3}_{\text{colour}} \times \underbrace{6}_{\text{flavour}} = 72$$

$$g_l = \underbrace{2}_{\text{spin}} \times \underbrace{2}_{\text{antiparticle}} \times \underbrace{3}_{\text{generation}} = 12$$

$$g_\nu = \underbrace{2}_{\text{spin}} \times \underbrace{1}_{\text{antiparticle (Majorana)}} \times \underbrace{3}_{\text{generation}} = 6$$

and where γ = photon, g = gluon, $W^\pm = W^\pm$ gauge boson, $Z^0 = Z^0$ gauge boson, H = standard-model Higgs boson, π = pion, t = top-quark, b = bottom-quark, c = charm-quark, s = strange-quark, u = up-quark, d = down-quark, τ = tauon, μ = muon, e = electron, ν_τ = tau neutrino, ν_μ = muon neutrino and ν_e = electron neutrino. Bosons, fermions, quarks, charged leptons and neutrinos are respectively denoted by b, f, q, l and ν.

At $T \sim 150$ MeV, the QCD phase transition (QCDPT) occurs. The quarks are no longer free and are trapped in baryons (p^+, n^0,...) and mesons ($\pi^\pm$, π^0,...). However, the sole relativistic hadron left below 150 MeV is the pion [22]. Therefore this is the only composite

particle which has to be taken into account in g_* and g_{*s}. The remaining elementary particles are μ^-, μ^+, e^-, e^+, ν_τ, $\bar{\nu_\tau}$, ν_μ, $\bar{\nu_\mu}$, ν_e, $\bar{\nu_e}$ and γ. With these considerations, we can obtain the evolution of g_* and g_{*s} during the thermal history of the Universe (see Tab. D.2).

Temperature	g_*	g_{*s}
$T \geq m_t$	$28 + \frac{7}{8}90 = 106.75$	106.75
$m_t > T \geq m_H$	$28 + \frac{7}{8}78 = 96.25$	96.25
$m_H > T \geq m_Z$	$27 + \frac{7}{8}78 = 95.25$	95.25
$m_Z > T \geq m_W$	$24 + \frac{7}{8}78 = 92.25$	92.25
$m_W > T \geq m_b$	$18 + \frac{7}{8}78 = 86.25$	86.25
$m_b > T \geq m_\tau$	$18 + \frac{7}{8}66 = 75.75$	75.75
$m_\tau > T \geq m_c$	$18 + \frac{7}{8}62 = 72.25$	72.25
$m_c > T \geq$ QCDPT	$18 + \frac{7}{8}50 = 61.75$	61.75
QCDPT $> T \geq m_{\pi^\pm}$	$5 + \frac{7}{8}14 = 17.25$	17.25
$m_{\pi^\pm} > T \geq m_{\pi^0}$	$3 + \frac{7}{8}14 = 15.25$	15.25
$m_{\pi^0} > T \geq m_\mu$	$2 + \frac{7}{8}14 = 14.25$	14.25
$m_\mu > T \geq m_e$	$2 + \frac{7}{8}10 = 10.75$	10.75
	neutrino decoupling	
$m_e > T \geq m_\nu$	$2 + \frac{7}{8}6\left(\frac{T_\nu}{T_\gamma}\right)^4 \simeq 3.36$	$2 + \frac{7}{8}6\left(\frac{T_\nu}{T_\gamma}\right)^3 \simeq 3.91$
$m_\nu > T \geq 0$	2	2

Table D.2 – Evolution of g_* and g_{*s} in the standard model as a function of the temperature of the Universe.

Bibliography

[1] D. B. Cline. The search for dark matter. *Sci. Am.*, 288:28–35, 2003. [Spektrum Wiss.2003N10,44(2003)].

[2] Joshua Ellis. TikZ-Feynman: Feynman diagrams with TikZ. *Comput. Phys. Commun.*, 210:103–123, 2017.

[3] Peter J. Mohr, David B. Newell, and Barry N. Taylor. CODATA Recommended Values of the Fundamental Physical Constants: 2014. *Rev. Mod. Phys.*, 88(3):035009, 2016.

[4] Alan L. Myers. Natural system of units in general relativity. `www.seas.upenn.edu/~amyers/NaturalUnits.pdf`, 2016.

[5] V. C. Rubin, N. Thonnard, and W. K. Ford. Extended rotation curves of high-luminosity spiral galaxies. IV - Systematic dynamical properties, SA through SC. *Astrophysical Journal, Part 2*, 225:L107–L111, 1978.

[6] Debasish Majumdar. *Dark matter: an introduction*. CRC Press, 2015.

[7] Yoshiaki Sofue and Vera Rubin. Rotation curves of spiral galaxies. *Ann. Rev. Astron. Astrophys.*, 39:137–174, 2001.

[8] Y. Sofue. Accurate rotation curves and distributions of dark matter in galaxies. In F. Hammer, T. X. Thuan, V. Cayatte, B. Guiderdoni, and J. T. Thanh Van, editors, *Building Galaxies; from the Primordial Universe to the Present*, page 127, 2000.

[9] Genzel et al. Strongly baryon-dominated disk galaxies at the peak of galaxy formation ten billion years ago. *Nature*, 543:397–401, March 2017.

[10] M. Swinbank. Astrophysics: Distant galaxies lack dark matter. *Nature*, 543:318–319, March 2017.

[11] D.H. Perkins. *Particle Astrophysics, Second Edition*. Oxford Master Series in Physics. OUP Oxford, 2008.

[12] Jaan Einasto. Dark Matter. *Braz. J. Phys.*, 43:369–374, 2013.

[13] Sidney van den Bergh. The Early history of dark matter. *Publ. Astron. Soc. Pac.*, 111:657, 1999.

[14] Douglas Clowe, Marusa Bradac, Anthony H. Gonzalez, Maxim Markevitch, Scott W. Randall, Christine Jones, and Dennis Zaritsky. A direct empirical proof of the existence of dark matter. *Astrophys. J.*, 648:L109–L113, 2006.

[15] A. Mahdavi, H. y Hoekstra, A. y Babul, D. y Balam, and P. Capak. A Dark Core in Abell 520. *Astrophys. J.*, 668:806–814, 2007.

[16] M. J. Jee, A. Mahdavi, H. Hoekstra, A. Babul, J. J. Dalcanton, P. Carroll, and P. Capak. A Study of the Dark Core in A520 with Hubble Space Telescope: The Mystery Deepens. *Astrophys. J.*, 747:96, 2012.

[17] David Harvey, Richard Massey, Thomas Kitching, Andy Taylor, and Eric Tittley. The non-gravitational interactions of dark matter in colliding galaxy clusters. *Science*, 347:1462–1465, 2015.

[18] Scott W. Randall, Maxim Markevitch, Douglas Clowe, Anthony H. Gonzalez, and Marusa Bradac. Constraints on the Self-Interaction Cross-Section of Dark Matter from Numerical Simulations of the Merging Galaxy Cluster 1E 0657-56. *Astrophys. J.*, 679:1173–1180, 2008.

[19] Richard Massey et al. The behaviour of dark matter associated with four bright cluster galaxies in the 10 kpc core of Abell 3827. *Mon. Not. Roy. Astron. Soc.*, 449(4):3393–3406, 2015.

[20] Viatcheslav Mukhanov and Sergei Winitzki. *Introduction to quantum effects in gravity*. Cambridge University Press, 2007.

[21] Don N. Page. Particle Emission Rates from a Black Hole: Massless Particles from an Uncharged, Nonrotating Hole. *Phys. Rev.*, D13:198–206, 1976.

[22] Daniel Baumann. Cosmology - Part III Mathematical Tripos. `www.damtp.cam.ac.uk/user/db275/Cosmology/Lectures.pdf`, 2013.

[23] JiJi Fan, Andrey Katz, Lisa Randall, and Matthew Reece. Dark-Disk Universe. *Phys. Rev. Lett.*, 110(21):211302, 2013.

[24] T. D. Lee and Chen-Ning Yang. Question of Parity Conservation in Weak Interactions. *Phys. Rev.*, 104:254–258, 1956.

[25] Paolo Ciarcelluti. Cosmology with mirror dark matter. *Int. J. Mod. Phys.*, D19:2151–2230, 2010.

[26] R. A. Sunyaev. Fluctuations of the microwave background radiation. In M. S. Longair and J. Einasto, editors, *Large Scale Structures in the Universe*, volume 79 of *IAU Symposium*, pages 393–402, 1978.

[27] Jean-Christophe Hamilton. What have we learned from observational cosmology? *Stud. Hist. Phil. Sci.*, B46:70–85, 2014.

[28] Gianfranco Bertone and Dan Hooper. A History of Dark Matter. *Submitted to: Rev. Mod. Phys.*, 2016.

[29] Joel R. Primack. Whatever happened to hot dark matter? *SLAC Beam Line*, 31N3:50–57, 2001.

[30] Adam G. Riess et al. Observational evidence from supernovae for an accelerating universe and a cosmological constant. *Astron. J.*, 116:1009–1038, 1998.

[31] Joel R. Primack. Cosmological Structure Formation. `https://arxiv.org/abs/1505.02821`, 2015.

[32] H. Mo, F. van den Bosch, and S. White. *Galaxy Formation and Evolution*. Galaxy Formation and Evolution. Cambridge University Press, 2010.

[33] Edward W. Kolb and Michael S. Turner. The Early Universe. *Front. Phys.*, 69:1–547, 1990.

[34] Julien Lesgourgues. An Overview of cosmology. 2004.

[35] M. Milgrom. A Modification of the Newtonian dynamics as a possible alternative to the hidden mass hypothesis. *Astrophys. J.*, 270:365–370, 1983.

[36] Antonino Del Popolo and Morgan Le Delliou. Small scale problems of the ΛCDM model: a short review. *Galaxies*, 5(1):17, 2017.

[37] Philip Bull et al. Beyond ΛCDM: Problems, solutions, and the road ahead. *Phys. Dark Univ.*, 12:56–99, 2016.

[38] Justin Khoury. Alternative to particle dark matter. *Phys. Rev.*, D91(2):024022, 2015.

[39] J. Bekenstein and M. Milgrom. Does the missing mass problem signal the breakdown of Newtonian gravity? *ApJ*, 286:7–14, November 1984.

[40] Jacob D. Bekenstein. Modified gravity vs dark matter: Relativistic theory for MOND. *PoS*, JHW2004:012, 2005.

[41] P. A. R. Ade et al. Planck 2015 results. XIII. Cosmological parameters. *Astron. Astrophys.*, 594:A13, 2016.

[42] V. Bonvin et al. H0LiCOW V. New COSMOGRAIL time delays of HE0435-1223: H_0 to 3.8% precision from strong lensing in a flat ΛCDM model. *Mon. Not. Roy. Astron. Soc.*, 465(4):4914–4930, 2017.

[43] Jonathan L. Feng. Supersymmetry and cosmology. *eConf*, C0307282:L11, 2003.

[44] Pat Scott. Searches for Particle Dark Matter: An Introduction. PhD thesis. `https://arxiv.org/pdf/1110.2757`, 2010.

[45] A. Del Popolo. Nonbaryonic Dark Matter in Cosmology. *Int. J. Mod. Phys.*, D23:1430005, 2014.

[46] Varun Sahni. Dark matter and dark energy. *Lect. Notes Phys.*, 653:141–180, 2004.

[47] David N. Spergel and Paul J. Steinhardt. Observational evidence for selfinteracting cold dark matter. *Phys. Rev. Lett.*, 84:3760–3763, 2000.

[48] Sean Tulin, Hai-Bo Yu, and Kathryn M. Zurek. Beyond Collisionless Dark Matter: Particle Physics Dynamics for Dark Matter Halo Structure. *Phys. Rev.*, D87(11):115007, 2013.

[49] Benjamin D. Wandelt, Romeel Dave, Glennys R. Farrar, Patrick C. McGuire, David N. Spergel, and Paul J. Steinhardt. Selfinteracting dark matter. In *Sources and detection of dark matter and dark energy in the universe. Proceedings, 4th International Symposium, DM 2000, Marina del Rey, USA, February 23-25, 2000*, pages 263–274, 2000.

[50] Sean Tulin. Self-interacting dark matter. *AIP Conf. Proc.*, 1604:121–127, 2014.

[51] James M. Cline, Zuowei Liu, Guy Moore, and Wei Xue. Composite strongly interacting dark matter. *Phys. Rev.*, D90(1):015023, 2014.

[52] JiJi Fan, Andrey Katz, Lisa Randall, and Matthew Reece. Double-Disk Dark Matter. *Phys. Dark Univ.*, 2:139–156, 2013.

[53] Mirco Cannoni. Exact theory of freeze out. *Eur. Phys. J.*, C75(3):106, 2015.

[54] E.C. Titchmarsh and D.R. Heath-Brown. *The Theory of the Riemann Zeta-function*. Oxford science publications. Clarendon Press, 1986.

[55] Steven Weinberg. *Gravitation and Cosmology*. John Wiley and Sons, New York, 1972.

[56] Paolo Gondolo and Graciela Gelmini. Cosmic abundances of stable particles: Improved analysis. *Nucl. Phys.*, B360:145–179, 1991.

[57] Robert J. Scherrer and Michael S. Turner. On the Relic, Cosmic Abundance of Stable Weakly Interacting Massive Particles. *Phys. Rev.*, D33:1585, 1986. [Erratum: *Phys. Rev.*D34,3263(1986)].

[58] Katherine Garrett and Gintaras Duda. Dark Matter: A Primer. *Adv. Astron.*, 2011:968283, 2011.

[59] V. A. Rubakov. Cosmology. In *Proceedings, 2011 European School of High-Energy Physics (ESHEP 2011): Cheile Gradistei, Romania, September 7-20, 2011*, pages 151–195, 2014.

[60] Michael E. Peskin and Daniel V. Schroeder. *An Introduction to quantum field theory.* 1995.

[61] Mark Srednicki, Richard Watkins, and Keith A. Olive. Calculations of Relic Densities in the Early Universe. *Nucl. Phys.*, B310:693, 1988.

[62] B. Holdom. Millicharged matter and a paraphoton. In *New and exotic phenomena.*, pages 637–642, 1987.

[63] Rouven Essig, John A. Jaros, and William Wester. Dark Sectors and New, Light, Weakly-Coupled Particles. `http://lss.fnal.gov/archive/2013/conf/fermilab-conf-13-653.pdf`, 2013.

[64] Kim Griest and David Seckel. Three exceptions in the calculation of relic abundances. *Phys. Rev.*, D43:3191–3203, 1991.

[65] C. Ngô and H. Ngô. *Physique statistique : Introduction - Cours et exercices corrigés.* Dunod, 2001.